THE CHARACTERIZATION AND ELECTROCHEMISTRY OF DYE-SENSITIZED SOLAR CELLS

University of Fort Hare
Together in Excellence

A dissertation submitted in fulfillment of the requirements for the degree of

MASTER OF SCIENCE (M.Sc)

By

CAGA NOLOYISO

In the Faculty of Science and Agriculture at the University of Fort Hare

Supervisor : Professor E.L Meyer

Co-Supervisor(s) : Doctor S. N Mamphweli

: Professor P.A Ajibade

December 2013

SUMMARY

In this study a presentation of the technology behind dye-sensitized solar cells, their design as well as the role of the different parts of the cell. The characterization of the cell is divided into four sections namely: the characterization of the paste required to make the TiO_2 film and its optical properties using SEM-EDX and XRD analytical techniques; Analysis of the various absorptions of three Ru-based dyes using UV-Vis spectroscopy, Photoluminescence and Fourier Transform Infra-Red spectroscopy; the characterization and the analyses of the entire cell using Electrochemical Impedance Spectroscopy.

The nine cells were prepared by examining $RuL_2(CN)_2$, $RuL_2(NCS)_2$ or N3 dye and $RuL_2(NCS)_2$ TBA^+ or N719 dye. [L = 2,2'-bipyridyl-4,4'-dicarboxylic acid ;TBA = tetra-butyl ammonium] were combined with three electrolytes namely: Z–150 , AN–50 and PN–50. The Iodolyte PN–50 is an iodide based low viscosity electrolyte with 50 mM of tri-iodide dissolved in a solvent called propionitrile (PN). The Iodolyte AN–50 is an iodide based low viscosity electrolyte with 50 mM of tri-iodide dissolved in a solvent called acetonitrile (AN). The Iodolyte Z–150 is an iodide based low viscosity electrolyte with 150 mM of tri-iodide dissolved in a solvent called 3-methoxypropionitrile (MPN) and with additives such an ionic liquid, alkylbenziimidazole and guanidine thiocyanate. A solar simulator was utilized with which the standard solar irradiation can be created in laboratory conditions. The fill factors as well as overall performance efficiencies of the these cells are quite low < 1.0%,.

Keywords: Dye-sensitized Solar Cells, Acetonitrile, Methoxypropionitrile, Propionitrile, Characterization Techniques, Overall Performance Efficiency.

ACKNOWLEDGEMENTS

- I would like to first and foremost to extend a Word of Gratitude to the Almighty God for enabling me to reach this milestone in my life and for the strength to finally finish this thesis by only His Grace. Ebenezer! Till thus far O Lord; Thou art with me and Your Mercies Endureth Forever… "Wena Ungundlela Azaziwa"
- I would like to thank my supervisor Professor Edson Meyer for all your patience and inspirational talks and all the FHIT staff particularly for all the assistance in trip bookings and giving support where necessary.
- I would like to sincerely thank Dr Sampson Mamphweli for all the unwavering support and for always being available in your office to give me direction. This thesis would not have been possible without the his help, kindness and patience.
- I would like to deeply appreciate Pastor Khaya Maphinda for mentoring, over-seeing this research project. You have actually seen the best in me even when I could not. Thank you for motivating and always give spiritual support at all times. Indeed Success is not an option but a must. I would like to thank you for your consistent, unwavering moral support and for always being there for me and listen; you have been a true father to me in so many ways. You have taught me that: victory is guaranteed for those to refuse to stop fighting …

- I wish to acknowledge Dr Adeloye Adewale for assisting me to perform experiments on the Ultra-Violet spectroscopy and Photoluminescence analytical instruments. Moreover he has assisted me with the most critical analysis of this project, without them, most of my piece of work would be meaningless.
- I would like to thank acknowledge SANERI for their financial assistance towards the completion of this thesis.
- I would like to acknowledge CSIR staff particularly Dr Lukas Le Roux for allowing me the opportunity to work of the fabrication, characterization of the dye solar cells.
- I would like to thank Walter Sisulu University staff for putting up with me under very difficult and trying times of my research.
- A special thank you to my biological family, spiritual family and friends for prayers individually and collectively; especially my aunt Mrs Mfengukazi Caga, Mrs Nocwaka Sino Klaas, and Mr Mzwandile Caga who worked tirelessly to inculcate the importance of the completion of this thesis.
- I will always cherish the wonderful conversations and great advises Dr Zoliswa Mali, Pt Nyayeni and Pt Maphinda which are full of wisdom conveyed to me during the hardest season of my life.
- To my beloved late mother, Nomahlubi Hlubie Caga, thank you for securing a bright future for me and my one and only brother Siviwe Caga. May Her soul Rest in Peace!

DEDICATION

I dedicate this piece of work to the Holy Spirit, My Ever-Present Help!

To God Be All The Glory!

LIST OF ABBREVIATIONS

AM – Air Mass

AN – Acetonitrile

CB – Conduction Band

CE – Counter Electrode

COOH – Carboxylic \Acid

CV – Cyclic Voltammetry

DSSC – Dye-sensitized Solar Cell

E_F – Fermi Level

EIS – Electrochemical Impedance Spectroscopy

EDX – Energy Dispersive X-Ray

FTO – Fluorine-Doped Tin Oxide ($F:SnO_2$)

FF – Fill Factor

FTIR – Fourier Transform Infra-Red

HOMO – Highest Occupied Molecular Orbital

IHP – Inner Helmholtz Plane (IHP)

IPCE – Induced Photon to Current Efficiency

I-V – Current Voltage

LUMO – Lowest Unoccupied Molecular Orbital

MLCT – Metal-to-Ligand Charge Transfer

MPN – Methoxypropionitrile

NCS – Thiocyanate

OHP – Outer Helmholtz Plane

PN – Propionitrile

PL – Photoluminescence

Q_D – Excess Charge in the Diffuse Layer

Q_E – Total Excess Charge

Q_{SC} – Space Charge

Redox – Reduction/Oxidation

R_{ct} – Charge-Transfer Resistance

SEM – Scanning Electron Microscope

TCO – Transparent Conductive Oxide

WE – Working Electrode

TBA – Tetra Butyl- Ammonium

UV-VIS – Ultra-violet and Visible

X_D – Thickness of the Diffuse Layer

X_{OH} – Distance for Locus of Centres for Solvated Ions

X_{SC} – Excess Charge Below Interface

XRD – X- Ray Diffraction

V_B – Valence Band

TABLE OF CONTENTS

LIST OF FIGURES

Page

LIST OF TABLES

CHAPTER 1

INTRODUCTION

1.1 BACKGROUND

As economic development takes place, energy demand is expected to grow significantly, driven particularly by important changes in livelihood patterns of the millions of people who live at or below the poverty line (Jaramillo, 2007). There is an increasing demand for renewable energy because there is an assumption that between the years 2000 and 2030 there will be an increase in the carbon dioxide emissions and world energy demand by about seventy percent (70%)(Smith, 2011).Generally, fossil fuels supply have a responsibility of supplying about 80% of all the energy that is consumed worldwide and unfortunately they are faced by rapid resource depletion(Sims, *et al.*, 2007).

Therefore, there is an urgent need for environmentally sustainable energy technologies, because of a growing demand for energy coupled with the depletion of fossil resources, global warming and its associated climate change**.** Renewable by definition refers to the production of electricity, transport fuel or heat from sources that do not run out. Surprisingly, renewable energy technologies that include photovoltaic, solar thermal, hydropower and biomass-fired electricity generation, only supplied 14% of all the energy consumed worldwide by 2011(IEA Fact Sheet).

Currently, solar electricity is a steadily growing energy technology and solar cells have gained different types of applications that range from consumer electronics and small scale distributed power systems to centralized huge power plants (Mills, 2011).The direct use of solar radiation so as to produce electricity is closely related to excellent ways of using the renewable energy flows in nature, such as photosynthesis. Power can be produced with the photovoltaic cells near the end user of the electricity and in the process avoiding the losses and costs of transmission. Furthermore, the high practical and theoretical potentials of the solar electricity make it attractive for large-scale utilization (Alsema, *et al.*, 2010).

1.2 RATIONALE OF THE STUDY

The existing commercial solar electricity technology relies on silicon-based solar cells whose energy production is based on charge separation. The charge separation, after the absorbed photon has generated an electron-hole pair, is monitored by an electric potential difference. Silicon cells are quite expensive and they require high purity, high illumination for them to avoidpremature recombination and to be highly efficient.The most studied and most famous unconventional photovoltaic system is the dye-sensitized nanostructured solar cell that was developed by Professor Gratzel in 1991 with the invention of the N3 dye. Currently, this dye-sensitized solar cell is based on a sponge-like TiO_2 film with a high surface and efficiencies of up to 10.4% are possible to achieve (Nazeeruddin, *et al*.,1991). This solar cell is called the dye-sensitized nanostructured solar cell or the Gratzel cell after its inventor. In contrast to the all-solid conventional semiconductor solar cells, the dye-sensitized solar cell is a photoelectrochemical solar cell i.e. it uses a liquid electrolyte or other ion- TiO_2 conducting

phase as a charge transport medium. Due to the high efficiencies and good long-term stability reported for the dye-sensitized solar cells, the research interest in this technology grew rapidly during the 1990's. Currently, the highest energy conversion efficiency is over 11% and further increase of the efficiency is possible by designing proper electrodes and sensitization dyes such as N719 dye (Chiba, *et al*., 2006).

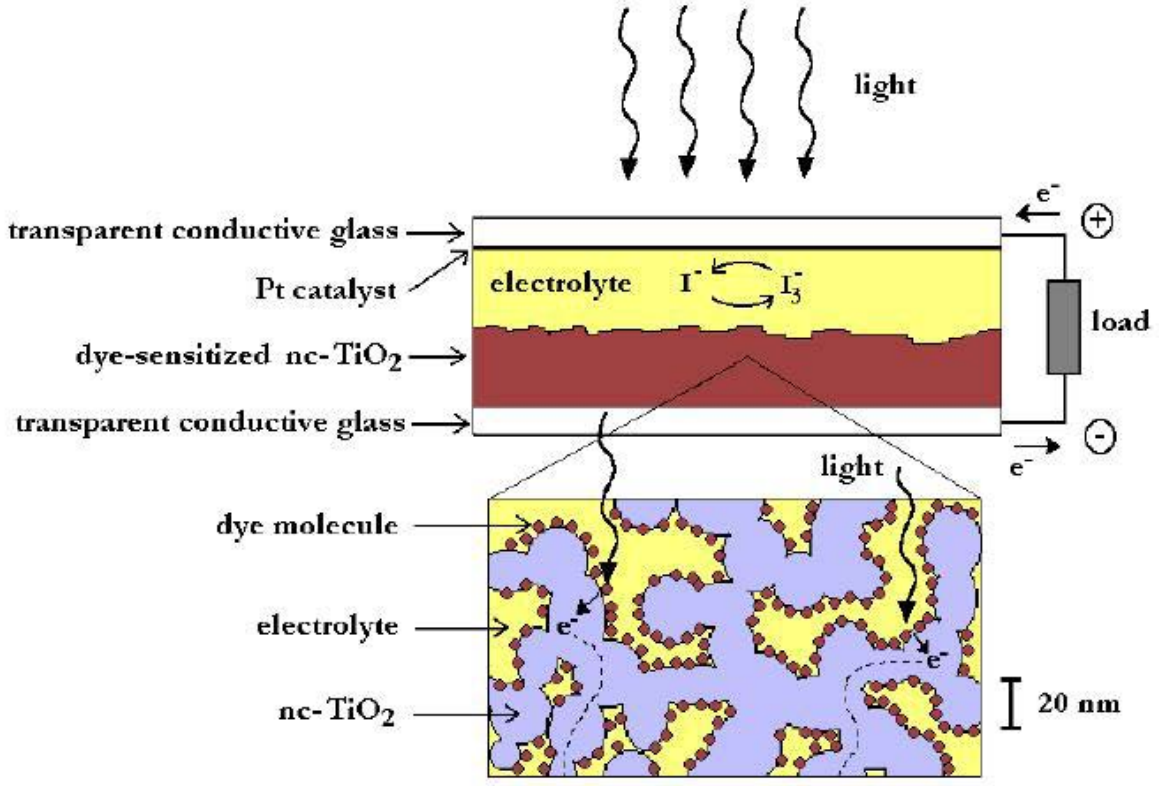

Figure 1.1 *A schematic diagram of a typical dye-sensitized solar cell with its components*

(Hagfeldt A, *et al*, 2009)

The dye-sensitization concept was invented in order to find a photoelectrochemical solar cell based on a semiconductor, which is stable against photo-corrosion and yet absorbs light in the visible region. Many metal oxides fulfill the former requirement, however, most only absorb UV-light. A way to extend their spectral response is to absorb dye molecules absorbing visible

light on the semiconductor surface: dye sensitization(Nazeeruddin, *et al*.,1993). By the use of a porous network of nanometer-sized crystals of TiO_2 deposited on a conducting substrate, the TiO_2 surface can become 100 times larger than the macroscopic area, per micrometer film thickness. The enlarged surface area of TiO_2 leads to increased dye adsorption (by the same factor) resulting in an increased harvesting of sunlight and an increased interface between the dye-sensitized semi-conductor and the electrolyte (O'Regan, *et al*. 2001). The stability of the dyes is coupled with three different electrolytes since they determine the lifetime of the entire cell, hence this research is mainly focused on this aspect.

1.3 OBJECTIVES OF THIS STUDY

This research project is aimed at the characterization of three ruthenium-based dyes with three different electrolytes for dye-sensitized solar cell application. To achieve this objective, the following aspects will be investigated:

i. Evaluation of the stability of the three ruthenium-based dyes under various characterization techniques;
ii. Determination of the elemental composition as well the optical properties of TiO_2 films;
iii. Investigation of the crystal phases of the TiO_2 films;
iv. Investigation of the spectral response characteristics of the cells;
v. Determination of the functional groups and the strengths of their bonds found on the various dyes;
vi. Determination of the electronic bands of the fabricated cells;

vii. Investigation of the kinematics with the electrolyte components and the construction and performance evaluation of the cells.

1.4 RESEARCH QUESTIONS

i. Which of the three dyes is more stable than the rest and why?
ii. Does the elemental composition of the various TiO_2 pastes differ significantly?
iii. What are the crystal-phases present in the various titania pastes?
iv. What is the spectral response of each of these cells fabricated and what impact does this have on the other aspects of the cells?
v. Do the functional groups present on the dyes affect the performance when they interact with the three different types of electrolytes?
vi. What are the electronic bands of the cells fabricated and their implications?

1.5 DELINEATION AND LIMITATIONS

The main focus of this project was to characterize the three ruthenium-based dyes with a view to investigate their possible application in solar cells with different electrolytes. The characterization techniques employed did not involve the electrical characterization in terms of performance evaluation or conversion efficiency of the dye-sensitized solar cells. This is therefore, the major limitation of this research project. However, it is recommended that this is undertaken as further research.

1.6 RESEARCH METHODOLOGY ANDOUTLINE OF THE DISERTATION

In this research, three dyes were purchased and these were characterized using the Ultraviolet-visible spectroscopy, Fourier Transform Infrared spectroscopy, and Photoluminescence to establish their stability and suitability for solar cell application. Furthermore, the Scanning Electron Microscopy coupled with Energy Dispersive X–Ray Diffraction and X–Ray Diffractionanalyzers were utilized for characterizing the optical properties of titania pastes prepared from Degussa P25 powder, as opposed to both commercially uncoated and coated pastes. Finally, Electrochemical Impedance Spectroscopy was used to establish the stability of the constructed cells.

This dissertation is composed of five chapters, as follows:

Chapter 1 is the introduction; this chapter gives an insight into the whole dissertation including the rationale and objectives of the study.

Chapter 2 is based on the literature review, which focuses on the fundamentals or the basics of dye-sensitized solar cells. The design of all the components of the dye solar cell, which are the TiO_2 film, the dye, the electrolyte and the counter electrode are clearly introduced. The operating principle of the dye solar cells is presented and the kinetics driving the cells are discussed and the parameters that relate to solar cell measurements are listed. It also concentrates on the interactions that occur at the semiconductor-electrolyte interfaces as well as dye-

electrolyte interfaces. Finally, the conductivity of the nanostructured TiO_2 film that serves as the semiconductor is dealt with in this chapter.

Chapter 3 deals with the description of how to manufacture dye-sensitized solar cells and it starts with the making of TiO_2 films, followed by dyeing of the films, preparing counter electrodes, preparing the electrolyte and ultimately assembling the dye solar cells. Furthermore, the characterization techniques, which include Scanning Electron Microscopy, X-ray Diffraction, Ultraviolet-Visible Spectroscopy, Fourier Transform Infrared Radiation Electrochemical Impedance Spectroscopy and I – V characterization and fill factor measurements for individual components and newly made dye solar cells, are discussed. After a brief description of the design and the physical principles underlying the operation of a dye-sensitized nanostructured solar cell, the performance will be presented

Chapter 4presents the results obtained using the methods and characterization techniques presented in Chapter 3. These results are presented and analyzed with reference to existing theories and literature.

Chapter 5 summarizes major findings and contributions based on the project anddraws conclusions on the outcome of the research experiment. The recommendations for further studies are also presented in this chapter.

CHAPTER 2

LITERATURE REVIEW

2.1 FUNDAMENTALS OF DYE-SENSITIZED SOLAR CELL

The dye-sensitized solar cell is designed to be made up of a working electrode, a counter electrode and an electrolyte. The DSSC can be made from a variety of different materials. The most conventional one will be described here. A 5-10 μm thick nanostructured TiO_2 film is deposited onto a transparent conducting substrate (back contact). The dye-sensitized TiO_2 forms the working electrode. A platinized conducting substrate constitutes the counter electrode of the solar cell.

2.1.1 THE SEMICONDUCTOR - TITANIUM DIOXIDE

The titanium dioxide (TiO_2) film forms part of the wide band gap semiconductor of the dye solar cell(Jasim, 2009). It is made up of three crystalline forms, anatase, rutile and brookite, but rutile and anatase play an important role in the applications of TiO_2. Anatase has pyramid-like crystals, is stable at low temperatures and is more prevailing. Rutile consists of needle-like crystals, and is stable at high temperatures. Brookite is very rare to find. TiO_2 has been extensively studied because of its excellent functionality as a charge collector, as an electron conductor, ability to allow fast electron movement, long-term stability, non-toxicity, very low

cost fabrication, high conversion efficiencies, support towards the sensitizer dye and is compatible with flexible substrates (Addamo M., *et al*., 2006).

Titanium dioxide (TiO_2) is one of the most promising material used for nano-porous thin film due to its appropriate energy levels, dye adsorption ability, low cost, and easy preparation (Diebold U., 2003). Extensive research on the photochemistry and photo-physics of TiO_2-based DSSCs has shown that the light harvesting efficiency of TiO_2 is influenced by its crystalline phase, particle size as well as its surface area, dye affinity, and film porosity. TiO_2 exists in two major phases: anatase and rutile. The anatase phase gained much attention due to its more active surface chemistry and smaller particles for more dye adsorption. Anatase is meta-stable and can be transformed irreversibly to thermodynamically more stable and condense rutile phase at higher temperature. The rutile phase TiO_2, due to the high refractive index, has excellent light-scattering characteristics, which is a profitable property from the perspective of effective light harvesting (Wang C., *et al.*,2004). Combination of anatase and rutile TiO_2 can be more effective than the pure phase owing to the electron-holes separation at the interface between phases and the formation of inter-band gap trap which may influence inter-particle carrier transportation. The commercial Degussa P-25 TiO_2 composed of anatase-TiO_2 and rutile-TiO_2 at a ratio of 80:20 is known to be one of the most active photo-catalysts due to the synergic effect (Park N.G., *et al*., 2003).

Titanium dioxide is a transition metal oxide (d^o) that is transparent to visible light and has a band gap of 3.2 eV mainly made up of the anatase phase(Monllor-Satoca, *et al.*, 2007). TiO_2 is composed of both the valence band that is having the O–2p character) and the valence band that

has the Ti–3d character. Its bonding type is intermediate between covalent and ionic (Henrich, *et al*., 1994).

Titanium has various stable oxidation states, which are Ti^{2+}, Ti^{3+} and Ti^{4+} and the extra electrons and band gap states are interpreted as one or two electrons occupying a metal site, i.e. in the upper half of the band gap region, therefore reducing the initial Ti^{4+} state.Point defects such as oxygenvacancies give rise to extra electrons that fill the band gap states (Agrell, 2003). Therefore, TiO_2 is found to be n-doped, because of the oxygen deficiencies. The electronic contact between the nanoparticles is achieved in a sintering process in the nanostructured TiO_2. Further defects in the crystal structure are expected due to the large number of grain boundaries, as well as the large TiO_2/dye/electrolyte interface (Lee, *et al*., 2009).

The Ti – O bonding, which mostly involves O 2p and Ti 3d atomic orbitals, has a strong ionic character. Thus, the partial densities of states are different for the valence band and conduction band, involving different contributions of the O and Ti atomic orbitals. According to the ionic character of TiO_2, the valence band is derived mainly from O 2p states and the conduction band originates mainly from Ti 3d states. Hence the valence orbitals are mainly associated with O^{2-} ions, whereas the conduction band states are mainly associated with Ti^{4+} ions. In the case of band gap excitation the electron density is shifted from oxygen to titanium sites. The upper valence band can be divided into three regions i.e. the sigma bonding in the lower part, middle and a higher pi bonding region, reaching to the valence band maximum. The unhybridized non-bonding molecular orbitals such as the O-p_π orbital at the valence band maximum (VBM) and the Ti-d_{xy} orbital at the conduction band maximum (CBM) are located near the band gap due to

symmetrical reasons (distortion of the $[TiO_6]^{2-}$ octahedrons). The rest of the conduction band states is of antibonding character, mainly derived from Ti 3d and Ti 4s atomic orbital. The anatase particles are spherical in shape and must be nanocrystalline in their application on their application in dye sensitized solar cells, because the nanocrystallinity of the anatase ensures a large dye uptake due to a large surface area. Consequently, the light absorption by the semiconductor electrode increases by several orders of magnitude compared to a flat dye-sensitized single crystal surface.

There are facts that need to be considered in a TiO_2 film for its excellent functionality. Firstly, the film has to be highly porous, therefore the particle size has to be increased. The electrolyte has to be able to go through the pores and be present where there is an adsorbed dye. Secondly, the particle size has to be optimized so as to maximize the effect of large surface area and the porosity of the film. Pores get smaller as the particle size decreases. Thirdly, a high surface area is necessary and when the surface area of the film increases, the particle size decreases. (Park, *et al*., 2009). Finally, the film has to be thicker so that there is more radiation that can be absorbed by the film. However, there is a probability of an increase in recombination when the thickness of the film increases(Wang, *et al*., 2003).

2.1.2 RUTHENIUM METAL COMPLEXES

Transition metals are defined as elements with one or more stable ions having incompletely filled d-orbitals.Therefore, Most of sensitizer dyes that are utilized in dye-sensitized solar cells are transition metal compounds. The majority of transition metal complexes have a tendency of

absorbing visible light and have different oxidation states,are therefore easily oxidized or reduced and are useful as redox catalysts. They are made up of a central transition metal (ruthenium) atom that is bonded to neutral and/or anionic ligands. The shape or geometry of a compound depends on the (coordination number) or ligand atoms that are directly bonded to the central metal atom. The most common geometry or shape for the ruthenium-based sensitizer dyes is the octahedral shape (i.e. it has six ligands) (Agrell, 2003).

There are two theories that can fully describe the bonding and the properties of a transition metal compound;the crystal field theory (CFT) and molecular orbital theory (MOT). The CFT outlines the fact the above-mentioned properties of the transition metal compounds result from the splitting of d-orbital energies as a result of electrostatic interactions between the central metal ion and ligands. The assumption of the CFT model is that, due to electrostatic attractions that are between the metal cation and the negative charges of the ligands, an ion compound results. The CFT does not explain the pi (π) bonding and the presence of properties other than crystal field based electronic transitions, but the MOT can fully describe them (Lee, 2006).

Molecular orbital theory (MOT), explains the interaction between the metal and ligands by the linear combinations of atomic orbitals (LCAO) and it allows the charge transfer between the central atom and its ligands. The interaction between orbitals is dependent on their energy differences and orbital overlaps. The boundary or cutting edge orbitals, for transition metal compounds, that are involved in the interactions are the s, p, and d orbitals on the metal and orbitals of the (sigma) δ- type and (pi) π-type with respect to the metal-ligand axis on the ligand.(Lee, 2006).

The oxidation of a molecule involves an occupied state and the reduction of a molecule involves an empty state, therefore, both processes exist at different energies being determined by the electronic structure of the molecule. The highest occupied molecular orbitals are commonly known as HOMO and the lowest unoccupied molecular orbitals are referred to as LUMO. The redox energy level of the excited molecule can be estimated by increasing the excitation energy to the energy level of the redox couple in the ground state. The excitation energy is given by the electronic transition between the lowest lying vibrational levels in the ground state and the excited state. The absorption and the redox properties of a dye complex can be changed by the use of different ligands(Ceroni, *et al.*, 2011).

According to crystal field theory in an octahedral metal complex, the d-orbitals of the ruthenium central atom split into degenerate t_{2g} (d_{xy}, d_{xz}, d_{yz}) and e_g (d_{x2-y2} , d_z^2) sets of orbitals. In these ruthenium-based dyes, the ruthenium atom in ruthenium 505 dye is coordinated by the two bivalent bipyridine, and two monovalent cyanide (CN) ligands. For ruthenium 535 dye or N3 dye is coordinated by the two bivalent bipyridine, and two monovalent thiocyanate (SCN) ligands. For ruthenium bis-535 or N719 dye is coordinated by the two bivalent bipyridine, two monovalent thiocyanate (SCN) ligands and two tetrabutylammonium ligands. On these dye molecules, the HOMO and LUMO orbitals are spatially separated from each other. Normally, the HOMO of the dyes is mainly located around the cyanide or thiocyanate group, whereas the LUMO is spread over the π-electron system of the bipyridine ligands (Rensmo, *et al*. 1998).

2.1.3 SENSITIZERS OR DYES

A ruthenium-based dye is adsorbed on the surface of the nanostructured TiO_2 film by soaking the film in an ethanolic solution of the dye. The bonding between the dye and the TiO_2 should give high stability, dense packing and efficient charge injection. The dye N719 is so far one of the most efficient and most studied dye of nanostructured solar cells. The dye exists in two redox states in the solar cell (Ru^{2+} and Ru^{3+}). The valence level of neutral ruthenium (Ru-4d) contains 8 electrons (d^8) (Chen, 2008).

For photovoltaic cells, an ideal sensitizer should absorb incident light of all wavelengths. Preferably, the energy level of the excited state corresponds to the conduction band of the semiconductor, and the ground state potential matches the redox level of the redox couple in the electrolyte, in order to avoid energy losses during the processes of electron transfer and regeneration (Gamstedt, 2005). The dye is usually anchored to the surface of the nanostructured semiconductor via its ligands, most often provided by carboxylate or phosphonate groups. However, for ligand-free organic sensitizers alternativeattaching strategies are known (Westermark, 2001).The dye serves as the heart of the nanocrystalline dye-sensitized solar cell since it plays different important roles including absorbing the incident light, injecting electrons into the semiconductor conduction band, reacting with the redox couple in order to be regenerated and blocking the TiO_2/Electrolyte interface to reduce the dark current. Therefore, the cell performance largely depends on the selection of an efficient light capturing antenna that normally consists of Ruthenium-based dyes and/or natural dyes **(**Grätzel, 2003).

The breakthrough in the dye-sensitization of semiconductor electrodes made the use of metallo-organic ruthenium complexes along with nanostructured TiO_2 electrodes. Thus, the selection of the dye is said to be easy. The dyes that have the general structure $ML_2(X)_2$ where L stands for 2,2'-bipyridyl-4,4'-dicarboxylic acid; M stands for ruthenium and X for a halide, cyanide or thiocyanate have been found promising. The dye that was introduced was *cis*-$RuL_2(NCS)_2$ which is also known as N3 dye and it showed a very good performance and ever since then it has been the most preferred option for nanocrystalline dye solar cells for quite some time. The N719 dye (tricyanato)-2,2',2''-terpyridyl-4,4',4''-tri(carboxylate)ruthenium(II)) or black dye (as effectually known) emerged to compete with the N3 dye and it had more advantages. The performance of the black dye exceeded that of the N3 dye by extending the absorption spectral range further to the infrared wavelengths, produced higher photovoltages and yielded the record cell efficiency of 10.4% (Halme, 2002).

Due to the distinct geometry of the ruthenium-based dye molecules, their orientation relative to the TiO_2 semiconductor is of prime importance for the performance of the dye-sensitized solar cells. These dye complexes anchor preferably with the carboxyl and thiocyanategroups on semiconductor surfaces. As the initial step for dye anchoring to the TiO_2 surface the coupling via only one carboxyl group takes place and in subsequential anchoring steps the dye can absorb with any of the other remaining uncoupled carboxyl group. The coupling via two carboxyl groups of the same bipyridine ligand allows the molecule to tilt sideways so that the thiocyanate (SCN) group can interact with the adsorption site. The IR has the ability to provide experimental evidence that the anchoring mechanism of the carboxyl group onto the TiO_2 substrate show three binding modes i.e. unidentate, bindentate and bridging are possible, but the one with the most

stable configuration is bridging anchoring mode. A beneficial side effect of dye-complexes that contain a thiocyanate ligand is that when they are coupled onto the TiO_2 surface they degrade under irradiation and loose sulfur. But upon anchoring the substrate, this degradation mechanism is suppressed due to the rapid transfer of the excited electron into the semiconductor, which deactivates the excited state of the molecule. The electron injection rate constant is estimated to be 10^9 times larger than the sulfur loss reaction.

2.1.3.1 RUTHENIUM 505 DYE

Ruthenium 505 Oxide Semiconductor Sensitizer is a dark orange color and its chemical name is *cis*-bis(cyanido) bis(2,2'-bipyridyl-4,4' dicarboxylato) ruthenium (II) and is normally shortened as $RuL_2(CN)_2$ (L = 2,2'-bipyridyl-4,4'-dicarboxylic acid). Ruthenium 505 sensitizes efficiently wide band-gap oxide semiconductors, like titanium dioxide, up to a wavelength of 650 nm. This sensitizer is suited for photochemical experiments, as it hasfavorable stability properties (Gimenez S., *et al*, 2011). The structure of Ruthenium 505 dye is as follows:

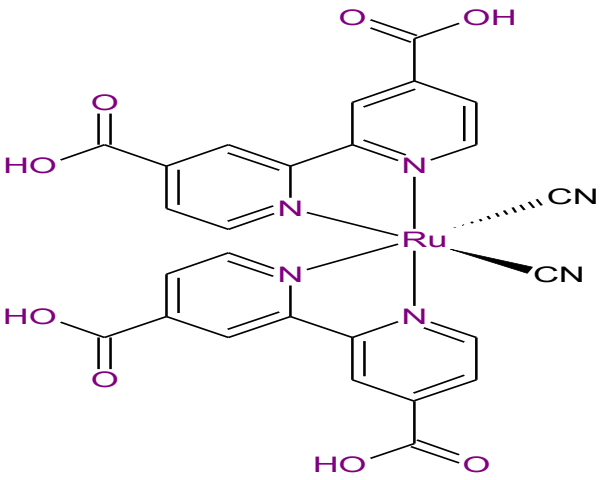

Figure 2.1 *The structure of the Ruthenium 505 Dye* (Gimenez S., *et al*, 2011)

2.1.3.2 RUTHENIUM 535DYE

Ruthenium 535 is also known as "N3" dark purple powder and its chemical name is *cis*-bis(isothiocyanato)bis(2,2'-bipyridyl-4,4'-dicarboxylato)-ruthenium(II),$RuL_2(NCS)_2.2H_2O$ (L = 2,2'-bipyridyl-4,4'-dicarboxylic acid).Ruthenium 535 very efficiently sensitizes wide band-gap oxide semiconductors, like titanium dioxide, up to a wavelength of 750 nm (Gimenez S., *et al*, 2011). The structure of Ruthenium 535 dye is shown in Figure 2.2.

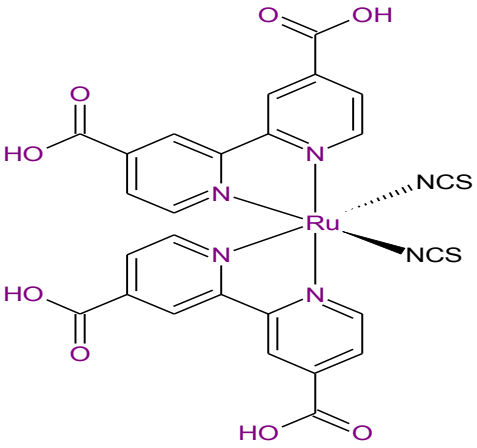

Figure 2.2*The structure of the Ruthenium 535 or N3 Dye* (Gimenez S., *et al*, 2011).

2.1.3.3 RUTHENIUM 535BIS-TBA DYE

Ruthenium 535 bis-TBA (also known as "N719" or "dye salt") is also dark purple powder and its chemical formula is *cis*-bis(isothiocyanato)bis(2,2'-bipyridyl-4,4'-dicarboxylato)-ruthenium(II)bis-tetrabutylammonium, $RuL_2(NCS)_2$: 2 TBA (L = 2,2'-bipyridyl-4,4'-dicarboxylic acid ;TBA = tetrabutylammonium). Ruthenium 535 bis-TBA very efficiently sensitizes very efficiently oxide semiconductors, such as titanium dioxide. It is more soluble than Ruthenium 535 in solvents, such as ethanol or acetonitrile.

Moreover, a photovoltage that is ~ 50 mV higher is obtained with this sensitizer (Athanasius J. *et al.*, 2012). The structure of Ruthenium 535 bis-TBA dye is as shown in Figure 2.3.

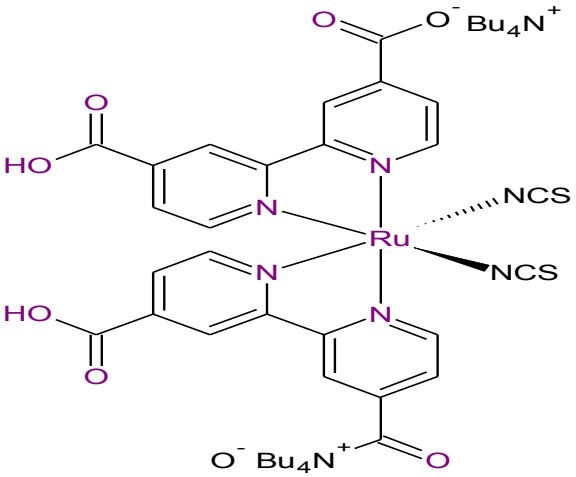

Figure 2.3*The structure of the Ruthenium 535 bis TBA or N719 Dye*(Athanasius J. *et al.*, 2012).

In ruthenium-based nanocrystalline dye-sensitized solar cells, the dye exists in two redox states (Ru^{2+} and Ru^{3+}). Therefore, Ru^{2+} has six d-electrons, Ru^{3+} has five d-electrons whereas the neutral ruthenium (Ru4d) consists of eight d-electrons. The highest occupied molecular orbitals (HOMOs) are mainly of ruthenium and thiocyanate (Ru-NCS) character and the lowest unoccupied molecular orbitals (LUMOs) are mainly of dicarboxybipyridine (dcbpy) character. When the dye is adsorbed onto the TiO_2 film there are two absorption maxima in the visible wavelength region (400nm and 550nm), because of the metal to ligand charge transfer (MLCT) transitions, in which an electron that is mainly on the Ru-NCS centre initially is transferred to the orbital set on the dcbpy ligands(Chen, 2008).

2.1.4 ELECTROLYTES

The electrolyte is found in the region between the working electrode and the platinized counter electrode of the dye-sensitized solar cell. It consists of iodide (I^-) and triiodide (I_3^-) that serves as a redox couple in a solvent which is either acetonitrile or propionitrile. In order for the electrolyte to penetrate the nanostructured system, it should have high conductivity. Other substances (referred to as additives) are also added so as to improve the properties of the electrolyte as well as the performance of the operating dye solar cell.An electrolyte is a chemical system that provides an electrolytic contact between the solar cell electrodes, and may exist in solid, liquid or solution form. The electrolytes usually employed in photoelectrochemical solar cells are based on salts dissolved in organic solvents, since the dye degenerates in the presence of water. For long-term operation these organic liquid-based electrolytes display many stability problems due to solvent evaporation, sensitivity to air and water, as well as elevated temperatures. The nc-DSC is a photoelectrochemical solar cell that requires a suitable electrolyte containing an adapted and electrochemically suitable redox couple. The iodide/triiodide redox couple (I^-/I_3^-) has given the best overall results so far(Yu, 2012).

The most suitable mediator known so far, to be used in dye-sensitized solar cells, consists of the iodide/triiodide redox couple (I^-/I_3^-). The mediator is active in the transfer of electrons from the external circuit, where triiodide ions are reduced to iodide ions at the counter electrode; a reaction catalyzed by a layer of platinum. After the injection of photo-excited electrons into the semiconductor, the oxidized dye is regenerated by iodide ions, which in the process are then converted back to triiodide ions. Iodide ions and triiodide ions are thus consumed at the working

electrode (the anode) and the counter electrode (the cathode), respectively. In the redox couple (I^-/I_3^-) there is a reduced state and oxidized state in the electron transfer reactions. The redox couple does not react (inert) with the other components of the dye solar cell and is highly reversible to facilitate the quick electron transfer kinetics. The reduced and the oxidized forms of the couple should be highly stable in order for the cell to have long operating life(Feldt, 2012).

The solvent contains the hydrogen bond and which assists to avoid photochemical degradation in the dye molecule, in particular. The thiocyanate ligand is sensitive to the ambient andUV-radiation i.e. due to an exchange reaction of this ligand with water molecules. Since the thiocyanate ligand is responsible for the electron uptake for re-reduction, this degradation can corrupt the performance of the cell. Also, water as a solvent for the redox couple causes an undesirable blue shift of the dye, which narrows the spectrum of absorbed incident light. A desired property of the solvent is a low viscosity, which facilitates high ion mobility. Overall the solvent should provide an inert environment for the redox couple to stabilize the electrolyte in harsh conditions like high thermal and UV input due to sunlight irradiation.

The electrolyte has to match a couple of requirements and as a basic prerequisite the electronic alignment of the redox couple relative to the dye must allow a re-reduction of the dye by means of electron donation from the reduced iodide ion (I^-). The more negative the redox potential of the mediator is, the larger the thermodynamic driving force of this re-reduction process. In addition, a lot more conditions have to be fulfilled which are as follows:

- The redox couple ions have to be soluble in the used solvent;
- The redox system must possess a high reversibility of involved charge transfer reactions;
- A high diffusion coefficient for a fast ion transport is highly demanded;
- A high stability of the reduced (I^-) and the oxidized (I_3^-) state within the solvent is also very important;
- To avoid loss of incident light, the electrolyte should not absorb light in the visible region;
- In order to prevent undesired side reactions a high resistance of the electrolyte against ambient conditions is necessary.

Drying up of the electrolyte is the main issue concerning long-term stability of the cell. Therefore many efforts have been attempted to get rid of the liquid electrolyte and despite the high viscosity of the liquid crystalline electrolyte, the I^-/I_3^- redox couple moves within ion conducting layers of the smectic phase formed by the cations. However, DSSCs employing liquid electrolytes overall still yield higher efficiencies than highly viscous electrolytes or solid hole conductors.

2.1.5 COUNTER ELECTRODE

The major role of the counter electrode is the reduction of triiodide to iodide. An amount of platinum has to be deposited on the electrode so as to catalyze the reaction, because if the SnO_2:F (FTO) layer is bare, its reduction is rather poor.

The performance of electrodes in an electron transfer process is measured by the charge transfer resistance. Therefore, the charge transfer resistance of a platinized counter electrode is normally far too low compared to the resistance of the plain electrode.

2.2 THE STRUCTURE AND OPERATING PRINCIPLE OF THE DSSC

The generative working cycle of the dye-sensitized solar cells, that schematically shows the relative energy levels of a working DSSC (Halme, 2002)is shown in Figure 2.4.

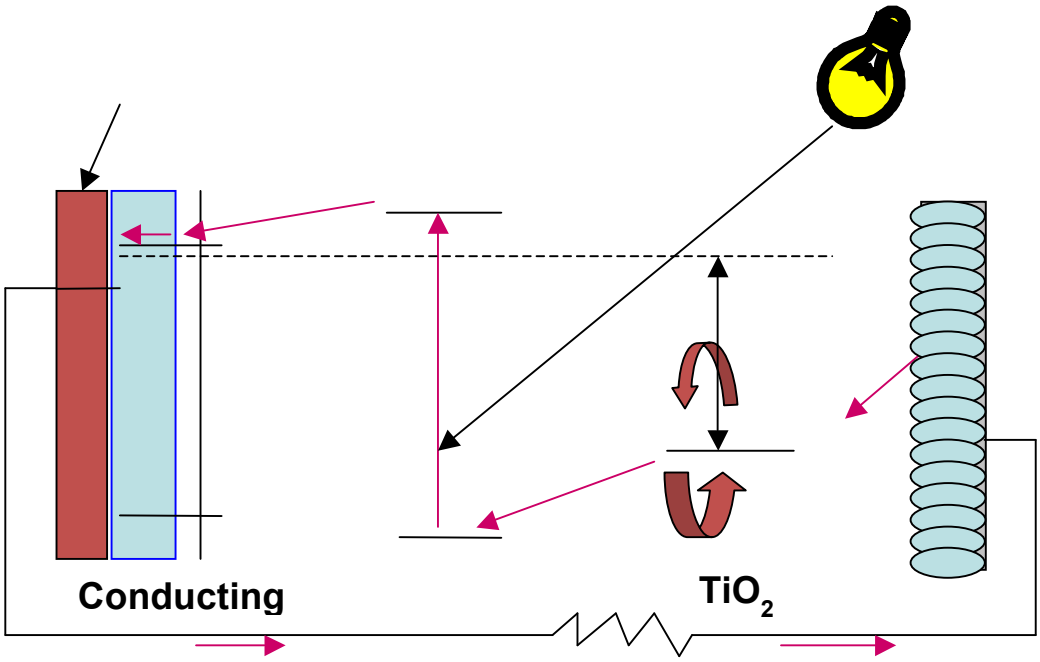

Figure 2.4 *The schematic diagram of a complete dye-sensitized solar cell (*Sokolsky, et. al. 2010).

1. The incoming photon is absorbed by the dye molecule adsorbed on the surface on the nano-crystalline TiO_2 particle and an electron from a molecular ground state S^o is excited to ahigher lying excited stateS*. This initial charge separation is a driven phenomenon called photo-excitation:

$$S^o + h\nu \rightarrow S^* \qquad \text{Photon Absorption} \qquad (1)$$

2. The excited electron is injected to the conduction band of the TiO_2 particle leaving the dyemolecule to oxidized state S^+. This jump or electron injection occurs very rapidly in a femto-second time regime, and it occurs through the carboxylate-titanium linkage:

$$S^* \rightarrow S^+ + e^- (TiO_2) \qquad \text{Electron Injection} \qquad (2)$$

3. The original state of the dye S^o is restored by the donation of an electron usually from iodide inthe electrode, this occurs in nanosecond regime. Therefore, from the HOMO level of the dye, the remaining hole is captured by the reduced iodide ions (I^-) of the redox couple resulting in re-reduction of the oxidized sensitizer:

$$S^+ + e^- \rightarrow S^o \qquad \text{Sensitizer Restoration} \qquad (3)$$

4. The injected electron percolates through the porous nanocrystalline structure of TiO_2 to thetransparent conducting oxide layer of the glass substrate (negative electrode, anode) and finally through an external load to the counter-electrode (positive electrode, cathode). Uponthis oxidation, triiodide ions (I_3^-) are formed which carry a positive charge to the counter electrode:

$$3I^- - 2e^- (Pt) \rightarrow I_3^- \qquad \text{Charge Percolation} \qquad (4)$$

5. At the counter-electrode the electrode is transferred to triiodide in the electrolyte to yieldiodine and when the triiodide is reduced, the iodide is regenerated and the cycle is closed by reduction of the oxidized dye iodine in the electrolyte:

$$I^-_3 + 2e^- (Pt) \rightarrow 3I^- \quad (5)$$

On the contrary, there is a "down-hill path" for an electron or "back-electron transfer" in the complete circuit from:

(i) The energy levels of the excited state of the dye S* to the ground state of the dye S which occurs in nanosecond to millisecond time regime,

(ii) The TiO_2 conduction band (CB) edge to the oxidized dye S* and it is strongly dependant on applied potential, light intensity and electrolyte and the conduction band electrons to the redox couple of the electrolyte I^-/I_3^-, this occurs in millisecond time regime.

2.3 SEMICONDUCTOR/DYE/ELECTROLYTE INTERFACE

When two phases that have varying electrochemical potentials are brought into contact, they tend to equilibrate by exchanging charges, whereby electrons from the substrate with highest level until $E_F \equiv E_{redox}$ to form charged electrochemical double layers. The three charged layers that appear at the semiconductor/dye/electrolyte are the space-charge double layer, a Helmholtz double layer and the Gouy-Chapman double layer. They lead to electrical double layers which consist of layers of positive charge, layers of negative charge, and regions of high electric field. These double layers govern the control of both electrical and chemical properties.

The space-charge charge double layer is the charged region between the bulk and the surface of the semiconductor. The space charge comes in various forms, such as immobile charged impurities near the surface of the semiconductor or as immobile trapped carriers, or can be in the form of mobile electrons or holes in the conduction or valence bands of the semiconductor. If majority carriers are extracted in moderate amounts, the surface region is assumed to be depleted of mobile carriers, because the surface region is completely ionized. A depletion layer is formed and the space charge (Q_{SC}) is the immobile charge of ionized donors. The density of a charge is usually assumed to be constant in the space charge region. The excess charge can be distributed over a considerable distance below the interface (X_{SC}).

The Helmholtz double layer results from two planes of charge, whereby one plane is due to charges at the surface of the solid and the other plane is due to ions in solution attracted by the charged surface. The charge occurs in three forms, such as an accumulation of free charge, free charge trapped from the solid onto surface states, or adsorbed ions. One layer of adsorbed solution species at the solid surface is usually called the Inner Helmholtz Plane (IHP). The solvated ions can only approach the solid to a distance (X_{OH}) and the locus of centres of these nearest solvated ions is called the Outer Helmholtz Plane (OHP).The possibility of storing charge in Helmholtz planes is related to the electrical capacitance.

The Gouy-Chapman double layer describes a region in the solution near the electrode in which there is a space charge due to an excess of free ions of one sign. The ions attracted to the Outer Helmholtz Plane are not sufficient to compensate all the charges on the electrode and the residual electric results in a charged Gouy-Chapman (diffusive) double layer. The thickness of the diffuse layer (X_D) is dependent on the total ionic concentration in the solution. If the solution is

concentrated, the layer becomes extremely thin and can be melted into the Outer Helmholtz Plane. The excess charge in the diffuse layer is (Q_D) and the total excess charge (Q_E) on the electrolyte side of the double layer is in the form $Q_E = Q_H + Q_D = -Q_{SC}$(Agrell H.G., 2003).

2.4 INTERFACE-INTERACTIONS IN DYE-SENSITIZED SOLAR CELL OPERATION

The dye-sensitized solar cell is composed mainly of the semiconductor, the dye that is a transition metal compound and the electrolyte. This is a quick review on the these components starting with general semiconductors that have the band structure, the energetic distribution of electrons, the perturbation of the electronic structure of semiconductors and the carrier transport that occurs on the semiconductors.

2.4.1 LIGHT ABSORPTION

A DSSC is able to acquire high efficiency only if there is a collective effect of numerous well-tuned physical-chemical nanoscale properties and the key principle is that there has to be a large band-gap semiconductor electrodes. To achieve this, the porous TiO_2 electrode must be coated on its internal surfaces with special dye molecules so as to absorb the incoming photons. There are three efficient photosensitizers for DSSCs that are appropriate for this research i.e. the Ruthenium 505 dye, Ruthenium 535 or N3 dye and the Ruthenium bis TBAor N719 dye.The dye is adsorbed to the semiconductor surface through the special anchoring groups that are attached to the dye molecule. These anchoring groups are the carboxylic groups (COOH) that are

found at the end of the pyridyl rings. At the surface of the TiO_2, the carboxylic group donates an electron to the TiO_2 lattice. The transfer of a charge between a dye molecule and the TiO_2 lattice occurs in three processes which are: (i) Metal to Ligand Charge Transfer (MLCT) excitation, (ii) Electron Injectionand (iii) Charge Recombination (Wang, *et al*., 2004).

A photon is absorbed by the dye molecule via the Metal to Ligand Charge Transfer excitation between the electronic states of the molecule. In the case of the N3 dye, in the visible region, there are two absorption maxima which are 380 nm and 518 nm. The excitation of the Ruthenium complexes via the absorption of a photon is of the MLCT type. Therefore, the Highest Occupied Molecular Orbital (HOMO) of the dye is situated near the central (ruthenium) metal atom (ruthenium) whereas the Lowest Unoccupied Molecular Orbital (LUMO) is situated at the ligand species (bipyridyl rings). During the process of MLCT excitation, an electron is transferred from the HOMO level to the LUMO level, from the LUMO level the electron is further transferred to the (carboxylic) COOH anchoring group that is close to the surface of the TiO_2 film. Ultimately, there is significant overlap between the electron wave-functions of the LUMO level of the dye and the conduction band of the TiO_2. This form of excitation is one of the reasons for the fast electron transfer process at the Dye-TiO_2 interface (Hara, *et al.*, 2003).

For efficient spectral sensitization, the spectral response of Induced Photon to Current Efficiency (IPCE) of Dye-sensitized Solar Cell for different dyes is compared with the spectral response of bare TiO_2 electrode and the ideal IPCE curve for a single band-gap device. Looking at the photon to current efficiency curves, the actual sensitization effect can be seen as a shift of the IPCE curve of the naked TiO_2 to the higher wavelengths when it is coated with the dye. The height of

the IPCE curve is related to the current efficiency of the dye-sensitized solar cell, which depends on the charge separation andcharge collection efficiencies (Moom, 2011).

2.4.2 CHARGE SEPARATION

The separation of charges in dye-sensitized solar cells is based on an electron transfer process from the dye molecule to the TiO_2 film, and a whole transport process from the thereby oxidized dye to the electrolyte. The electron transfer mechanism is strongly dependant on the electronic structure of the adsorbed dye molecule and the energy level matching between the excited state of the dye and the conduction band of the TiO_2.The charge separation at the DSSC in a nanoparticle electrode-electrolyte interface, which is quite different from the charge separation in the semiconductor p-n junction, arises from the electric field in the space-charge layer in the junction layer. The individual particle size in the nanostructured electrode is too small for the formation of a space charge layer inside the particle. Moreover, there are no significant macroscopic electric fields present between the individual nanoparticles in the bulk of the electrode. Therefore, the absence of band bending is a result of the individuality of each nanocrystalline particle. If the film behaved as an ensemble, then a thick nanoparticle film could have a collective space charge. However, in the vicinity around the electrolyte all the particles decouple the particles and screens any existing electric field within about a nanometer(Agrell, 2003).

There is an electric field at the semiconductor-electrolyte interface due to the dye molecules adsorbed while the band bending inside the particles is inhibited. Since the dye molecules have

carboxylic groups (COOH) that are attachment groups, a proton (H^+) is released to the oxide surface and the dye molecule becomes negatively charged. Consequently, a Helmholtz's layer is formed with a potential difference of approximately 0.3 eV that will help to separate charges and to reduce recombination.The main mechanism for the separation of a charge is all about energy level positioning between the dye molecule and the nanoparticle. The HOMO level (ground state) of the dye is less than the chemical potential of the redox pair iodide/triiodide in the electrolyte and the LUMO level (excited state) of the dye is above the conduction band edge of the TiO_2 and they both present an energetic driving force for the electron and hole separation. Furthermore, entropic factors arise due to the addition of the favorable energetics for charge separation. The electron injection to the TiO_2 conduction band is associated with the entropy increase that presents a driving force of approximately 0.1 eV for the charge separation, because the large density of delocalized states in the nanoparticle compared to small number of dye molecules on the particle surface (Agrell, 2003).

2.4.3 CHARGE TRANSPORT

The transportation of a charge in dye-sensitized solar cells occurs in two regions i.e. in the nanostructured TiO_2 electrode (electron transport) and in the electrolyte (hole transport) as I_3^-. Both of these charge transport mechanisms are equally significant for the operation of the cell, but recently electron transport has attracted an intensive study due several interesting fundamental questions concerning it.The semiconductor nanoparticle functions as a large surface area substrate for the dye-molecule and also as a transport medium for the electrons injected from the dye-molecules. The nature of the highly efficient electron transport in the dye-sensitized

electrode is particularly intriguing and has puzzled researchers ever since the invention of the dye-sensitized solar cell. The electrode can be viewed as a network of individual particles through which electrons percolate by jumping from one particle to the next, because of the porous structure of the electrode and the screening effect of the electrolyte (Haque, *et al*,2005).

The diffusion of electrons is characterized by the distribution of diffusion coefficients that has been related to the jumping of electrons via surface traps of different depths. These electron traps are localized energy states that are situated below the conduction band edge of the TiO_2 and they play a major role in the electron transport. The trapping of electrons in the bulk states does not lead to recombination losses due to the majority carrier nature of the TiO_2 electrode. However, the trapping of electrons at the TiO_2 surface may be a pathway for recombination that results in photocurrent losses and also photovoltage losses for kinetic reasons. Furthermore, the trap states lead to a lower quasi-Fermi level for the electrons under illumination and thus to a reduced photovoltage. The diffusion coefficient of electrons depends on the electron quasi-Fermi level under illumination. Only deep traps participate in the electron transport, causing a low diffusion coefficient at low light conditions. The deep traps are filled at steady state conditions as the increased light intensity raises the electron quasi-Fermi level, whereas the shallow traps contribute to the electron motion and all of that results in a larger diffusion coefficient. When the illumination level is increased, then the conductivity of the TiO_2 electrode is increased by filling the trap states (Labat, *et al.*, 2011).

The motion of the electrons in the semiconductor is coupled to the species in the electrolyte at the semiconductor-electrolyte interface. The screening by the electrolyte keeps the electrons

near the particle surface, consequently with the picture of the electron transport via the surface electron traps. The electron, together with its screening charge in the electrolyte side of the particle surface, can be viewed as a polaron moving by electron diffusion towards the back contact where the electron is subsequently separated. The organic solvent serves as an electrolyte in the dye-sensitized solar cells and contains the redox pair I^-/I_3^- that works as a hole-conducting medium. At the TiO_2 electrode, the oxidized dye, which is the one left behind by the electron injected to the TiO_2, is regenerated by I^- in the electrolyte (Gratzel,*et al*., 1991)Hence we have the reaction equation:

$$2S + 3I^- \rightarrow 2S + I_3^- \quad (1)$$

whereas, at the counter-electrode, I_3^- is reduced to I^- as:

$$I_3^- + 2e^-(Pt) \rightarrow 3I^- \quad (2)$$

Therefore, the triiodide ion is produced at the TiO_2 electrode and is consumed at the counter-electrode and thus diffused across the electrolyte correspondingly, and that is the reason triiodide is often labeled as the hole carrier to draw similarities with the conventional p-n junction solar cells. The same applies to the iodide, because it is produced at the counter-electrode and diffused to the opposite direction in the electrolyte. The redox electrolyte chemistry appears to be a more or less standard and established area of chemistry, or at least it is only rarely discussed in much more detail than this in conjunction with dye-sensitized solar cell research. Nevertheless, the simplest way of dealing with the electrolyte might be to think of it as an essential neutral sink of $I^-$and I_3^- feeding reactions (1) and (2) at the electrodes and maintaining the redox potential in the bulk of the electrolyte via the fast redox reaction of the I^-/I_3^- pair(Cahen, 2000).

2.4.4 RECOMBINATION

Recombination of the generated electrons with holes in the dye-sensitized nanostructured TiO_2 electrode can occur either after the electron injection or during its migration in the TiO_2 electrode on its way to the electrical back contact. When the dye-sensitized electrode is initially illuminated in the dark (at equilibrium) a transient electric field is generated between the injected electrons in the TiO_2 and the oxidized species in the electrolyte. This electric field could both oppose the further charge separation and promote the recombination process. However, in the dye-sensitized solar cell the mobile ions in the electrolyte can easily rearrange and effectively screen the light induced opposing fields and steady state conditions throughout the electrode film, and thus enable an efficient charge separation(Haque, *et al.*,2005).

A semiconductor material of high crystal purity is required, because in the silicon solar cells the recombination of charge carriers in trap states in surfaces, grain boundaries, and in bulk degrades the cell performance very easily. However, in the dye-sensitized TiO_2 electrode, there is a vast amount of particle boundaries and a huge surface to volume ratio. Yet the dye solar cell does not seem to suffer from the recombination losses at the grain boundaries at all due to the fact that only electrons are transported through the semiconductor particles, while holes (oxidized ions) are carried by the electrolyte. In other words, the dye cell works as a majority carrier device, similar to the metal-semiconductor junction, which is a Schottky Diode (Huang, *et al*., 1997).

The recombination process occurs mostly by the loss of electron to an oxidized dye molecule or to a hole in the electrolyte (i.e. the oxidized triiodide) in the absence of holes in the

semiconductor particles. The recombination process occurs mostly by the loss of an electron to an oxidized dye molecule. The assumption of most electrical models of the cell is that the former recombination process is negligible, but there is a possibility that it may be important in near open circuit conditions, where there is the accumulation of electrons into the TiO_2 particles(Daeneke, et al., 2012). The latter recombination pathway, on the other hand, is made inefficient by the reaction kinetic reasons and then the net recombination reaction at the TiO_2-Electrolyte interface is a two electron reaction as follows:

$I_3^- + 2e^- \rightarrow 3I^-$, which is made-up of the following sub-reactions (1)

$I_3^- \leftrightarrow I_2 + I^-$ (2)

$2I_2^- \rightarrow I_3^- + I^-$ (3)

Equation (2) shows that the actual electron acceptor in the recombination reaction is I_2 and the final reaction [equation (3)] is a slow dismutation reaction and rate limiting in the net recombination reaction. The conducting glass substrate may be partly exposed to the electrolyte, setting up a potential recombination pathway between the electrons in the conducting substrate and hole carriers in the electrolyte, because of the porous structure of the electrode. However, due to low electro-catalytic activity of Platinum-free SnO_2:F surface for the iodine/triiodide redox system, there is experimental evidence that this effect is insignificant (Lobato, *et al*., 2009).

2.4.5 INTERFACIAL KINETICS

The dye-sensitized solar cell is based on photo-electrochemical reactions at the semiconductor-electrolyte interface and the operation of the cell is therefore an outcome of competing opposite chemical reactions having different rate constants. Fast wanted reactions with high rate constants are responsible for the accomplishment of the desired direction for the electrochemical reactions, as well as the slow unwanted reactions with low rate constants. Thus, the greater the difference between the rate constants, the higher the efficiency of the system.(Bisquert, *et al*.,2006).

On the kinetics of the dye-sensitized solar cell, the desired reaction is through the electron injection from the dye molecule (HOMO level) to the conduction band of the TiO_2 (LUMO level) in a range of 50 femtoseconds to 1.7 picoseconds. This desired reaction exceeds any unwanted reaction in an order of magnitude or more. This electron injection process between the N3 dye and the TiO_2 in the dye-sensitized solar is one of the fastest chemical processes known. The relaxation of the excited state occurs in 60 nanoseconds. The other desirable reaction is a very fast reaction that occurs in 10 nanoseconds when the dye is regenerated by the iodide (I^-) at normal conditions in the dye-sensitized solar cell. This process is important for obtaining a high life cycle for the dye, because if there is a deficiency of adequate conditions for the regeneration process, then there can be dye degradation. Recombination of the electron in the TiO_2 conduction band with a hole triiodide (I_3^-) in the electrolyte occurs and this electron percolation through the nanostructured TiO_2 has been estimated to occur in the millisecond to second range (Tolvanen, 2003).

CHAPTER 3

RESEARCH METHODOLOGY

3.1 PREPARATION OF THE COMPONENTS OF DSSC

Thischapter deals with the materials and the engineering behind the dye solar cells. The standard DSSC consists of electrodes that are prepared onto the transparent conducting oxide (TCO) coated glass substrates. The substrate material has two functions, which are to hold up the structure of the cell and to close up the layer that is between the cell and the ambient air. Furthermore, the conducting coating of the substrate collects current. The most frequently used transparent conducting oxide in thin film solar cells is fluorine-doped tin oxide (SnO_2:F), since it is stable even at high temperatures.

The choice of sheet resistance of the tin oxide-coated glass plates is a compromise between the contradictory valuable properties of the TCO-coated glass, such that when the transmittance is high then the conductance is low and vice versa. Dyesol (Pty) Ltd has optimized the performance of the cells by using TEC 15 (15 Ω/sq) for high transmittance in the working electrode (semiconductor) and TEC 8 (8 Ω/sq) for high conductance in the platinized counter electrode.

3.1.1 PREPARATION OF THE TEST PLATE

In a ventilated fume-cupboard, 6g of colloidal Degussa P25 TiO_2 and 10 mL of nitric acid were added together by incrementally adding nitric acid 1ml at a time, nine times, while grinding in mortar and pestle. 1mL addition of dilute acid solution was done only after the previous mixing created a uniform and a lump-free paste. The process took about 30 minutes and was later allowed to equilibrate at room temperature, for 15 minutes. The other titanium dioxide paste was Ti-Nanoxide D/SP, which was purchased from Solaronix (Ltd) in Switzerland, and was doctor-bladed on tin oxide-coated glass plates.

3.1.2 DEPOSITION OF THE TEST PASTE

Latex gloves were used to handle the transparent conducting oxide (TCO) glass to avoid fingerprint contamination of the glass substrate. Also, it should be noted that the hazy side, i.e. the one that feels "sticky" when passing gently with the fingernail, is the conducting side for the SnO_2 glasses.The 3M Scotch Magic tape from 3M was doubled to 6 μm and was used as an adhesive tape over the glass substrate. The thickness of the adhesive tape determines the thickness of the titanium oxide that is deposited on the glass. Also, the magic tape provides some consistency in the active cell area. This tape was easily removed from the glass without leaving traces of the adhesive materials. The nanocrystalline TiO_2 pastes were stirred well before use. During the deposition process the doctor-blading or squeegee technique was used, whereby the titanium oxide paste was deposited and spread out using a rigid glass rod.

Figure 3.1 shows the titanium dioxide coated on the glass substrate by the doctor-blading method.

Figure 3.1*The titanium oxide paste which is coated on a glass substrate*

The nanocrystalline titanium oxide paste on the electrode was allowed to dry gently until the solvent evaporated. When using the two layers of tape, it was imperative to note that there was no sign of peeling off of the TiO_2 film and no air-bubbles visible on the back side of the electrode. Therefore, a slow dry-out of the solvent and progressive heating was necessary to ensure optimal adhesion of the titanium oxide layer to the transparent conducting oxide glass.

3.1.3 SINTERING PROCESS

The sintering process is a process that allows the titanium oxide nanocrystals to dissolve partially together so as to ensure electrical contact and mechanical adhesion to the glass electrode. Promising results have been obtained when the TiO_2 film was heated to 450^oC for 30 minutes, using a furnace. When the sintering process was completed, there was an indication that the electrode first turned brownish and at times fumes were released. Later on, the electrode turned yellowish due to the narrowing of the band-gap that is temperature dependant in the pure

titanium oxide. To avoid the cracking of the glass electrode, an excellent cooling rate had to be considered i.e. by cooling down from 450^{o}C to 60-80^{o}C in three minutes. The other titanium dioxide films were prepared from commercial screen-printing paste by Dye-sol (Ltd).

3.1.4 SENSITIZER IMPREGNATION

After sintering, the TiO_2 film was ready to be dyed. The sintered electrode was allowed to cool to 100^{o}C and it was slowly and gently immersed into the dye solution so as to avoid the cracking of the glass. The impregnation process was done at room temperature for 5 to 10 hours. The duration of impregnation largely depends on the actual titanium oxide layer thickness. In order for the dyeing to be properly done, the electrode was impregnated overnight to avoid non-uniformity in the spread of the dye.

In dye-sensitized solar cells, dyes have a role of being sensitizers. The three sensitizers were prepared by dissolving 0.1 mg Ruthenium 505, Ruthenium 535 and Ruthenium 535 bis-TBA dyes with 500 ml of pure ethanol. The dye molecules were adhered to the nanostructured TiO_2 electrode by immersing the sintered electrode into a dye solution for 24 hours to fully impregnate the electrode. During the impregnation process the electrode is sensitive to water. To minimize the water vapor content inside the pores of the electrode, the electrode should be warm upon immersion to the dye solution.

The water was not allowed to enter the dye solution and also not permitted to be in contact with the electrodes, because the condensed water blocks the dye solution from reaching all parts of the

film thus reducing dye adsorption. Furthermore, the effect of water is magnified by a strong capillary effect of the nanopores. After the dyeing process, the dyed electrodes were stored in a closed container.

3.1.5 PLATINIZATION OF THE COUNTER ELECTRODE

The counter electrode is made up of anelectrically conducting glass plate and a thin layer of platinum, to catalyze the reduction reaction triiodide. There are many methods of producing platinized counter electrodes, but in this study the platinum catalyst was obtained by using the Pt-Catalyst T/SP that was purchased from Solaronix in Switzerland. There were 5 to 6 drops of this invisible product that were distributed on the glass by squeegee printing, using a glass rod.

The thickness of the platinum depended on the thickness of the Scotch Magic tape, which was attached on the edges of the glass plates. The platinum catalyst was dried at 100^{o}C before heating to 400^{o}C for 30 minutes. The temperature was carefully monitored, for it not to rise and exceed 400^{o}C, because the charge transfer resistance of the platinized counter electrode would rise steeply. When platinum is deposited it is practically invisible, but its absence in the counter electrode dye solar cell will cause malfunctioning.

3.1.6 TYPES OF ELECTROLYTES USED

The main purpose for using an electrolyte in a dye-sensitized solar cell is to transfer electrons between the TiO_2 electrode and the counter electrode through the I^-/I_3^- redox couple.

Current in liquid electrolytes is carried by ions which are formed by the dissociation of salts in polar solvents. There are two types of charge carriers i.e. holes and electrons (positively and negatively charged ions) that are present in equal concentrations in the electrolyte. The electrolyte in the dye-sensitized solar cell consists of a redox couple dissolved in an organic solvent. Redox couples are characterized by molecules or ions (in solution) which can be in a reduced state (Red) and an oxidized state (Ox) in electron transfer reactions.

There are three types of electrolytes which have been tested for this research purchased from Solaronix namely: Iodolyte PN–50, Iodolyte AN–50 and Iodolyte Z–150. The Iodolyte PN–50is an iodide based low viscosity electrolyte with 50 mM of tri-iodide dissolved in a solvent called propionitrile (PN). This electrolyte is intended for high performance cells and it has a low boiling point of ≈ 100^{o}C. Additives which are found on this electrolyte include an ionic liquid, as well as pyridine a derivative.

The Iodolyte AN–50 is an iodide based low viscosity electrolyte with 50 mM of tri-iodide dissolved in a solvent called acetonitrile (AN). This electrolyte is intended for high performance cells and it has a low boiling point of ≈ 80^{o}C. Additives which are found on this electrolyte include an ionic liquid, lithium salt as well as a pyridine derivative.

The Iodolyte Z–150 is an iodide based low viscosity electrolyte with 150 mM of tri-iodide dissolved in a solvent called 3-methoxypropionitrile (MPN). This electrolyte is intended for high performance cells and temperature stable cells due to its boiling point ≈ 160^{o}C. Additives which are found on this electrolyte include an ionic liquid, alkylbenziimidazole and guanidine thiocyanate.

The propionitrile and methoxypropionitrile solvents found on these electrolytes are known to be non-toxic. Acetonitrile is hazardous in nature and can cause cyanide poisoning. Acetonitrile is less viscous in nature than methoxypropionitrile and propionitrile solvents, therefore its capillary forces are stronger than the other solvents and this electrolyte fills the cells quickly, which makes filling more difficult [Yu Z., (2012)].

3.2 CONSTRUCTION AND ASSEMBLY OF THE DSSCs

The dye-sensitized solar cell has to be assembled as soon as the electrodes have been prepared, because long storage of electrodes is harmful to the solar cell. The two electrodes, i.e. working electrode (dyed TiO_2)and the counter electrode that is coated with platinum, were attached together with the Hermetic Sealant along the edges. The role of the sealant was to prevent the electrolyte from entering the cell, as water can have a degrading effect on the cell components. Through a tiny hole, three drops of the electrolyte was injected into the cell. The function of the electrolyte is to transfer electrons between the TiO_2 electrode and the counter electrode through the redox couple (I^-/I_3^-).

Figure 3.2 presents assembled dye-sensitized solar cells made up the doctor-bladed Ti – nanoxide D/SP film which were not properly sealed and ended drying up due to the high vapor pressure of the electrolyte.

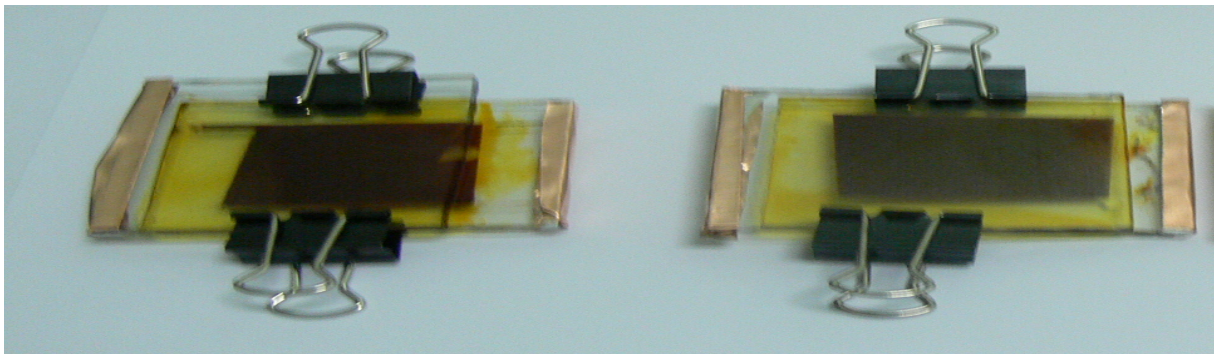

Figure 3.2: *Assembled dye-sensitized solar cells of the doctor-bladed Ti – nanoxide D/SP film*

Figure 3.3 presentsthree assembled electrochemical cells made up of the Ruthenium 505 dye combined with Z – 150 electrolyte that contains methoxypropionitrile solvent in (a) or Cell 25, Ruthenium 505 dyecombined with AN – 50 electrolyte that contains acetonitrile solvent in (b) or Cell 27 and Ruthenium 505 dye combined with PN – 50 electrolyte that contains propionitrile solvent in (c) or Cell 22 on commercially screen-printed TiO_2 films.

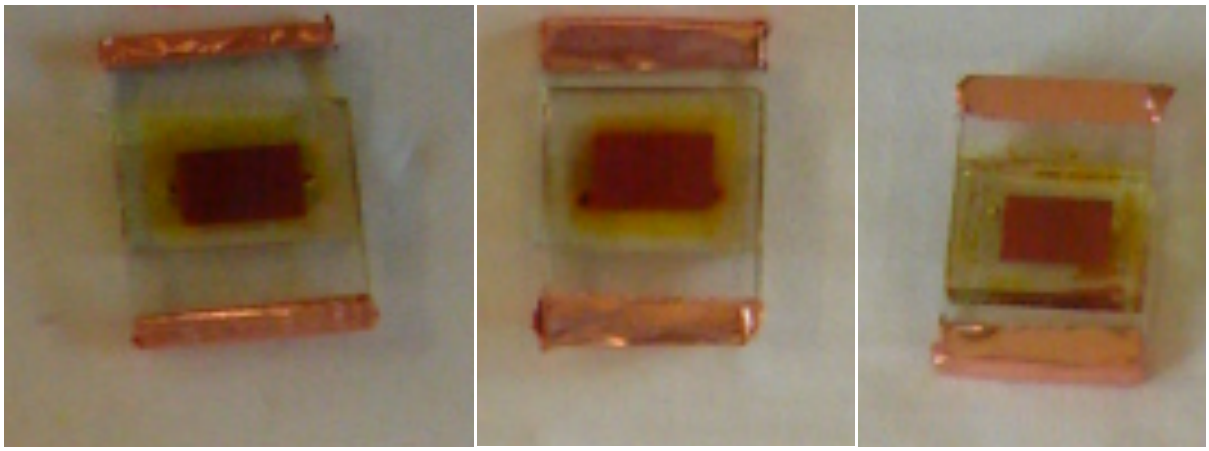

(a) (b) (c)

Figure 3.3*:Assembled cells made up of the Ruthenium 505 dye combined with Z – 150 electrolyte (Cell 25) (b) AN – 50 electrolyte (Cell 27) and (c) PN – 50 electrolyte (Cell 22).*

Figure 3.4 presents three assembled electrochemical cells made up of the Ruthenium 535 dye combined with Z – 150 electrolyte that contains methoxypropionitrile solvent in (a) or Cell 28, Ruthenium 535 dye combined with AN – 50 electrolyte that contains acetonitrile solvent in (b) or Cell 24 and Ruthenium 535 dye combined with PN – 50 electrolyte that contains propionitrile solvent in (c) or Cell 23 on commercially screen-printed TiO_2 films.

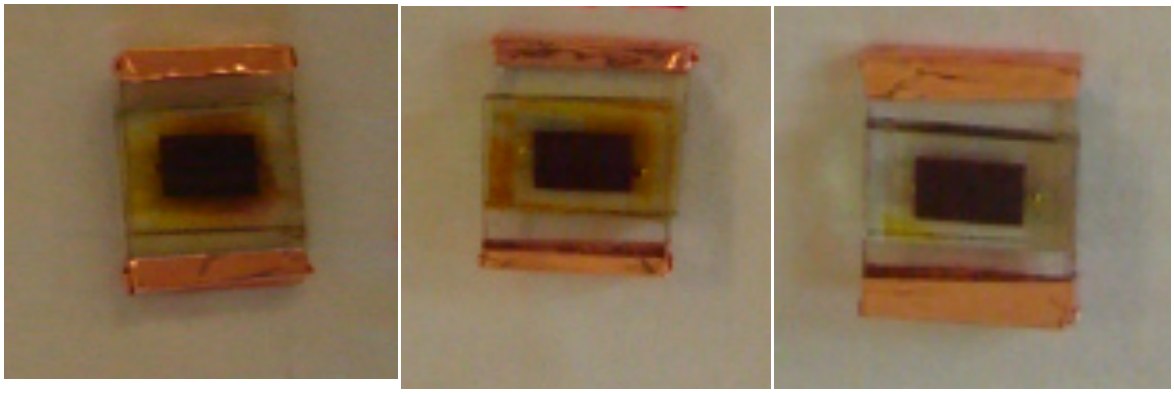

(a) (b) (c)

Figure 3.4:*Assembled cells made up of the Ruthenium 535 (N3) dye combined with (a) Z – 150 electrolyte (Cell 28) (b) AN – 50 electrolyte (Cell 24) and (c) PN –50 electrolyte (Cell 23).*

Figure 3.5illustrates three assembled electrochemical cells made up of the Ruthenium 535 bis-TBA (N719) dye combined with Z – 150 electrolyte that contains methoxypropionitrile solvent in (a) or Cell 17, Ruthenium 535 bis-TBA (N719) dye combined with AN – 50 electrolyte that contains acetonitrile solvent in (b) or Cell 26 and Ruthenium 535 bis-TBA (N719) dye combined with PN – 50 electrolyte that contains propionitrile solvent in (c) or Cell 21 on commercially screen-printed TiO_2 films.

(a) (b) (c)

Figure 3.5*: Assembled electrochemical cells made up of the Ruthenium 535 bis-TBA (N719) dye combined with (a) Z – 150 electrolyte (Cell 17) (b) AN – 50 electrolyte (Cell 26) and (c) PN – 50 electrolyte (Cell 21).*

The electrodes were placed a little off-centre to accommodate the electrical contacts. Prior testing, it was recommended to put silver paint onto the contact areas so as to ensure optimal electrical connections and to minimize serial resistance losses, especially when testing large cells. The working electrode (TiO_2) should never be connected to a positive terminal unless reverse bias occurs.

Figure 3.6 presents a typical constructed dye-sensitized solar cell that is properly sealed and electrically connected at room temperature conditions.

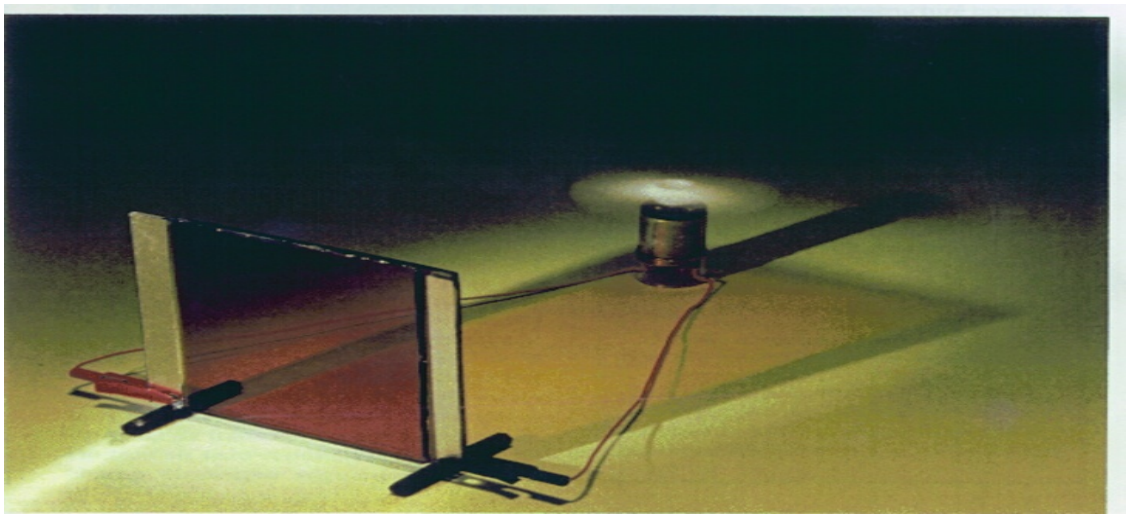

Figure 3.6: *A typical constructed dye-sensitized solar cell that is properly sealedand electrically connected.*

3.3 CHARACTERIZATION TECHNIQUES

3.3.1 SCANNING ELECTRON MICROSCOPE (SEM-EDX)

SEM provides detailed high resolution images and surface morphology of the sample by rastering a focussed electron beam across the surface and detecting secondary or backscattered electron signal. SEM provides high magnification images with rapid, high resolution imaging with identification of elements present. An Energy Dispersive X-Ray analyzer (EDX) is an analytical technique used for the elemental identification or chemical characterization and quantitative compositional information of a sample. It relies on the investigation of an interaction of some source of X-ray excitation and a sample. Its characterization capabilities are due in large part to the fundamental principle that each element has a unique atomic structure, allowing unique set of peaks on its X-ray spectrum. (Dykstra M. J., 1993)

The scanning electron microscope (SEM) is nearly always used in combination with an energy dispersive X-ray analyzer (EDX) and are combined into one unit (SEMEDX), greatly reducing the need for complex operations. There is a growing need to understand the composition and distribution of elements in addition to observing sample material shape. SEMEDX has been designed to allow smooth, easy operation of SEM image observation functions as well as easy EDX element analysis setup and execution. Also, in order to provide more accurate, rapid analysis, a recipe function has been added that makes it possible to simultaneously set and save optimum analysis conditions for both SEM and EDX parameters. The SEM and EDX with conventional systems are independent units. A sample is observed as an SEM image under optimal conditions for the SEM, and then the test sample position is repeatedly adjusted between the SEM and EDX to achieve maximum X-ray detection efficiency during EDX analysis.. The SEMEDX is an excellent example of the fusion of various device functions into one unit to create a whole that is greater than the sum of its parts. (Yurugi T., *et al*,(2001).

3.3.2 X-RAY DIFFRACTION (XRD)

X-ray diffraction (XRD) is a technique in crystallography in which the pattern produced by the diffraction of X-rays through the closely spaced lattice of atoms in a crystal is recorded and then analyzed to reveal the nature of that lattice. The information obtained includes types and nature of crystalline phases present, structural make-up of phases, degree of crystallinity, amount of amorphous content, micro-strain and size, and orientation of crystallites. This generally leads to an understanding of the material and molecular structure of a substance. The spacing in the

crystal lattice can be determined using Bragg's law. The electrons that surround the atoms, rather than the atomic nuclei themselves, are the entities which physically interact with the incoming X-ray photons (Connolly J. R., 2007).

These factors are combined in Bragg's Law, $n\lambda = 2d\sin\theta$, where n = an integer 1, 2, 3 etc wavelength in angstroms, d (d-spacing) is the interatomic spacing in angstroms; θ (theta) and the diffraction angle in degrees.

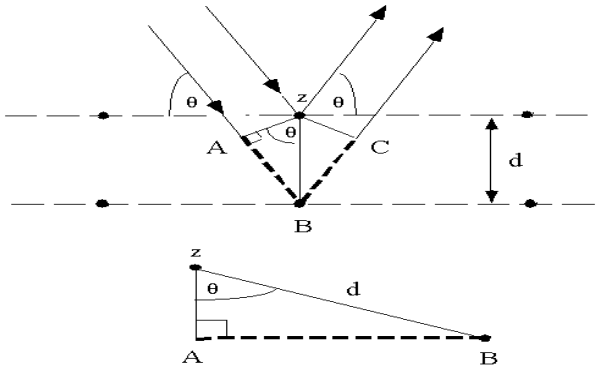

Figure 3.7: *Schematic diagrams of Braggs Law and Diffraction*(Miller F.P., et al, 2010)

Diffraction occurs as waves interact with a regular structure whose repeat distance is about the same as the wavelength. The phenomenon is common in the natural world, and occurs across a broad range of scales. For example, light can be diffracted by a grating having scribed lines spaced on the order of a few thousand angstroms, about the wavelength of light. It happens that X-rays have wavelengths on the order of a few angstroms, the same as typical inter-atomic distances in crystalline solids. That means X-rays can be diffracted from minerals which, by definition, are crystalline and have regularly repeating atomic structures. When certain geometric requirements are met, X-rays scattered from a crystalline solid can constructively interfere, producing a diffracted beam(Zhang S., *et al*., 2009).

3.3.3 ULTRA-VISIBLE SPECTROSCOPY (UV-VIS)

The ultraviolet-visible spectroscopy characterizes light in the ultraviolet and visible regions in terms of wavelength expressed in nanometers, whereby the human eye is only sensitive to a tiny proportion of the total electromagnetic spectrum between approximately 380 and 780 nm and within this area we perceive the colors of the rainbow from violet through to red. When white light falls upon a sample, the light may be totally reflected, in which case the substance appears white or the light may be totally absorbed, in which case the substance will appear black. A close relationship exists between the color of a substance and its electronic structure. A molecule or ion will exhibit absorption in the visible or ultraviolet region when radiation causes an electronic transition within its structure. Thus, the absorption of light by a sample in the ultraviolet or visible region is accompanied by a change in the electronic state of the molecules in the sample(Owen T., 1996).

The energy supplied by the light will promote electrons from their ground state orbitals to higher energy, excited state orbitals or antibonding orbitals. A transition in which a bonding s electron is excited to an antibonding σ orbital is referred to as σ to σ* transition. In the same way π to π* represents the transition of one electron of a lone pair (non-bonding electron pair) to an antibonding π orbital. Thus the following electronic transitions can occur by the absorption of ultraviolet and visible light: σ to σ*, n to σ* n to π* and π to π* molecular orbitals (Spectro-Educational Booklet, 2007), which were determined from the prepared cells.

Therefore, electronic transitions take place from highest occupied molecular orbital (HOMO) levels to lowest unoccupied molecular orbital (LUMO) levels. In dyes, the excitation involves the promotion of an electron from the metal centre to the π* of the ligand via Metal-to-Ligand Charge Transfer (MLCT). The absorption bands observed are due to electronic transitions from the ground state to excited state.

3.3.4 FOURIER TRANSFORM INFRARED RADIATION (FTIR)

Infrared spectroscopy is a technique based on the vibrations of the atoms of a molecule. An infrared spectrum is commonly obtained by passing infrared radiation through a sample and determining what fraction of the incident radiation is absorbed at a particular energy. The energy at which any peak in an absorption spectrum appears corresponds to the frequency of a vibration of a part of a sample molecule. In this introductory chapter, the basic ideas and definitions associated with infrared spectroscopy will be described. The vibrations of molecules will be looked at here, as these are crucial to the interpretation of infrared spectra. Infrared spectroscopy is certainly one of the most important analytical techniques available to today's scientists. One of the great advantages of infrared spectroscopy is that virtually any sample in virtually any state may be studied. Liquids, solutions, pastes, powders, films, and surfaces can all beexamined with a judicious choice of sampling technique. As a consequence of the improved instrumentation, a variety of new sensitive techniques have now been developed in order to examine formerly intractable samples(Stuart B., 2004).

Fourier Transform Infrared Radiation (FTIR) is most useful for identifying chemicals that are either organic or inorganic and is perhaps the most powerful tool for identifying types of chemical bonds (functional groups). Molecular bonds vibrate at various frequencies depending on the elements and the type of bonds. For any given bond, there are several specific frequencies at which it can vibrate. The interactions of infrared radiation with matter may be understood in terms of changes in molecular dipoles associated with vibrations and rotations. In order to begin with a basic model, a molecule can be looked upon as a system of masses joined by bonds with spring-like properties. Taking first the simple case of diatomic molecules, having three degrees of translational freedom and two degrees of rotational freedom. The atoms in the molecules can also move relative to one other, that is, bond lengths can vary or one atom can move out of its present plane. This is a description of stretching and bending movements that are collectively referred to as vibrations. For a diatomic molecule, only one vibration that corresponds to the stretching and compression of the bond is possible. This accounts for one degree of vibrational freedom (Gremlich, H.U.,*et al*., 2000).

The infrared (IR) region of the electromagnetic spectrum covers the range from just above the visible to approximately 10^{-4} m, but only the mid-portion from 2.5×10^{-6} m to 2.5×10^{-5} m is used by organic chemists to identify the functional groups present in a molecule. The full interpretation of an infrared spectrum is difficult, because most organic molecules are so large that they have dozens of different bond stretching and bending motions. Thus, an infrared spectrum contains dozens of absorptions. Nevertheless, this complexity is valuable, because an infrared spectrum serves as a unique fingerprint of a specific compound. The complex region of the infrared spectrum from 1500 cm^{-1} to around 400 cm^{-1} is called the fingerprint region. If two or more compounds have identical infrared spectra, they are almost identical. Fortunately, there

is no need to interpret an infrared spectrum fully to get useful structural information. Most functional groups have characteristic infrared absorption bands that do not change from one compound to another.

3.3.5 PHOTOLUMINESCENCE (PL)

Photoluminescence (PL) is the spontaneous emission of light from a material under optical excitation. The excitation energy and intensity are chosen to probe different regions and excitation concentrations in the sample. PL investigations can be used to characterize a variety of material parameters. PL spectroscopy provides electrical characterization, and it is a selective and extremely sensitive probe of discrete electronic states. The intensity of the PL signal provides information on the quality of surfaces and interfaces. Under pulsed excitation, the transient PL intensity yields the lifetime of non-equilibrium interface and bulk states(Hannewald K., *et al*., 2002).

When light of sufficient energy is incident on a material, photons are absorbed and electronic excitations are created. Eventually, these excitations relax and the electrons return to the ground state. If radiative relaxation occurs, the emitted light is called PL. This light can be collected and analyzed to yield a wealth of information about the photo-excited material. The PL spectrum provides the transition energies, which can be used to determine electronic energy levels. The PL intensity gives a measure of the relative rates of radiative and non-radiative recombination.

Variation of the PL intensity with external parameters like temperature and applied voltage can be used to characterize further the underlying electronic states and bands (Sauer M., *et al*., 2011).

3.3.6 ELECTROCHEMICAL IMPEDANCE SPECTROSCOPY (EIS)

Electrochemical impedance spectroscopy (EIS) is a useful tool to study complete DSSCs and the DSSC counter electrode and the redox electrolyte. The EIS is very important for the determination or obtaining parameters such as series resistance, charge transfer resistance at the counter electrode, diffusion resistance of the electrolyte, the resistance of electron transport and recombination in the TiO_2 matrix, and the chemical capacitance of the porous TiO_2 electrode. It is used to investigate electronic and ionic processes in dye-sensitized solar cells (DSC). Furthermore, it is a steady-state method measuring the current response to the application of an ac voltage as a function of the frequency.An important advantage of EIS over other techniques is the possibility of using tiny AC voltage amplitudes exerting a very small perturbation on the system. EIS has been widely employed to study the kinetics of electrochemical and photo-electrochemical processes including the elucidation of salient electronic and ionic processes occurring in the DSC.

The Nyquist diagram features typically three semicircles that in the order of increasing frequency are attributed to the Nernst diffusion within the electrolyte, the electron transfer at the oxide/electrolyte interface, and the redox reaction at the platinum counter electrode.However, owing to the complexity of the system, the unambiguous assignment of equivalent circuits and

the elucidation of processes occurring on dye-sensitized TiO_2 electrode is difficult and remains a topic of current debate. The present study employs EIS as a diagnostic tool for analyzing in particular photovoltaic performance changes detected during accelerated high-temperature durability tests on dye-sensitized solar cells. A theoretical model is presentedinterpreting the frequency response in terms of the fundamental electronic and ionic processes occurring in the photovoltaic device. From applying appropriate equivalent circuits, thetransport rate and lifetime of the electron in the film are derived and the values are checked by transient photocurrent and photovoltage measurements.(Barsoukov, *et al*., 2005)

The DSC contains three spatially separated interfaces formed by FTO/TiO_2, TiO_2/electrolyte, and electrolyte/Pt-FTO. Electron transfer is coupled to electronic and ionic transport. In the dark under forward bias electrons are injected in the conduction band of the nanoparticles and their motion is coupled to that of I^-/I_3^- ions in electrolyte. Illumination gives rise to new redox processes at the TiO_2/dye/electrolyte interface comprising sensitized electron injection, recombination with the parent dye, and regeneration of the sensitizer. During photovoltaic operation, this "internal current generator" drives all the electronic and ionic processes in the solar cell.

The concentration of triiodide is much lower thanthat of iodide and the latter is diffuses faster than the formerion. Hence, I^- contributes little to the overall diffusion impedance,which is determined by the motion of I_3^-. Nernst diffusion impedance in the Nyquist plot shows typically a straight line at higher frequency along with a semicircle at lower frequency. The charge-

transfer resistance R_{CT} associated with the heterogeneous electron exchange involving the I_3^-/I^- redox couple at the electrolyte/Pt-FTO interface is typically given for the equilibrium potential.

Normally the description of charge transfer over a metal/electrolyte interface, which is not determined by diffusion limitation in the electrolyte. It consists of exchange current density of the reaction, the frequency response of charge-transfer impedance under small sinusoidal perturbation with the double layer capacitance. The charge-transfer resistance manifests itself as a semicircle in the Nyquist diagram and a peak in the Bode phase angle plot. For electrodes having a rough surface the semicircle is flattened and the double-layer capacitance is replaced bya constant phase element (CPE) (Macdonald J.R, *et al*.,2005).

Under these conditions, the Nyquist plot shows a short straight line at higher frequencies due to diffusion and a large semicircle in the lower frequency regime, indicating fast electron transport and long lifetime of electron in the film. By contrast, if the electron collection efficiency is low, i.e., a major part of the electron reacts with I_3- in the electrolyte before they are recovered at the current collector, the condition *R*d. For a nanoporous electrode, the infinite transmission line is normally used as the equivalent circuit for modeling. For simplicity, only the representative elements displayed in Figure 3 are employed here to model DSC at different states.

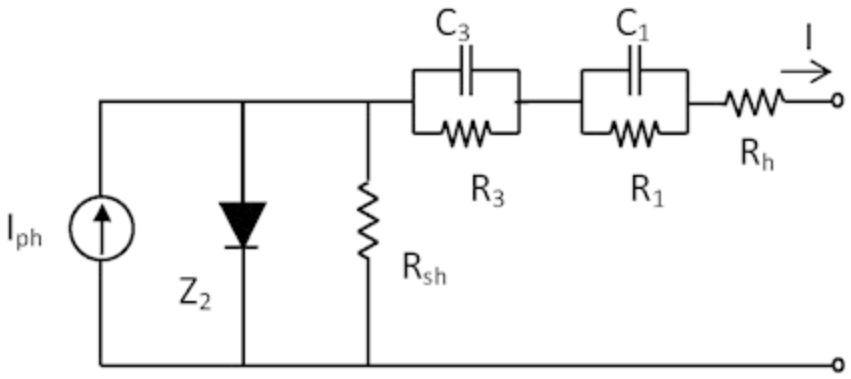

Figure 3.8*The equivalent circuit of a dye-sensitized solar cell (DSSC)* (Han L., *et al*., 2006).

The Nyquist plots of dye-sensitized solar cells are characterized by having three semi-circles which are in the increasing order of frequency (ranging from 10^{-1} Hz to 10^{6} Hz) range. These frequencies correspond to three types of impedances namely Z_1, Z_2 and Z_3. Impedance Z_1 is for the redox reaction which is related to charge-transport at the Pt electrode in the high frequency (10^{6} – 10^{3} Hz) region. Impedance Z_2 is for the electron transfer which is observed in the middle frequency (100 Hz – 10 Hz) region at TiO_2/dye/interface. Impedance Z_3 is observed in a low frequency range (10 Hz – 0.1 Hz) due to an integrated viscosity and Nernst diffusion resistance within the electrolyte. Therefore, the actual dye-sensitized solar cell model consists of series resistance, shunt resistance and capacitive parts. Z is parallel combination of R_1 and C_1, Z_2 is parallel combination of R_2 and C_2, and Z_3 is parallel combination of R_3 and C_3. The real part of Z_1 is related to charge –transfer process occurring at the Pt counter electrode denoted by R_1 and the imaginary part C1 is capacitance of Helmholtz double layer at the electrodes. Similarly R_2, the real part of Z_2 corresponds to diode like behavior. Resistance R_3 of Z_3 is proportional to the distance between TCO and Pt counter electrode and is related to diffusion of iodide and trioxide within the electrolyte. The series resistance Rs can be written as$R_s=R_h+R_1+R_3$Where R_h is the sheet resistance of TCO glass substrate(Han L., *et al*., 2004).

CHAPTER 4

RESULTS AND DISCUSSION

4.1 PARTICLE AND SURFACE MORPHOLOGIES OF TITANIUM DIOXIDE FILMS

The particle and surface morphologies of the all titania pastes were studied by scanning electron microscopy using JEOL JSM – 6390 LV Scanning Electron Microscope which is linked to an Energy Dispersive X-ray Analyzer at an accelerating voltage of 15.0 kV and magnification of 8500 which was decreased from 250 µm, 50 µm, 10µm and 2.5 µm to investigate the surface area of the films.

Figure 4.1 (a – d) shows the titanium paste which was prepared from Degussa P25 powder and was coated on the glass substrate by the doctor-blading method to expose the unevenness as well as their roughness with evident lumps which would greatly affect charge transportation as well as the dye or sensitizer impregnation.

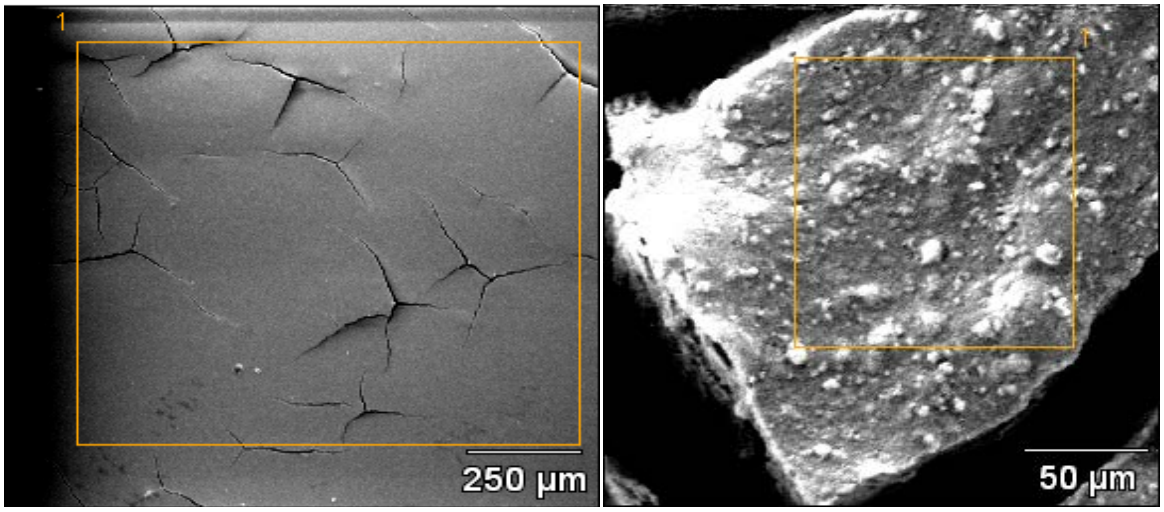

(a) (b)

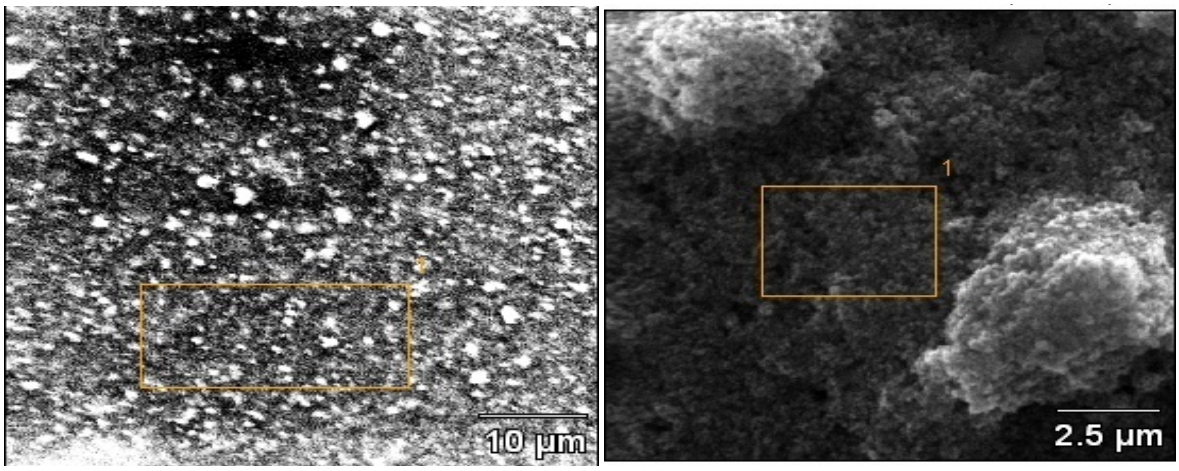

(c) (d)

Figure 4.1:*SEM images TiO2 films that were prepared from pastes that are based from Degussa P25 powder where (a) is a burnt and a cracked film (b) shows rough surfacearea (c) and (d) shows the presence of lumps both at 2.5 µm and 10 µm of the titania pastes.*

The SEM images were obtained when the titania paste was prepared from the Degussa P25 powder. The sintering process was done at a temperature range between 400 – 450^{o}C. The edges of the coated film accumulated a black color and cracks were observed, in the middle of the glass substrate. As the magnification scan was decreased from 250 µm, 50 µm, 10µm and 2.5 µm the surface area of the films exposed the unevenness as well as their roughnesswith evident lumps, which would greatly affect charge transportation as well as the dye or sensitizer impregnation. As a result, when these coated glass substrates were dipped in dye solution, the sintered films detached from glass substrates and no dye stained these films.

Figure 4.2 presents the EDX spectrum of a TiO_2 paste prepared from Degussa P25 powder coated on a glass substrate by doctor-blading method. The paste was coated with gold before the EDX was performed to produce the elemental analysis of the sample.

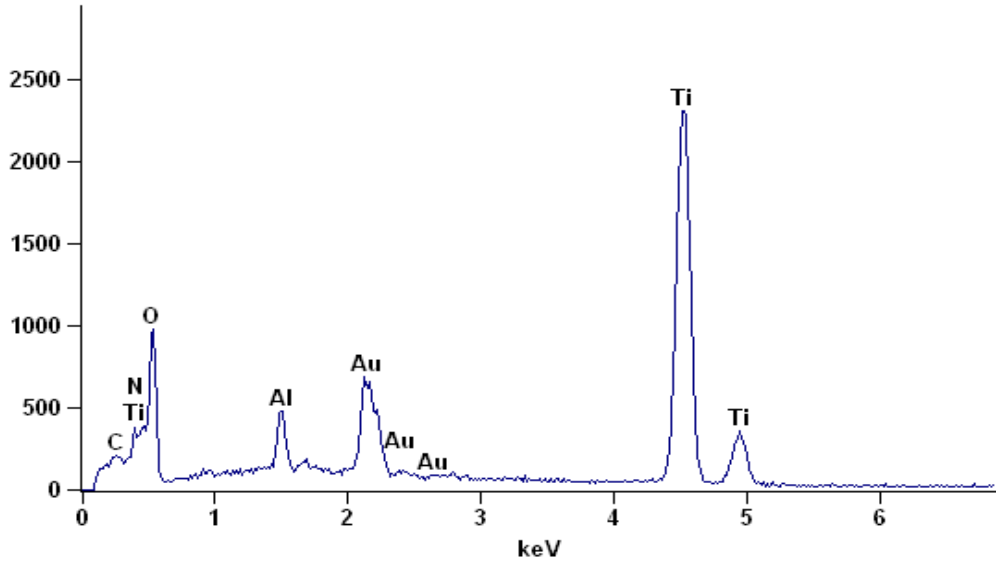

Figure 4.2 *EDX spectrum of TiO_2 paste prepared from Degussa P25 powder coated on a glass substrate by doctor-blading method.*

The typical EDX pattern of TiO_2 paste prepared from Degussa P25 powder confirmed the presence of titanium and oxygen atoms shown in Figure 4.2 was interpreted using the x-ray microanalysis periodic table. Titanium is initially observed at 0.326 keV and is overlapping with oxygen at 0.523 keV due to the high oxidation state of Ti (IV). Oxygen was observed at 0.523 keV. The highest peak for titanium was observed at 4.35 keV followed by the one at 4.89 keV because of a decline of an oxidation state to Ti(III). Other trace elements such as carbon, nitrogen, aluminium and gold were observed at 0.233keV, 0.467 keV, 1.594 keV, and 2.280 keV respectively. These are the elements that emanated from the traces of the coating applied on the titania film before SEM micrographs were generated. The elemental analysis for the composition of TiO_2 paste prepared from Degussa P25 powder commercial TiO_2 film was found to be as follows: Ti = 54.32 % by mass; O = 22.18 % by mass; N = 13.0 % by mass; Al = 2.0 % by

mass; C = 1.2 % by mass and Au = 7.3 % by mass. Therefore, the film analyzed contained = 76.5 % TiO_2 compound.

Figure 4.3 (a – b) shows SEM images of a coated glass substrate with titanium dioxide film called Ti-nanoxide D/SP that was purchased at Solaronix as an alternative for the Degussa P25 paste at an acceleration voltage of 15.0 kV and a magnification scan of 20 μm and 10 μm. This paste is a screen processable opaque titanium dioxide that consists of a mixture of nanocrystalline TiO_2 and optically dispersing anatase particles. These anatase nanocrystals are highly porous with 15 – 20 nm. It is highly recommended for either doctor-blading / screen-printing methods. The aim of this figure is to present the surface morphology of the Ti-nanoxide D/SP to detect any non-uniformity and defects such as lumps and cracks.

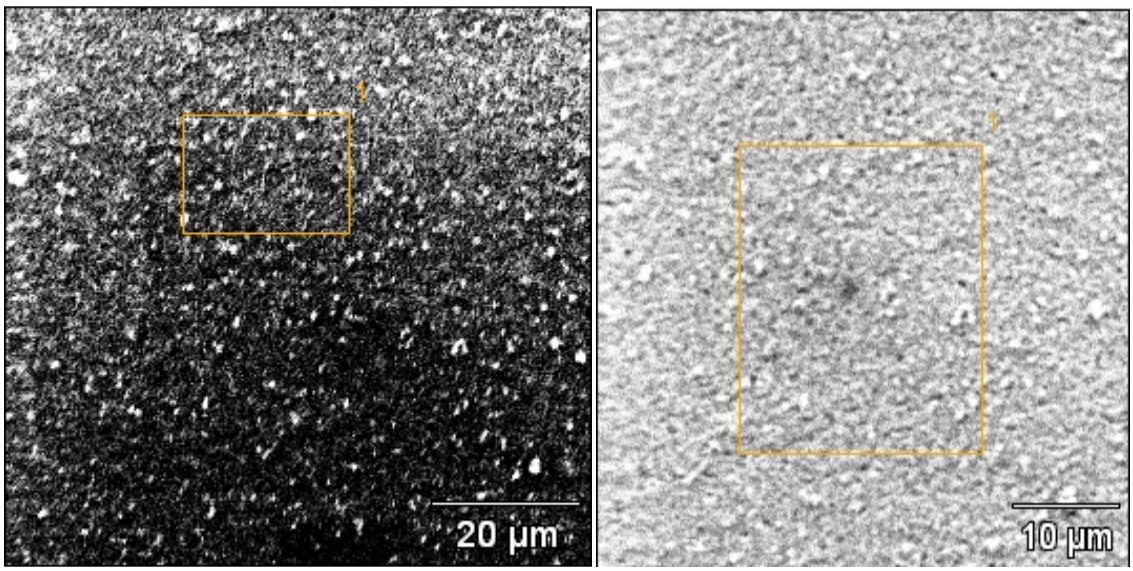

(a) (b)

Figure 4.3: *SEM images TiO_2 films that were prepared from pastes that are based from the Ti-nanoxide D/SP where (a) and (b) show a rough surface area and the presence of lumps both at (a)2.5 µm and (b)10 µm of the titania pastes operating at 8500 magnification and accelerating voltage of 15.0 kV.*

Figure 4.4 presents the EDX spectrum of a TiO_2 paste prepared from Degussa P25 powder coated on a glass substrate by doctor-blading method. The paste was coated with gold before the EDX was performed to produce the elemental analysis of the sample.

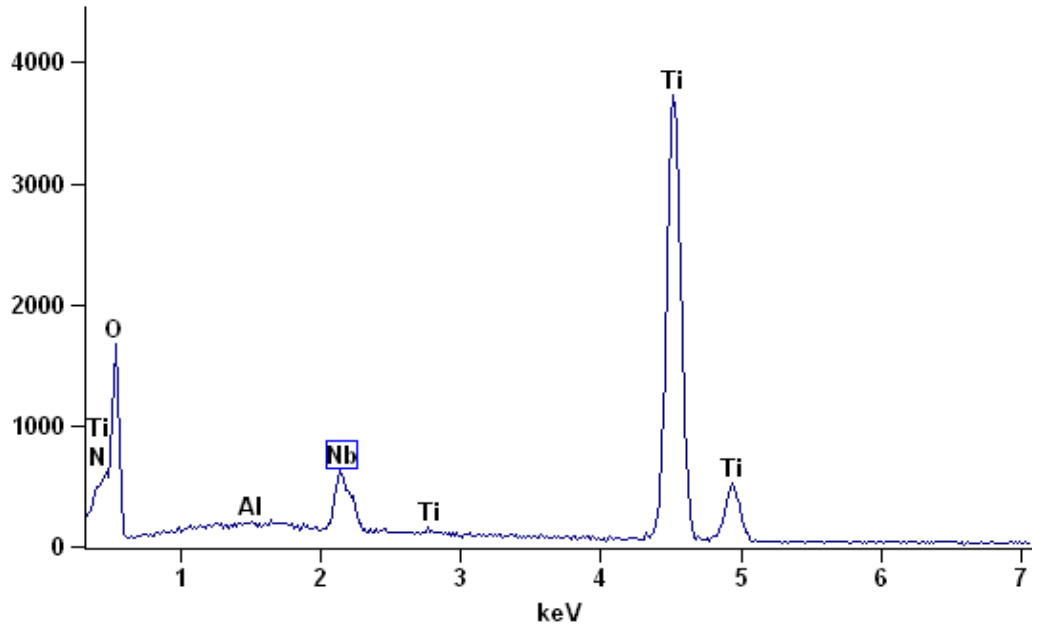

Figure 4.4: *EDX spectrum of TiO_2 paste prepared from Ti-nanoxide D/SP that was purchased at Solaronix coated on a glass substrate by doctor-blading method.*

The typical EDX pattern of the TiO_2 paste prepared from Ti-nanoxide D/SP Degussa P25 powder confirmed the presence of titanium and oxygen atoms from the TiO_2 sample shown in Figure 4.4 was interpreted using the x-ray microanalysis periodic table. Titanium is initially observed at 0.326 keV and is overlapping with oxygen at 0.523 keV due to the high oxidation state of Ti (IV).Also, titanium is observed at 2.876 keVthough the peak is minimal. Oxygen was observed at 0.523 keV; the highest peak for titanium was observed at 4.35 keV followed by the one at 4.89 keV because of a decline of an oxidation state to Ti(III). Other elements such as nitrogen, aluminium and niobium were observed at 0.265 KeV, 1.594 keV, and 2.166 keV respectively. These are the elements that emanated from the traces of the coating applied on the titania film before SEM micrographs were generated. The elemental analysis for the composition of TiO_2 film prepared from Ti-nanoxide D/SP paste was found to be as follows: Ti = 46.21 % by

mass; O = 37.93 % by mass; N = 5.13 % by mass; Al = 3.5 % and Nb = 7.23 % by mass. Therefore, the film analyzed contained = 84.14 % TiO_2 compound.

Figure 4.5 (a – b) illustrates SEM images of a commerciallycoated glass substratewith titanium dioxide film at 8500 magnification and accelerating voltage of 15.0 kV where (a) has a magnification scan of 2.5 µm and (b) has a magnification scan of 1 µm in order to study the smooth surface morphology, particle size, surface area, porosity and dispersion of TiO_2 nanoparticles are the various influencing factors which determine the performance of a photo-anode and no lumps and cracks are observed.

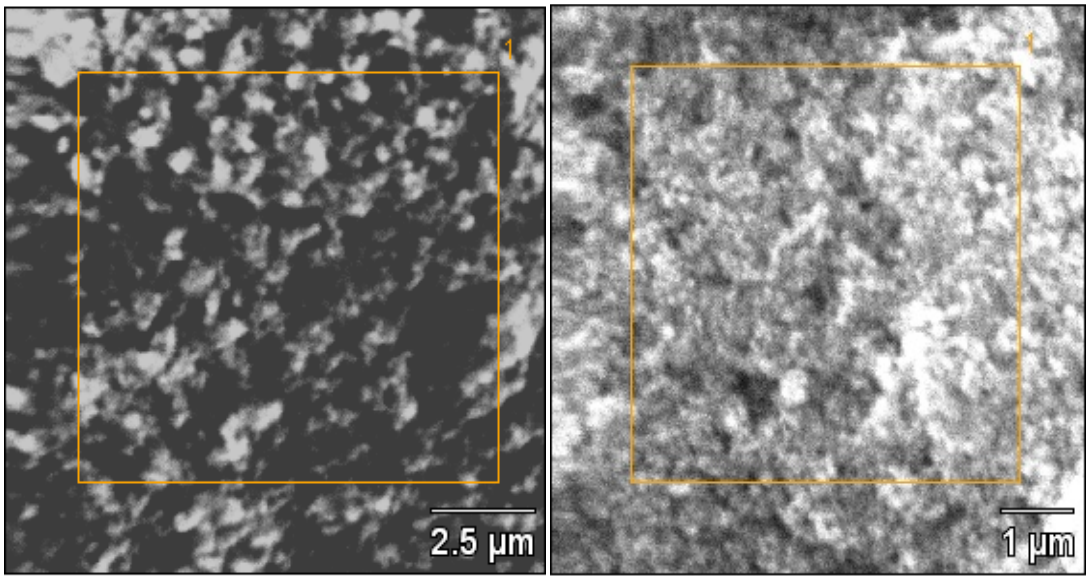

(a) (b)

Figure 4.5*: SEM images of commercially TiO_2films observed at (a) 2.5 µm and (b) 1 µm operating at 8500 magnification and accelerating voltage of 15.0 kV.*

The structure, morphology and optical properties of the commercial TiO_2 films were studied to have amorphous crystalline particles, which are highly porous with high surface area and a

sponge-like structure. The average particle size of a pure titania film is known to range from 2.4 nm to 4.6 nm. The surface area of TiO_2 increases with the decrease in the particle size, which cannot be reduced indefinitely, since porosity also plays a vital role in the performance of a semiconductor. If porosity is low, then that means that the particle size decreases, which is very important because the electrolyte has to be able to penetrate the pores and exist where the adsorbed dye is. Moreover, larger particles have a tendency of scattering light more effectively than smaller ones and that has a positive effect on the efficiency of the cell.

Figure 4.6 presents the EDX spectrum of a commercially coated glass substrate with titanium dioxide film by screen-printing method. The paste was coated with gold before the EDX was performed to produce the elemental analysis of the sample.

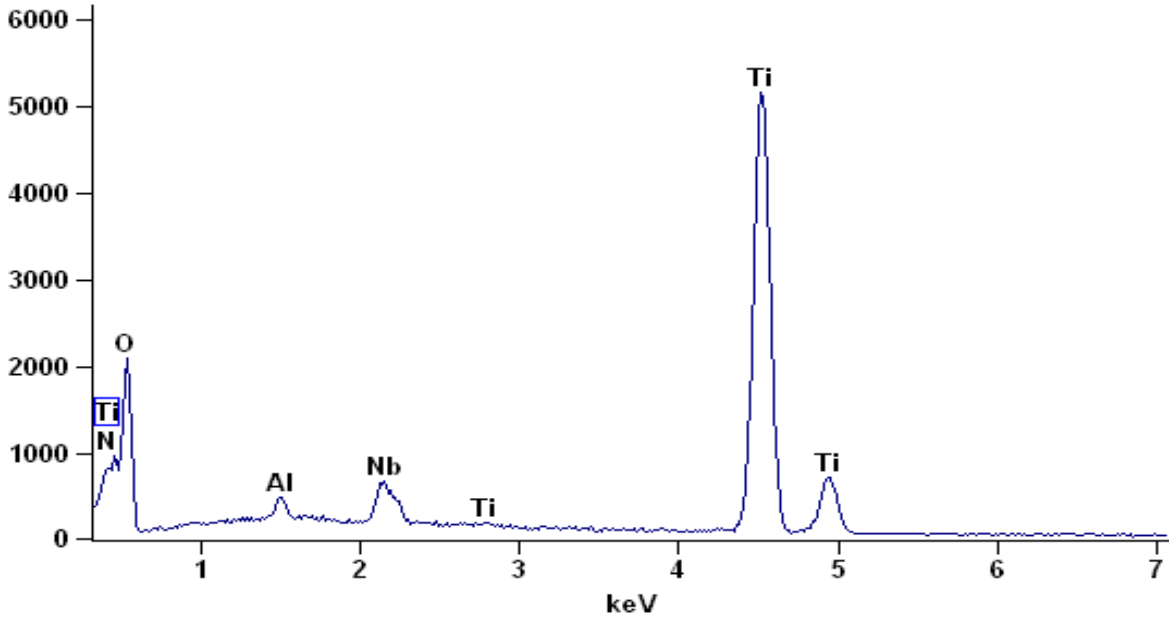

Figure 4.6:*EDX spectrum of a commercially coated glass substrate with titanium dioxide film by screen-printing method.*

The EDX analysis was carried out, so as to confirm and characterize the presence of TiO_2 attained on the film. The typical EDX pattern of the commercial TiO_2 film sample shown in Figure 4.6 was interpreted using the x-ray microanalysis periodic table. Titanium is initially observed at 0.326 keV and is overlapping with oxygen at 0.523 keV due to the high oxidation state of Ti (IV). Oxygen was observed at 0.523 keV; the highest peak for titanium was observed at 4.35 keV followed by the one at 4.89 keV because of a decline of an oxidation state to Ti(III). Other elements such as nitrogen, aluminium and niobium were observed at 0.265 KeV, 1.594 keV, and 2.166 keV respectively. These are the elements that emanated from the traces of the coating applied on the titania film before SEM micrographs were generated. The elemental analysis for the composition of commercial TiO_2 film was found to beas follows: Ti = 52.53 % by mass; O = 39.72 % by mass; Al = 2.0 % by mass; N = 0.92 % by mass andNb = 4.83 % by mass. Therefore, the film analyzed contained= 92.25 %TiO_2 compound.

4.2 CRYSTALLINE PHASES OF TITANIUM DIOXIDE FILMS

All the XRD patterns for titanium dioxide films were recorded and studied on a PHILIPS upright X-ray Powder (Philips PW 1050/25) Diffractometer at room temperature.XRD measurements have been undertaken to determine and establish the major and minor crystalline phasesof the Degussa P25 powder of TiO_2, Ti – nanoxide D/SP and of the commercially coated TiO_2 as well as determining their particle sizes.

Figure 4.7 presents the phase characterization of a Degussa P25 powder by a XRD pattern that shows strong diffraction peaks which confirm that this powder is mainly composed of the anatase phase and rutile phase.

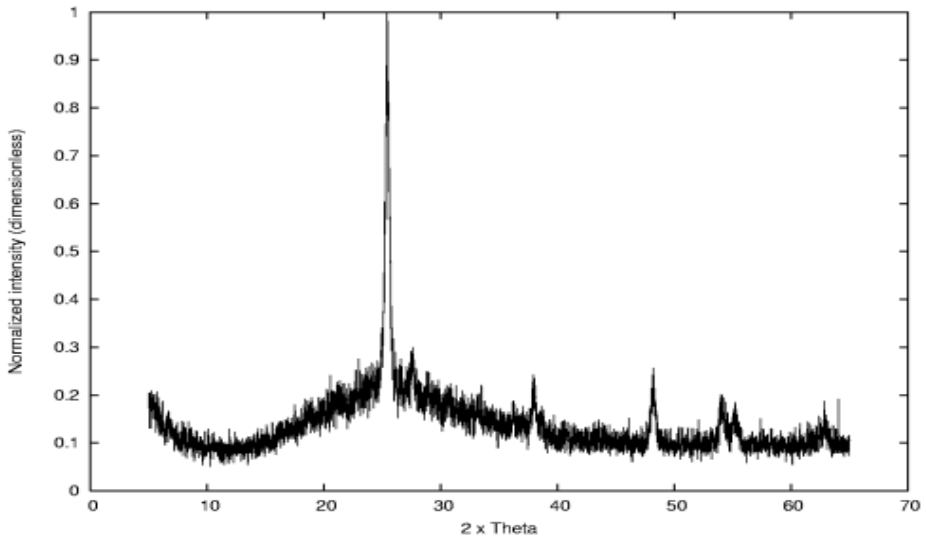

Figure 4.7: *XRD pattern of Degussa P25 TiO_2 powder at room temperature.*

The XRD pattern shown in Figure 4.7 illustrated distinctive diffraction peaks at $2\theta = 25.3^o$, 37.7^o, 47.8^o, 54^o and 55^o for (101), (004), (200), (105) and (211) anatase phase respectively. Moreover, distinctive peaks were observed at $2\theta = 27^o$ and 62^o for (110) and (310) rutile planes respectively. All peaks are in good agreement with the standard spectrum (JCPDS no.: 88-1175 and 84-1286). These results suggest that the Degussa P25 TiO_2 powder is composed of irregular amorphous polycrystalline structures that are composed of both the anatase phase and the rutile phase. The diffraction peak $2\theta = 25.3^o$ is broadened and the intensity is increased which confirms the increase of the increased particle sizes of the powder.

Figure 4.8 (a) and (b)show XRD patterns for the phase characterization of a TiO_2 film prepared from Ti – nanoxide D/SP paste andcommercially coated TiO_2 film at room temperature shows strong diffraction peaks which confirm that this powder is mainly composed of the anatase phase and rutile phase.

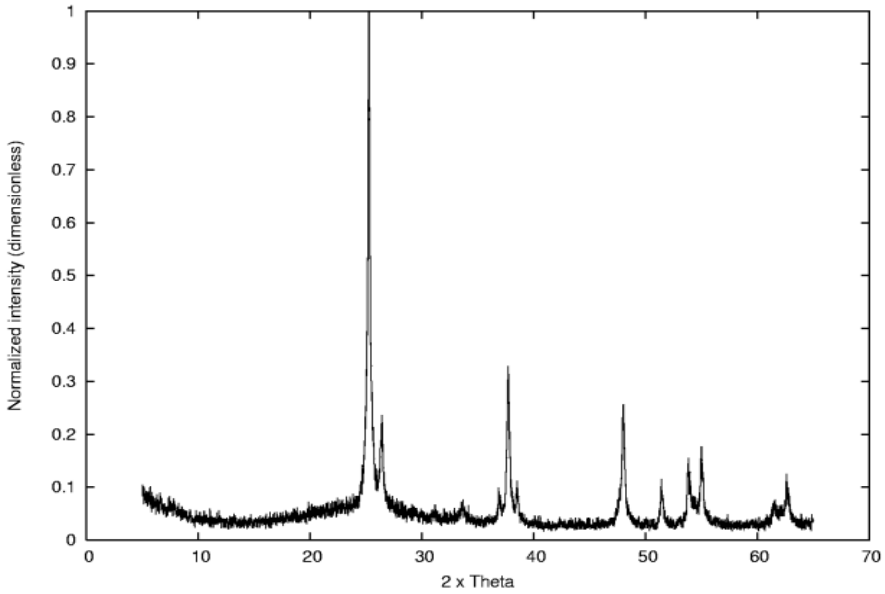

Figure 4.8(a): *XRD pattern of a TiO_2 film prepared from Ti – nanoxide D/SP paste at room temperature.*

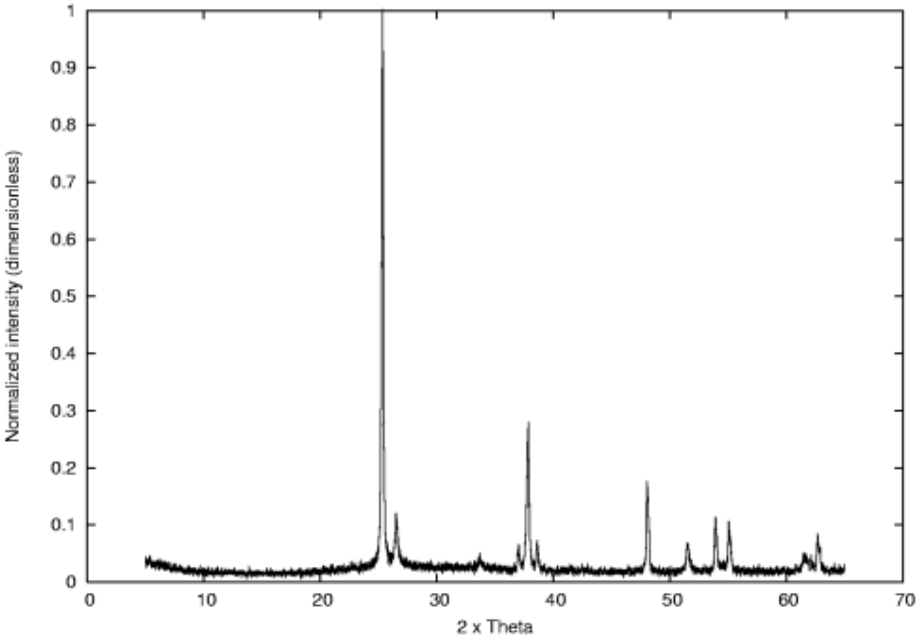

Figure 4.8 (b): *XRD pattern of the commercially coated TiO_2 film on a glasssubstrate at room temperature.*

Figure 4.8 (a) and (b) XRD patterns that exhibited strong diffraction peaks at 2θ = 25.3^{o}, 37^{o}, 37.7^{o}, 39^{o}, 47.8^{o}, 54^{o}, 55^{o}, and 63^{o} for (101), (103), (004), (112), (200), (105), (211) and (118) anatase planes respectively. On the other hand, these XRD patterns exhibited strong diffraction peaks at 2θ = 27^{o}, 52^{o} and 62^{o} for the (110), (211) and (310) rutile planes respectively. All the peaks presented on these patterns are in good agreement and have been compared with reference towith the standardspectrum (JCPDS no.: 88-1175 and 84-1286) database for the diffraction patterns of both anatase and rutile phase. The size of the particles was in the range 32–62 nm for anatase and 27–32 nm for rutile.The narrowing of the distinctive (101) peak at 25.3^{o} on Figure 4.9(b) compared to Figure 4.8 (a) illustrates the increase in particle size. Furthermore, the diffraction pattern peak intensity of the Ti – nanoxide D/SP TiO_2 film in Figure 4.8 (a) commercial titania paste was higher compared to that of the commercially coated TiO_2 film in Figure 4.8 (b) to its increased particle size.The intensity of the titania film in Figure 4.8(b) is lower than the titania film in Figure 4.8 (a) because the commercially coated TiO_2 film is commercialized and has been detected to be fully synthesized.

4.3 SPECTRAL RESPONSE CHARACTERIZATION OF THE DYES

The ultraviolet – visible spectral data of all the ruthenium-based sensitizers were collected on a Perkin Elmer Lambda 35 UV-Vis Light Spectrophotometer at room temperature.This was done to investigate the spectral response of the sensitizers, which is an important aspect that determines the efficiency of the dye-sensitized solar cells.

Figure 4.9 shows the UV-Vis spectrum of the Ruthenium 505 dye or *cis*-bis(cyanido) bis(2,2'-bipyridyl-4,4' dicarboxylato) ruthenium (II) dye at room temperature which is normally shortened to have a formula of $RuL_2(CN)_2$ (L = 2,2'-bipyridyl-4,4'-dicarboxylic acid) with a visible optical electronic transition of the ruthenium complex called Metal-to-Ligand Charge Transfer (MLCT).

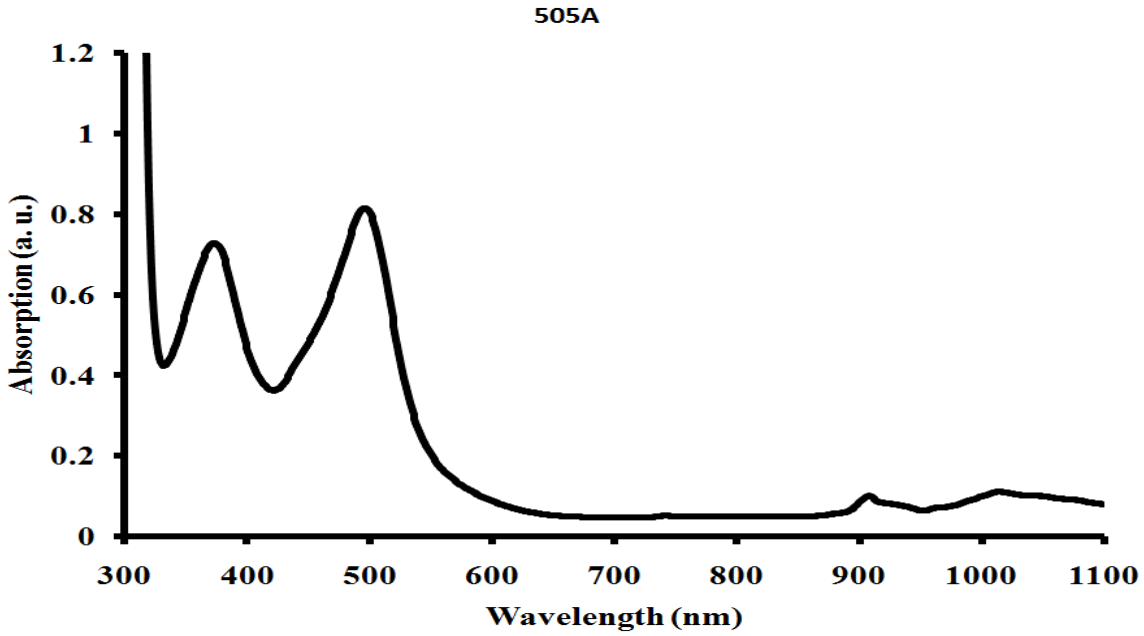

Figure 4.9: *UV-Vis spectrum of Ru505 or cis-bis(cyanido) bis(2,2'-bipyridyl-4,4' dicarboxylato) ruthenium (II) dye at room temperature.*

The excitation of Ruthenium-505 dye in Figure 4.10 involves the promotion of an electron from the ruthenium metal centreto π* orbitals on the pyridyl ligand. This *cis*-bis(cyanido) bis(2,2'-bipyridyl-4,4' dicarboxylato) ruthenium (II) dye has two such electronic transitions in the visible region of the spectrum, at 493 nm and 370 nm with absorptions 0.80859 and 0.72279 respectively. The molar absorptivities (ε)for these transitions absorbing 493 nm and 370 nm are 1.34×10^4 $L.mol^{-1}.cm^{-1}$ and 1.32×10^4 $L.mol^{-1}.cm^{-1}$ respectively(Adeloye A.O., 2011).

Figure 4.10 shows the UV-Vis spectrum of the N3 or -bis(isothiocyanato)bis(2,2'-bipyridyl-4,4'-dicarboxylato)-ruthenium(II) dye and its shortened formula is $RuL_2(NCS)_2.2H_2O$ (L = 2,2'-bipyridyl-4,4'-dicarboxylic acid) at room temperature.

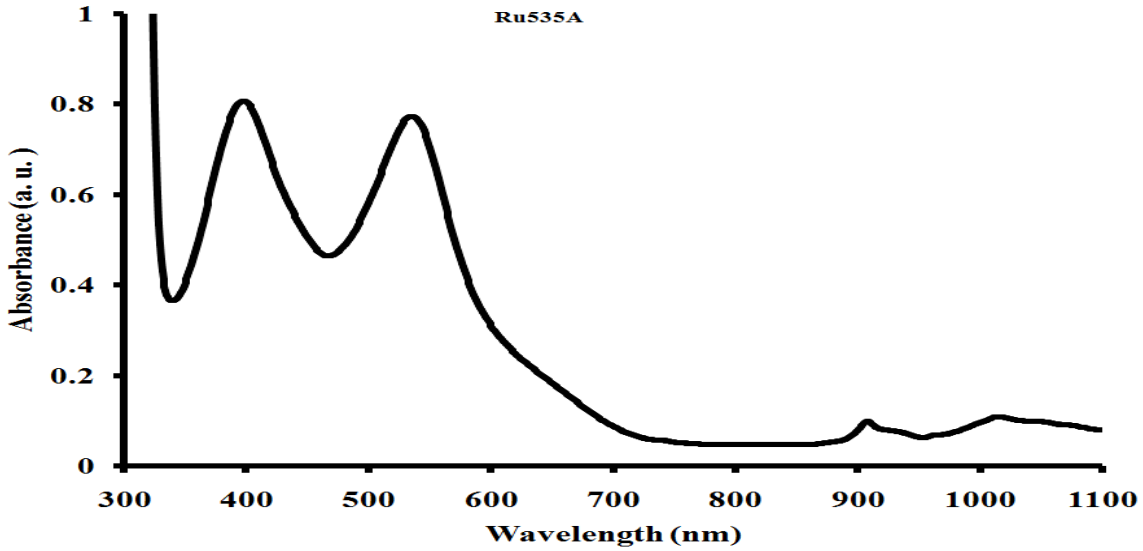

Figure 4.10: *UV-Vis spectrum of the Ru535 (N3) or cis-bis(isothiocyanato)bis(2,2'-bipyridyl-4,4'-dicarboxylato)-ruthenium(II) dye at room temperature.*

The N3 dye in Figure 4:10 illustrates two absorption bands at 532 nm and 395 nm with absorptions 0.7704 and 0.80518 respectively due to the metal-to-ligand charge transfer (MLCT) from ruthenium metal centre to π* orbitals on the pyridyl ligand. Also, in this complex, the cyanide (CN^-) ions are replaced by thiocyanate (SCN^-) ions hence the decrease in the absorption levels. The thiocyanate groups are bound through the nitrogen although the S-bonded isomer does appear as an intermediate species. The molar absorptivities (ε) for these transitions absorbing 532 nm and 395 nm are 1.48 x 10^4 $L.mol^{-1}.cm^{-1}$ and 1.46 x 10^4 $L.mol^{-1}.cm^{-1}$ respectively (Adeloye A.O., 2011).

Figure 4.11 shows the UV-Vis spectrum of Ruthenium 535 bis-TBA(N719) *or cis*-bis(isothiocyanato)bis(2,2'-bipyridyl-4,4'-dicarboxylato)-ruthenium(II)bis-tetrabutylammonium dye and is shortened to be $RuL_2(NCS)_2$: 2TBA . (L = 2,2'-bipyridyl-4,4'-dicarboxylic acid ;TBA = tetrabutylammonium) with a visible optical electronic transition of the ruthenium complex called Metal-to-Ligand Charge Transfer (MLCT).

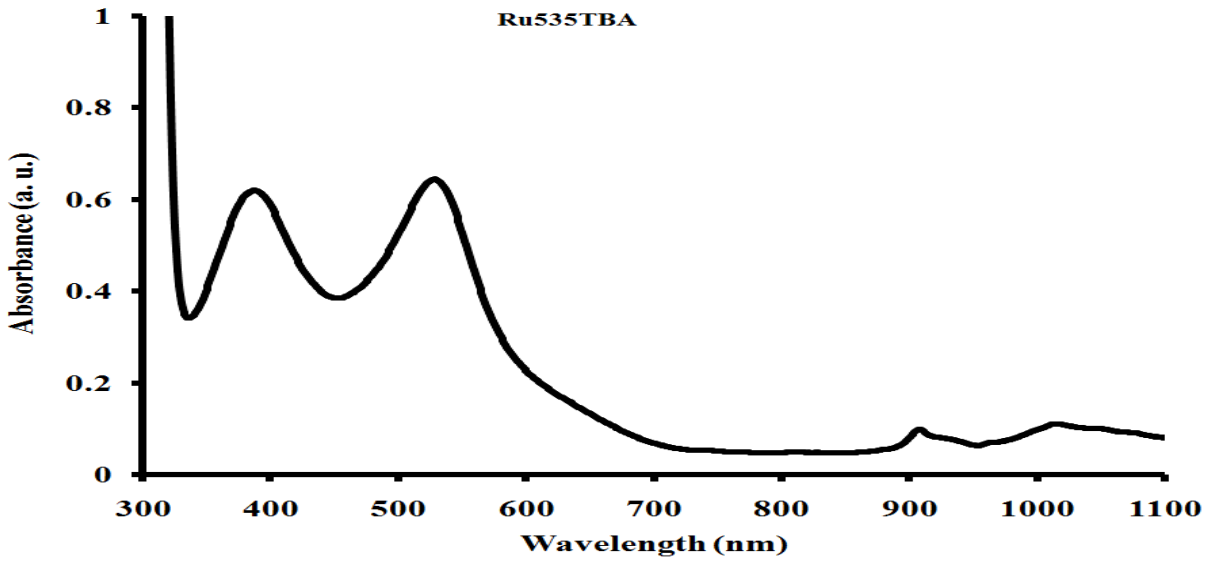

Figure 4.11: *UV-Vis spectrum of Ruthenium 535 bis-TBA (N719) or cis-bis(isothiocyanato) bis(2,2'-bipyridyl-4,4'-dicarboxylato)-ruthenium(II)bis-tetrabutylammonium dye at room temperature.*

Figure 4.11 is showing the excitation of the N719 dye resulting in two absorption bands at 524 nm and 383 nm with absorptions 0.64043 and 0.61660 respectively due to the metal-to-ligand charge transfer (MLCT) from ruthenium metal centre to π* orbitals on the pyridyl ligand. Also, in this complex, the hydride (H^-) ions are replaced by tetrabutylammonium ions (B_4N^+) ions hence the decrease in the absorption levels. The molar absorptivities (ε) for these transitions

absorbing 524 nm and 383 nm are 1.54 x 10^4 $L.mol^{-1}.cm^{-1}$ and 1.52 x 10^4 $L.mol^{-1}.cm^{-1}$ respectively.

These dyes adopt a distorted octahedral metal geometry and bind to the oxide layer via two of carboxylic acid group, at least one of them being anchored via bindentate configuration bridging two adjacent titanium sites.There different spectral responses exhibited by these dye complexes in the visible region of the spectrum due to the different structures they possess. The complexes exhibit a very broad and intense metal-to ligand charge transfer (MLCT) absorption throughout the visible spectrum (300 – 700 nm), characteristic of many other ruthenium (II) polypyridyl complexes, and which can be assigned to electronic transitions from Ru II based orbital to the ligand based π* orbitals. All of these complexes have similar ligands hence there are no multiple MLCT transitions in the visible region, therefore there was no enhancement of the oscillator strength in the blue and green portions of the spectrum which improve light absorption cross-sections at higher energy in similar complexes. The line that appears on the individual spectra of the dyes slightly below 300 nm are attributed by the π-π* absorption band(Adeloye A.O., 2011).

The absorption peaks for Ruthenium 535 dye (λ_1 = 395 nm λ_2 = 532 nm)were observed to be higher than those of the Ruthenium 505 dye (λ_1 = 370 nm λ_2 = 493 nm) and of Ruthenium 535 bis-TBA (λ_1 = 383 nm λ_2 = 524 nm). This is due to the fact that the cyanide ion in Ru-505 dye was replaced by the thiocyanate ion to form the Ru-535 or N3 dye and the absorption levels of Ru-535 bis-TBA were decreased by the substitution of hydrogen (H^+) ionsby the tert-butyl ammonium ions (TBA^+). The interaction between the carboxylic groups and the TiO_2 is of

fundamental importance in determining the geometrical orientation of the absorbed dye state and influences the electronic coupling with the Ti (3d) conduction band orbital.

4.4 DETERMINATION OF FUNCTIONAL GROUPS

The Perkin Elmer Spectrum 2000 FTIR spectrophotometer was utilized to record the infrared spectra of all the ruthenium-based dyes at room temperature.This was performed to investigate the impact of the different functional groups of the dye molecules on the efficiency of solar cells.

Figure 4.12 shows the spectrum of FTIR for the Ruthenium 505 dye or *cis*-bis(cyanido) bis(2,2'-bipyridyl-4,4' dicarboxylato) ruthenium (II) dye at room temperature to study the impact of the presence of two cyanide (CN) ligands attached to the ruthenium metal through the carbon atom on the efficiency of the solar cells.

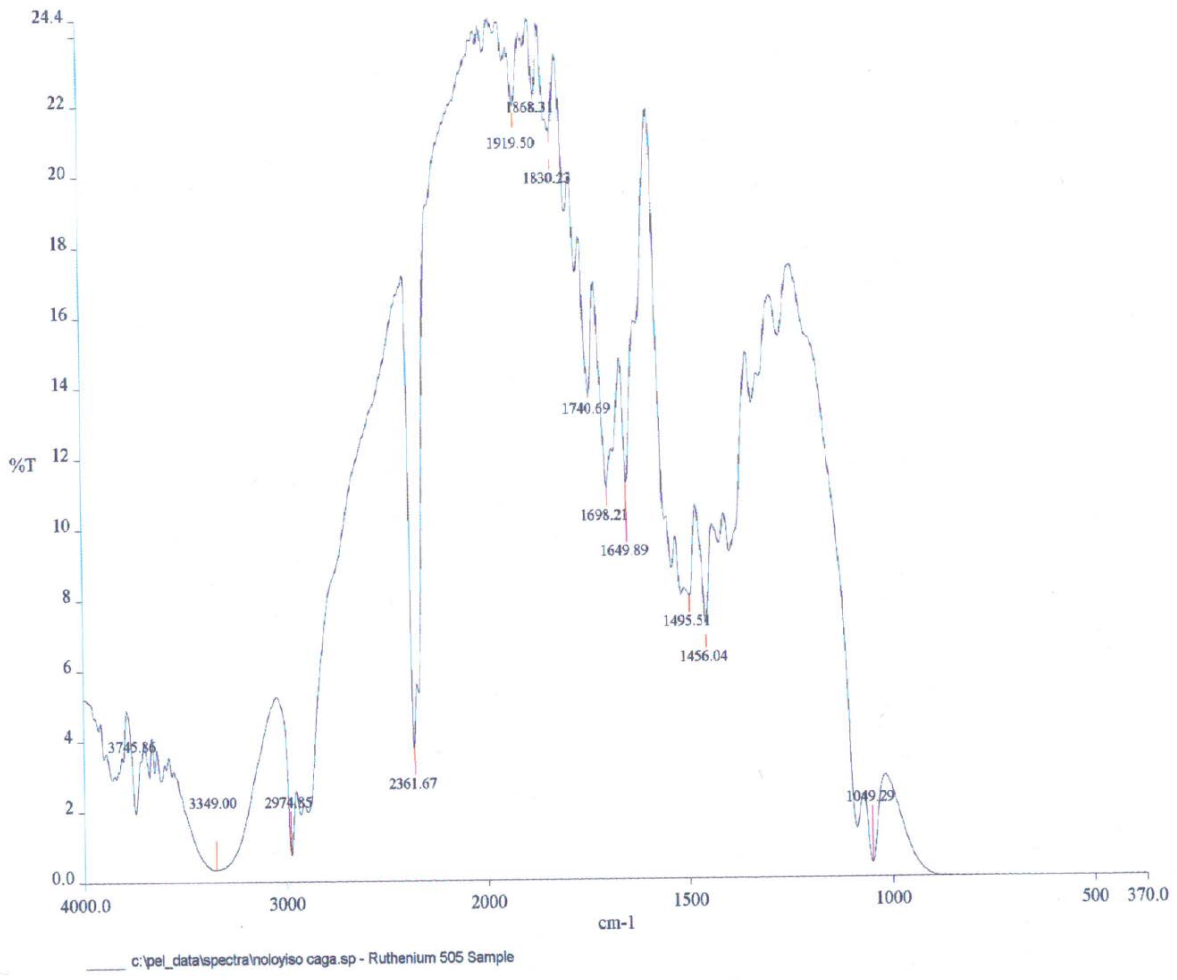

Figure 4.12: *FT-IR spectra of Ru505 or cis-bis(cyanido) bis(2,2'-bipyridyl-4,4' dicarboxylato) ruthenium (II) dye at room temperature dye dissolved in ethanol as a solvent.*

The FTIR spectrum of Ru-505 dye observed in Figure 4.12 revealed that at 3746 cm^{-1}, 3353 cm^{-1} and at 2974 cm^{-1} there are single-bond stretching motions which correspond to absorptions caused by N – H, O – H and C – H bond stretching which are found on the bipyridyl rings

respectively. A sharp peak is observed at 2361 cm^{-1} and is attributed to the existence of a triple bond motion with increased intensity of the stretching band of ν(C≡N). The absorptions observed at 1919 cm^{-1}, 1858 cm^{-1}, 1830 $cm^{-1}$and 1740 cm^{-1} are attributed to the existence of the carboxylic groups (COOH). Strong peaks of interest appeared at 1698 $cm^{-1}$and at 1649 cm^{-1}which indicate the carbonyl ν(C=O) stretch mode of the protonated carboxylic acid COOH (i.e. the ester-like linkage) and the absorption peaks at 1495$cm^{-1}$and at 1456 cm^{-1} confirm the presence of (C=C) in the bipyridine ring.The absorptions bands at 1361 cm^{-1} and 1285 $cm^{-1}$is assigned to the asymmetric carboxylate ionsν(COO^-) of the carboxylic groups and the symmetric carboxylate ions ν(COO^-) respectively. The vibrational band at 1049 cm^{-1} confirms the presence ofν(C–O) stretching of the carboxylic groups.

Figure 4.13 shows the FTIR spectrum of N3 or -bis(isothiocyanato)bis(2,2'-bipyridyl-4,4'-dicarboxylato)-ruthenium(II) dye at room temperature to study the impact of the presence of two thiocyanate (SCN) ligands attached to the ruthenium metal through the sulfur atom and the anchoring mechanisms of the carboxylic acid groups on the titanium oxide films on the efficiency of the cells.

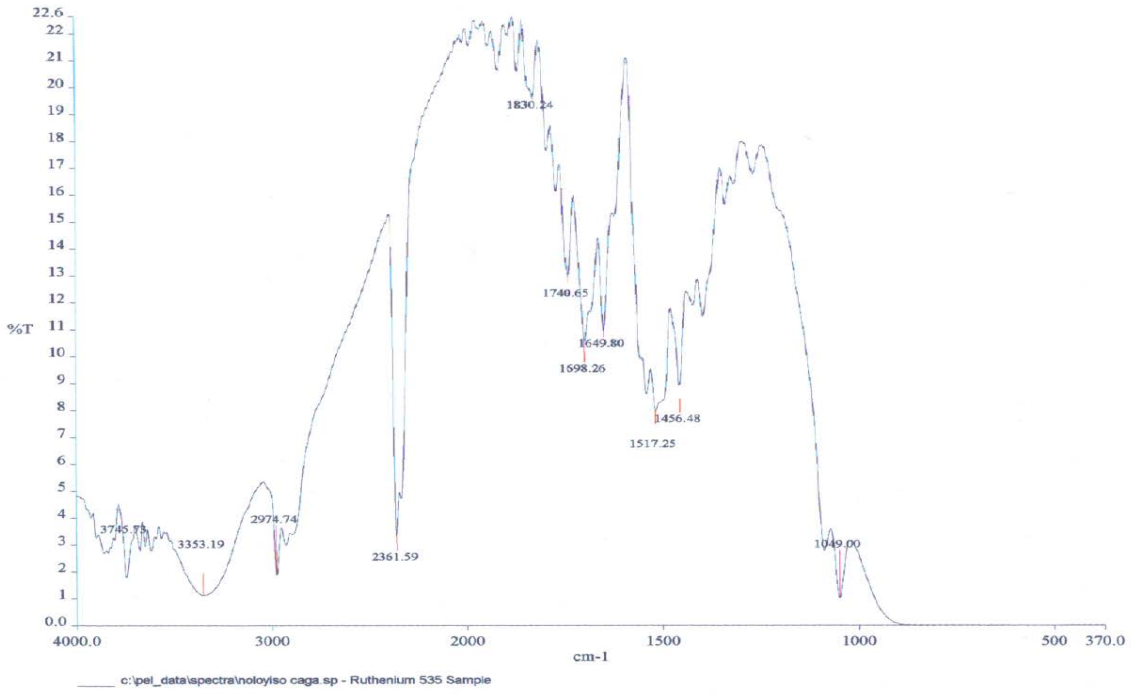

Figure 4.13: *FT-IR spectra of Ru535 (N3)or -bis(isothiocyanato)bis(2,2'-bipyridyl-4,4'-dicarboxylato)-ruthenium(II) dye at room temperature dissolved in ethanol as a solvent.*

The FT-IR spectrum of Ru-535 dye presented on Figure 4.13 show absorptions at 3746 cm^{-1}, 3353 cm^{-1} and at 2974 cm^{-1} there are single-bond stretching motions which correspond to absorptions caused by N – H, O – H and C – H bond stretching which are found on the bipyridyl rings respectively. A sharp peak is observed at 2361 cm^{-1} and is attributed to the existence of a triple bond motion with increased intensity of the stretching band of ν(C≡N) instead of a stretching band of the thiocyanate ligand ν(N=C=S) at 2100 cm^{-1}. The absorptions observed at 1830 cm^{-1} and 1740 cm^{-1} are attributed to the existence of the carboxylic groups (COOH). Strong peaks of interest appeared at 1698 cm^{-1} and at 1649 cm^{-1} which indicate the carbonyl ν(C=O) stretch mode of the protonated carboxylic acid COOH (i.e. the ester-like linkage) and the

absorption peaks at 1517 $cm^{-1}$and at 1456 cm^{-1} confirm the presence of (C=C) in the bipyridine ring. The absorptions bands at 1361 cm^{-1} and 1285 cm^{-1} is assigned to the asymmetric carboxylate ions $\nu(COO^-)$ of the carboxylic groups and the symmetric carboxylate ions $\nu(COO^-)$ respectively. The vibrational band at 1049 cm^{-1} confirms the presence of ν(C–O) stretching of the carboxylic groups.

Figure 4.14 shows the FTIR spectrum of Ruthenium 535 bis-TBA (N719) *or cis*-bis(isothiocyanato) bis(2,2'-bipyridyl-4,4'-dicarboxylato)-ruthenium(II)bis-tetrabutylammonium dye to study the impact of replacing two (H^+) ions on carboxylic acid groups with tetrabutylammonium ion (TBA^+) ions on the efficiency of the solar cells at room temperature and the role played by the anchoring mechanisms of the carboxylic acid groups on the titanium oxide films on the efficiency of the cells.

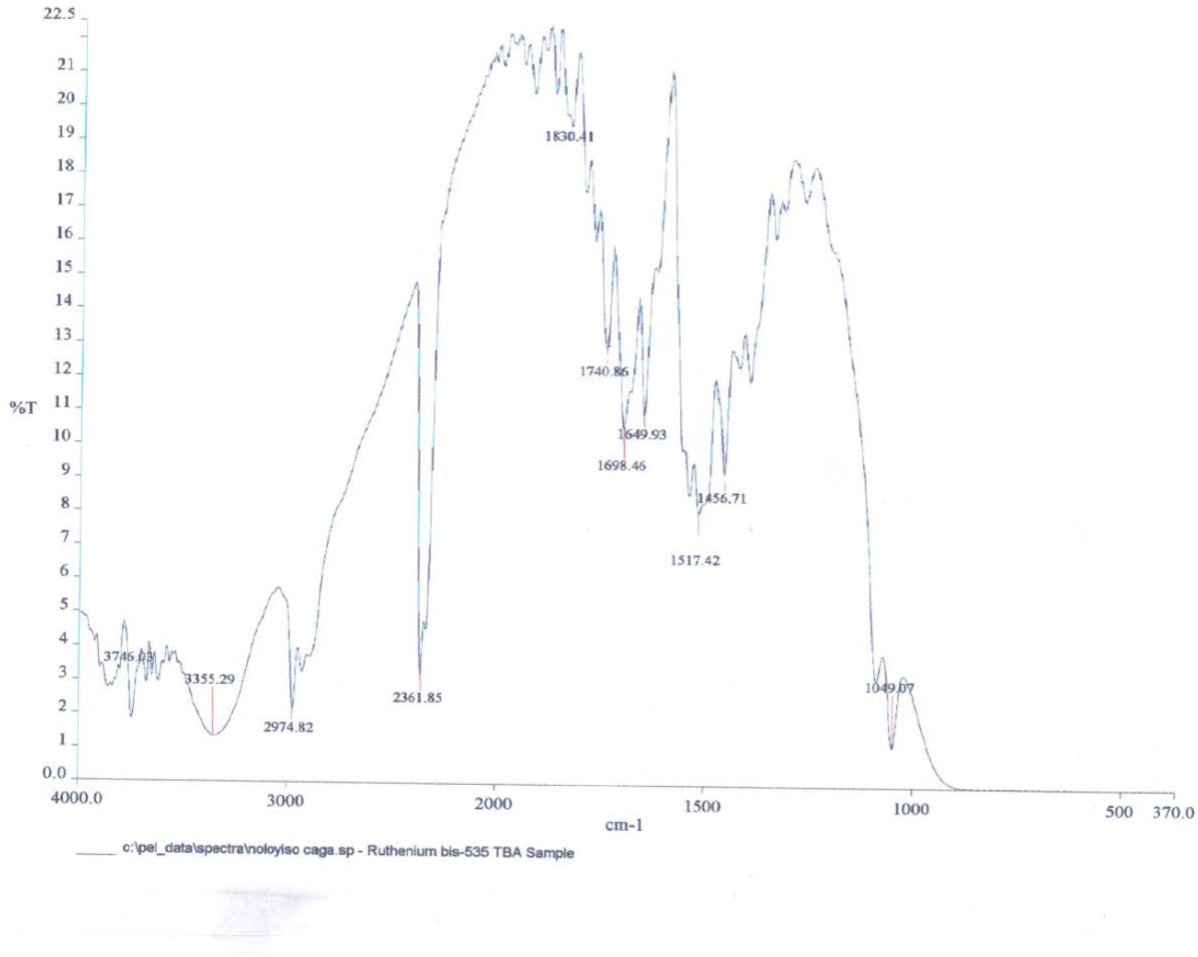

Figure 4.14: *FT-IR spectra of Ru535 bis-TBA (N719) or cis-bis(isothiocyanato) bis(2,2'-bipyridyl-4,4'-dicarboxylato)-ruthenium(II)bis-tetrabutylammonium dye dissolved in ethanol as a solvent.*

The FT-IR spectrum of Ru-535 bis-TBA in Figure 4.14 illustrate absorptions at 3746 cm^{-1}, 3353 cm^{-1} and at 2974 cm^{-1} there are single-bond stretching motions which correspond to absorptions caused by N – H, O – H and C – H bond stretching which are found on the bipyridyl rings respectively. A sharp peak is observed at 2361 cm^{-1} and is attributed to the existence of a triple bond motion with increased intensity of the stretching band of ν(C≡N) instead of a stretching

band of the thiocyanate ligand ν(N=C=S) at 2100 cm^{-1}. The absorptions observed at 1830 cm^{-1} and 1740 cm^{-1} are attributed to the existence of the carboxylic groups (COOH). Strong peaks of interest appeared at 1698 cm^{-1} and at 1649 cm^{-1} which indicate the carbonyl ν(C=O) stretch mode of the protonated carboxylic acid COOH (i.e. the ester-like linkage) and the absorption peaks at 1517 $cm^{-1}$and at 1456 cm^{-1} confirm the presence of (C=C) in the bipyridine ring. A very weak vibrational and a stretching band of *tert*-butyl ammonium (TBA) was observed at 1435 cm^{-1}. The absorptions bands at 1361 cm^{-1} and 1285 cm^{-1} is assigned to the asymmetric carboxylate ions $\nu(COO^-)$ of the carboxylic groups and the symmetric carboxylate ions $\nu(COO^-)$ respectively. The vibrational band at 1049 cm^{-1} confirms the presence of ν(C–O) stretching of the carboxylic groups.

The three infrared spectra of the dyes illustrated similar traits with regards to the ligands they possess with slight differences in some of their distinctive vibrational absorption peaks since they differ because of the existence of the C≡N at 2224 cm^{-1}, N=C=S 2100 cm^{-1} and TBA 1436 cm^{-1} in Ruthenium 505, Ruthenium 535 and Ruthenium 535 bis-TBA respectively. Absorptions beyond 2500 $cm^{-1}$of the infra-red region are assigned to aromatic C – H stretching and are considered to be indicative of the presence of O – H groups in the respective dyes.Also, broadened absorption peaks below 1000 cm^{-1}form part of the fingerprint regionof the infrared and they confirm the coordination of nitrogen atoms of the ancillary ligands to ruthenium central metal atom (Zhang J., et al., 2008).

4.5 DETERMINATION OF ELECTRONIC BANDS

The photoluminescence emission spectra of Ruthenium 505 or $RuL_2(CN)_2$ dye, Ruthenium 535 or $RuL_2(NCS)_2$dye and Ruthenium 535 bis-TBA or$RuL_2(NCS)_2$:2TBA dye complexes are performed in were collected by the Perkin Elmer Lambda 45 Fluorescence Spectrophotometer at room temperature to establish the maximum wavelengths of these dye complexes .

Figure 4.15 shows electronic bands with different wavelengths at which these three dye complexes fluoresce to study the impact of molecular weights and molar absorptivities on the efficiency of the solar cells.

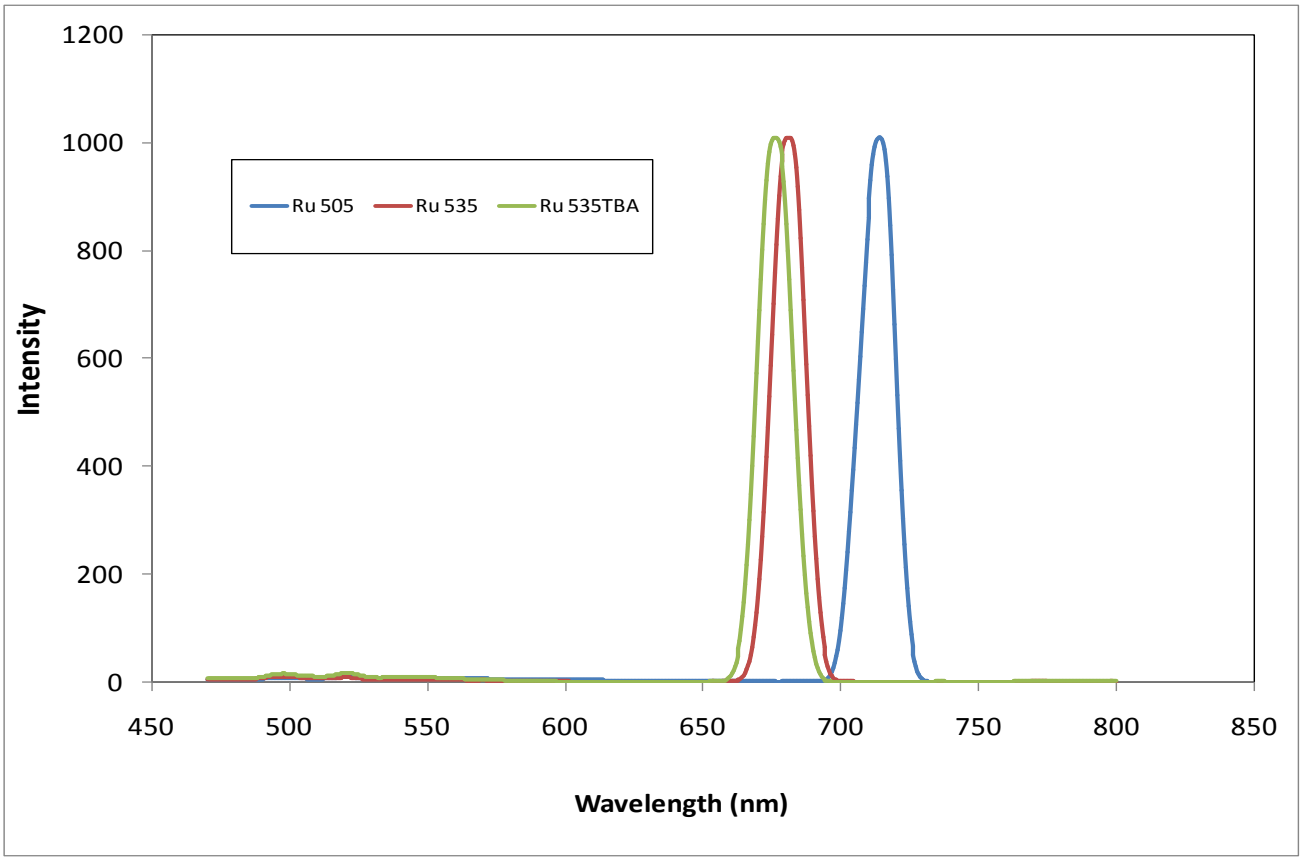

***Figure 4.15**: Photoluminescence emission spectra of Ru505,Ru535 and 535TBA in ethanol.*

Upon excitation into the Ligand-Centered (LC) and Metal-to-Ligand Charge Transfer (MLCT) bands (λ_{exc} = 500 nm), all the dye complexes in Figure 4.15 show appreciable good luminescence at room temperature with a similar well-defined peaks of intensity at 1000 a.u. The emission wavelengths maxima were found at 723, 686 and 673 nm for Ruthenium 505 dye, N3 dye and N719 dye respectively. A direct correlation has been observed between emission intensity, molar extinction co-efficients and the molecular weights of these ruthenium-based compounds.

The *cis*-bis(cyanido) bis(2,2'-bipyridyl-4,4' dicarboxylato) ruthenium (II) or Ruthenium 505 dye has a molecular formula of $C_{26}H_{16}O_8N_6Ru$ with a molecular weight of 641g/mol and a molar extinction coefficient (ε) of about 1.34 x 10^4 $L.mol^{-1}.cm^{-1}$. The N3 dye is *cis*-bis(isothiocyanato)bis(2,2'-bipyridyl-4,4'-dicarboxylato)-ruthenium(II) or Ruthenium 535 dye has a molecular formula of $C_{26}H_{20}O_{10}N_6S_2Ru$ with a molecular weight of 741.7 g/mol and a molar extinction coefficient (ε) of about 1.48 x 10^4 $L.mol^{-1}.cm^{-1}$.

The N719 is *cis*-bis(isothiocyanato)bis(2,2'-bipyridyl-4,4'-dicarboxylato)-ruthenium(II)bis tetrabutylammonium or Ruthenium 535 bis-TBA dye has a molecular formula of $C_{58}H_{86}O_8N_6S_2Ru$ with a molecular weight of 1188.6 g/mol and a molar extinction coefficient (ε) of about 1.54 x 10^4 $L.mol^{-1}.cm^{-1}$. There is a direct proportionality between molecular weights and molar extinction coefficients of the dyes. Consequently,there is an inverse proportionality between the molecular weights of the dyesand emission wavelengths of the dyes. Hence, the dye with the least molecular weight was observed near the infrared region at 723 nm (Adeloye A.O., 2009).

The conjugated functional organic molecules are useful for the study of electron transport at the molecular scale. The most stable and effective dye is expected to be the N719 dye which has the least wavelength and greater solubility than all the dyes.

4.6 DETERMINATION OF RESISTIVE STABILITIES OF ASSEMBLED CELLS

The PGSTAT 12/30/230 Potentiostat was used to carry out the electrochemical impedance measurements of the assembled electrochemical cells at a scan rate of 50mV/s with the main aim of studying the internal resistances as well as transfer kinetics of dye-sensitized solar cells. The EIS spectra were measured over of frequency range of 10^{-1} – 10^{6} Hz at room temperature under open circuit conditions whereby a two electrode configuration was utilized by connecting TiO_2 as the working electrode and the counter electrode as the reference electrode.

Figure 4.16 shows Nyquist plots were produced for three cells which all consisted of the N719 dye whereby the first cell had Z-150 electrolyte, which is composed of 150 mM triiodide that is dissolved in a methoxypropionitrile (MPN) solvent. **Table 4.1 shows** the percentage differences between the Nyquist plots presented in Figure 4.16. The second cell was made up of N719 dye and the AN-50 electrolyte, which is composed of 50 mM triiodide that is dissolved in an acetonitrile (AN) solvent. The third cell was made up of N719 dye and the PN-50 electrolyte, which is composed of 50 mM triiodide that is dissolved in a propionitrile (PN) solvent.

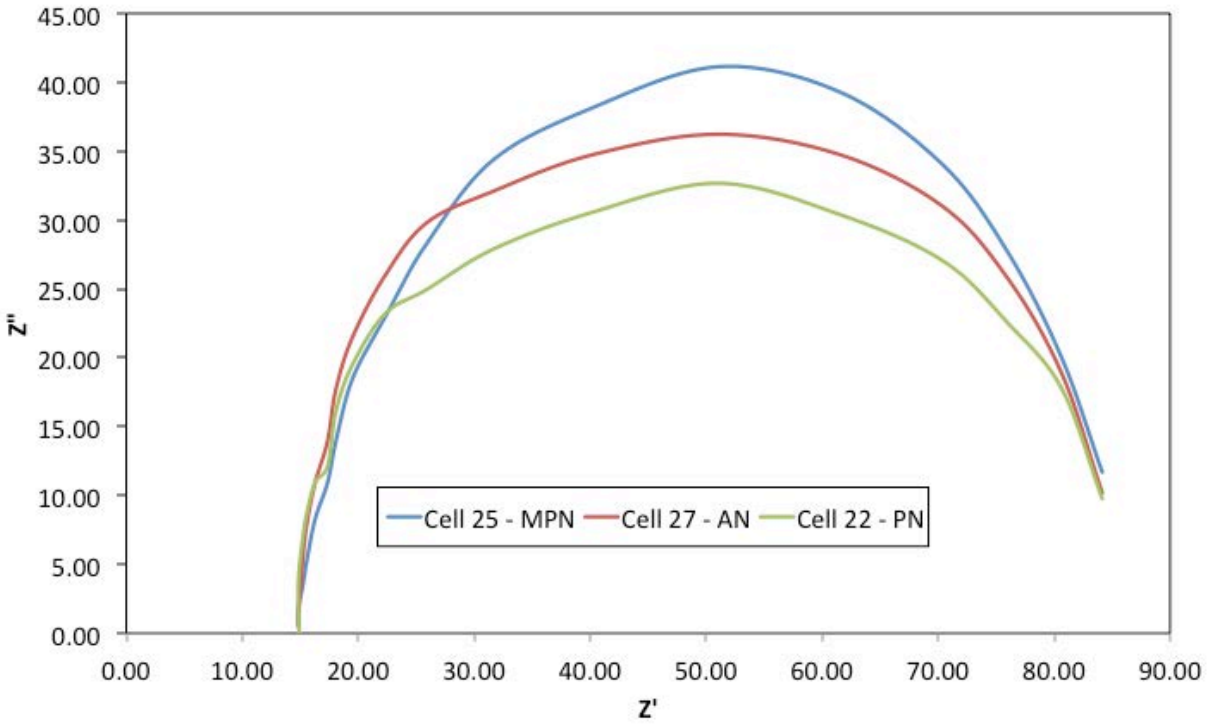

Figure 4.16: *Nyquist plots of dye-sensitized solar cells withRuthenium 535-bis-TBA or N719 dye combined with (a) Z-150 electrolyte, (b) AN-50 electrolyte and (c) PN-50 electrolyte.*

Table 4.1 Percentage differences between the Nyquist plots of cell 25, cell 27 and cell 22 which contain ruthenium 535 bis – TBA (N719) dye and methoxypropionitrile (MPN), acetonitrile (AN) and propionitrile (PN) based electrolytes.

% Difference, Cell 25/ Cell 27	% Difference, Cell 25/ Cell 22	% Difference Cell 27/ Cell 22
0	100	100
40	102.8708134	238.1180223
55.55555556	100.3349282	28.78673958
50	64.5608339	9.707222602
31.81818182	32.01818182	0.151724138
27.5862069	10.70450421	13.23160481
27.02702703	15.41704384	9.139774
16.32653061	5.57562738	9.242004533
13.1147541	0.917213115	10.78333333
5.333333333	11.808	16.27341772
6.593406593	18.84010989	13.11117647
8.910891089	19.87029703	12.03152174

	11.9266055	20.57293578	9.8171875
	11.53846154	22.64038462	12.55
	8.888888889	20.47055556	12.71158537
	6.849315068	18.50342466	12.51102941
	5.660377358	11.15	5.819
	12.90322581	16.39677419	4.011111111
SUM	340.0327612	592.6516276	517.9964546
Mean	**18.89070895**	**32.92509042**	**28.77758081**
STDEV.P,Cell25/Cell27			
12.5456022			
STDEV.P,Cell22/Cell25			
11.71548012			
STDEV.P, Cell27/Cell22			
10.77347689			

A significant difference was established between the three plots as evident in the percentage difference data presented in Table 4.1.This was also confirmed through calculation of the *P* values to compare the three plots as could be seen in the table.

In Figure 4.16 each cell produced only one large semicircle located in the middle of the Nyquist plot which is attributed to the dark reaction impedance caused by charge transport resistance (R_{ct}) at the TiO_2/Dye/Electrolyte interface. The other two semicircles, where one is located in the low frequency region assigned to the charge transport resistance at the counter electrode and the other semicircle is located on the high frequency region assigned to charge transport resistance for the diffusion the triiodide ion in the electrolyte.

The semicircle radius of each cell increases with the change of an electrolyte which could lead to the increase of the efficiency of the cells due to the interaction between the tert-butyl ammonium ion (TBA^+) on Ruthenium 535 bis-TBA or N719 dye with the methoxypropionitrile, acetonitrile and propionitrile solvents on the different electrolyte and ionic liquids.

Figure 4.17 presents Nyquist plots were produced for three cells which all consisted of the N3 dye whereby the first cell had Z-150 electrolyte, which is composed of 150 mM triiodide that is dissolved in a methoxypropionitrile (MPN) solvent. The second cell was made up of N3 dye and the AN-50 electrolyte, which is composed of 50 mM triiodide that is dissolved in an acetonitrile (AN) solvent. The third cell was made up of N3 dye and the PN-50 electrolyte, which is composed of 50 mM triiodide that is dissolved in a propionitrile (PN) solvent.

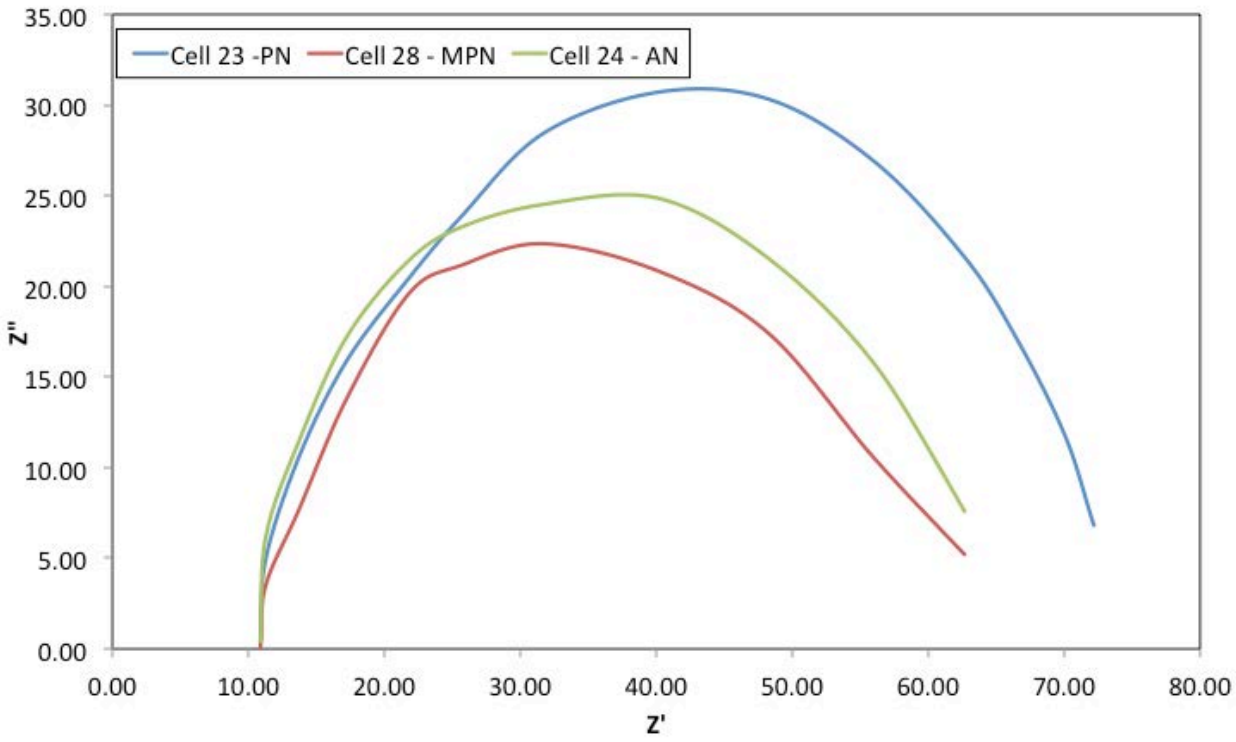

Figure 4.17: *Nyquist plots of dye-sensitized solar cells with Ruthenium 535 or N3dye combined with (a) Z-150 electrolyte, (b) AN-50 electrolyte and (c) PN-50 electrolyte.*

Table 4.2 Percentage differences between the Nyquist plots of cell 23, cell 28 and cell 24 which contain ruthenium 535 (N3) dye and propionitrile (PN), methoxypropionitrile (MPN) and acetonitrile (AN) and based electrolytes.

	% Difference, Cell 23 / Cell28	% Difference, Cell 23/ Cell 24	% Difference Cell 28 / Cell 24
	89.29803206	10.7723372	93.06511863
	29.22980685	24.59156862	76.05090939
	27.40498411	8.236340473	49.09610411
	13.02527638	8.278607085	24.4943388
	4.164537669	4.767361111	9.320035155
	11.3548634	2.538095238	9.946138614
	21.39999098	13.77133333	9.705670197
	32.11957534	19.05154321	19.2515474
	42.55718706	28.95234375	23.68415231
	60.77954846	41.3806338	49.46122214
	75.87989213	64.87960526	45.60629216
SUM	407.2136944	227.2197691	409.6815289
Mean	37.01942677	20.65634264	37.24377535
STDEV.P, Cell23/Cell28			
9.391518185			
STDEV.P, Cell23/Cell24			
0			
STDEV.P, Cell28/Cell24			
7.910220007			

A significant difference was established between the three plots as evident in the percentage difference data presented in Table 4.2. This was also confirmed through calculation of the *P* values to compare the three plots as could be seen in the table.

Figure 4.17 showed that each cell produced only one large semicircle located in the middle of the Nyquist plot which is attributed to the dark reaction impedance caused by charge transport resistance (R_{ct}) at the TiO_2/Dye/Electrolyte interface. The other two semicircles, where one is

located in the low frequency region assigned to the charge transport resistance at the counter electrode and the other semicircle is located on the high frequency region assigned to charge transport resistance for the diffusion the triiodide ion in the electrolyte. The semicircle radius of each cell increases with the change of an electrolyte which lead to the increase of the efficiency of the cells due to the interaction between the, thiocyanate ion (SCN^-) on Ruthenium 535 or N3 dye with the methoxypropionitrile, acetonitrile and propionitrile solvents on the different electrolyte and ionic liquids.

Figure 4.18 shows Nyquist plots were produced for three cells which all consisted of the ruthenium-505 dye whereby the first cell had Z-150 electrolyte, which is composed of 150 mM triiodide that is dissolved in a methoxypropionitrile (MPN) solvent. The second cell was made up of ruthenium-505 dye and the AN-50 electrolyte, which is composed of 50 mM triiodide that is dissolved in an acetonitrile (AN) solvent. The third cell was made up of ruthenium-505 dye and the PN-50 electrolyte, which is composed of 50 mM triiodide that is dissolved in a propionitrile (PN) solvent.

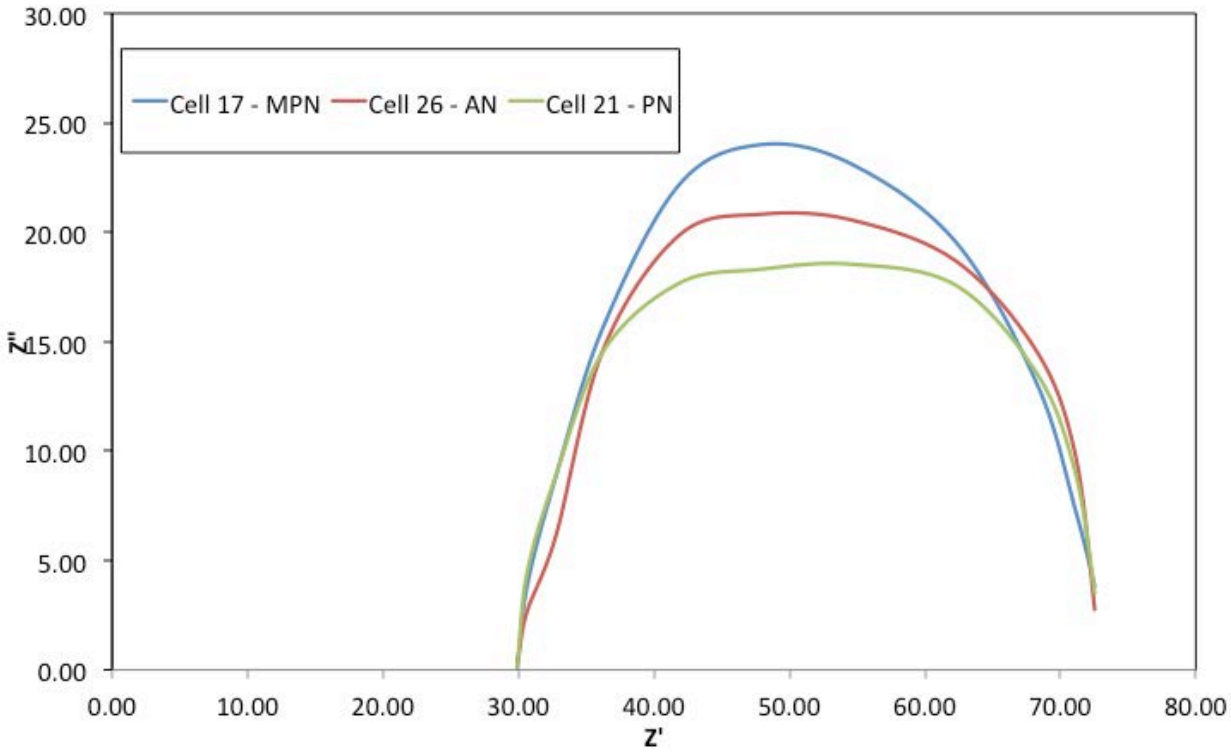

Figure 4.18: *Nyquist plots of dye-sensitized solar cells with Ruthenium 505 dye combined with (a) Z-150 electrolyte, (b) AN-50 electrolyte and (c) PN-50 electrolyte.*

Table 4.3 Percentage differences between the Nyquist plots of cell 17, cell 26 and cell 21 which contain ruthenium 505 dye and methoxypropionitrile (MPN), acetonitrile (AN) and propionitrile (PN) based electrolytes.

% Difference, Cell 17 / Cell 26	% Difference, Cell 17 / Cell 21	% Difference Cell 26 / Cell 21
30.33333333	15.73839095	66.13166165
30.76604555	0.740964894	45.50803243
6.587195122	7.147238456	0.599535936
10.45431034	20.3637931	11.06639839
13.25	23.7257217	12.07575988
11.0527841	19.80576083	9.840641595
4.379084967	10.04803922	5.928571429
11.41544118	3.731617647	6.896551724
34.475	23.38719097	8.24525676

	27.895	8.1469219	27.3879455
SUM	**180.6081946**	**132.8356397**	**193.6803553**
Mean	**18.06081946**	**13.28356397**	**19.36803553**

STDEV.P, Cell 17/ Cell 26
7.886270986
STDEV.P, Cell 17 / Cell 21
7.373614207
STDEV.P, Cell 17 / Cell 21
7.373614207

A significant difference was established between the three plots as evident in the percentage difference data presented in Table 4.3. This was also confirmed through calculation of the *P* values to compare the three plots as could be seen in the table.

Each cell produced in Figure 4.18 only one large semicircle located in the middle of the Nyquist plot which is attributed to the dark reaction impedance caused by charge transport resistance (R_{ct}) at the TiO_2/Dye/Electrolyte interface. The other two semicircles, where one is located in the low frequency region assigned to the charge transport resistance at the counter electrode and the other semicircle is located on the high frequency region assigned to charge transport resistance for the diffusion the triiodide ion in the electrolyte (Hui X. *et al*., 2009).

The semicircle radius of each cell increases with the change of an electrolyte which lead to the increase of the efficiency of the cells due to the interaction between the, cyanide ion ($C\equiv N^-$) on the Ruthenium 505 dye with the methoxypropionitrile, acetonitrile and propionitrile solvents on the different electrolyte and ionic liquids.

4.7 EFFICIENCY MEASUREMENTS AND CURRENT-VOLTAGE (I – V) CURVES

The conversion efficiencies were calculated by using the equation: $\eta = J_{sc} \times V_{oc} \times FF / P_{in}$ where $P_{input} = 0.088W$.

Figure 4.19 presents efficiency performances and measurements of dye-sensitized solar cells with Ruthenium 505, Ruthenium 535 or N3 dye and Ruthenium 535-bis-TBA or N719 dyes combined with Z–150 electrolyte.

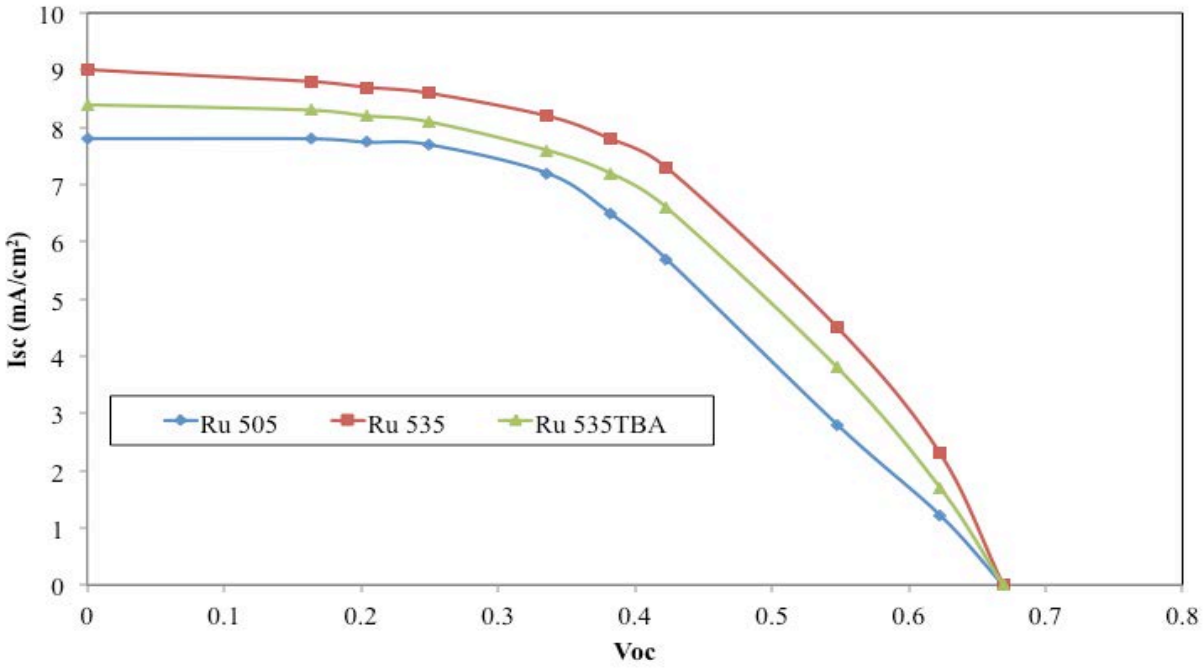

Figure 4.19*: Photocurrent-Voltage (I-V) curves of dye-sensitized solar cells with Ruthenium 505, Ruthenium 535 or N3 dye and Ruthenium 535-bis-TBA or N719 dyes combined with Z–150 electrolyte.*

Three dye-sensitized solar cells were constructed, measured and their I-V curves are presented in Figure 4.19. Cell 17 contained Ruthenium 505 dye and Z–150 electrolyte and it was measured to give a short-circuit current of 0.78 mA/cm^2, an open-circuit voltage of 0.0655 V, a fill factor of 0.30 and an overall cell efficiency of 0.174 %. Cell 28 contained Ruthenium 535 (N3) dye and Z–150 electrolyte and it was measured to give a short-circuit current of 0.90 mA/cm^2, an open-

circuit voltage of 0.0698 V, a fill factor of 0.34 and an overall cell efficiency of 0.243 %. Cell 25 contained Ruthenium 535 bis-TBA (N719) dye and Z–150 electrolyte and it was measured to give a short-circuit current of 0.84 mA/cm^2 , an open-circuit voltage of 0.0669 V, a fill factor of 0.44 and an overall cell efficiency of 0.281 %.

Table 4.4: *I – V Characteristics of dye-sensitized solar cells shown in Figure 4.19*

Cell	**Dye**	**I_{SC} (mA/cm^2)**	**V_{OC} (V)**	**Fill Factor (FF)**	**Efficiency (η) %**
Cell 17	Ru-505	0.78	0.0655	0.30	0.174
Cell 28	Ru-535	0.90	0.0698	0.34	0.243
Cell 25	Ru-535 TBA	0.84	0.0669	0.44	0.281

Efficiency performances and measurements of dye-sensitized solar cells are shown in Figure 4.20 with Ruthenium 505, Ruthenium 535 or N3 dye and Ruthenium 535-bis-TBA or N719 dyes combined with AN–50 electrolyte.

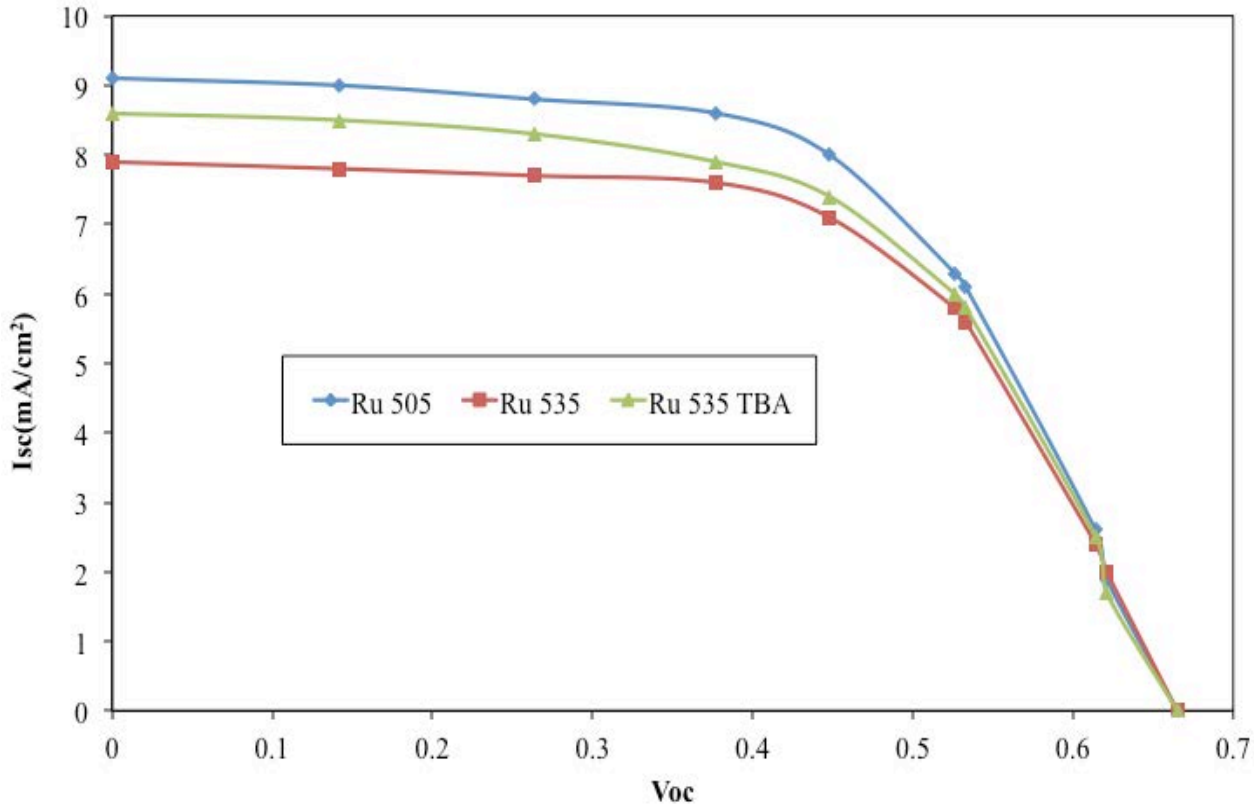

***Figure 4.20**: Photocurrent-Voltage (I-V) curves of dye-sensitized solar cells with Ruthenium 505, Ruthenium 535 or N3 dye and Ruthenium 535-bis-TBA or N719 dyes combined with AN–50 electrolyte.*

Three dye-sensitized solar cells were constructed, measured and their I-V curves are presented in Figure 4.20. Cell 26 contained Ruthenium 505 dye and AN–50 electrolyte and it was measured to give a short-circuit current of 0.91 mA/cm^2, an open-circuit voltage of 0.0599 V, a fill factor of 0.27 and an overall cell efficiency of 0.167 %. Cell 24 contained Ruthenium 535 (N3) dye and AN–50 electrolyte and it was measured to give a short-circuit current of 0.79 mA/cm^2 , an open-circuit voltage of 0.0662 V, a fill factor of 0.37 and an overall cell efficiency of 0.220 %. Cell 27 contained Ruthenium 535 bis-TBA (N719) dye and AN–50 electrolyte and it was measured to give a short-circuit current of 0.86 mA/cm^2 , an open-circuit voltage of 0.0623 V, a fill factor of 0.43 and an overall cell efficiency of 0.262 %.

Table 4.5: *I – V Characteristics of dye-sensitized solar cells shown in Figure 4.20*

Cell	Dye	I_{SC} (mA/cm^2)	V_{OC} (V)	Fill Factor (FF)	Efficiency (η) %
Cell 26	Ru-505	0.91	0.0599	0.27	0.167
Cell 24	Ru-535	0.79	0.0662	0.37	0.220
Cell 27	Ru-535 TBA	0.86	0.0623	0.43	0.262

Figure 4.21illustrates efficiency performances and measurements of dye-sensitized solar cells with Ruthenium 505, Ruthenium 535 or N3 dye and Ruthenium 535-bis-TBA or N719 dyes combined with PN–50 electrolyte.

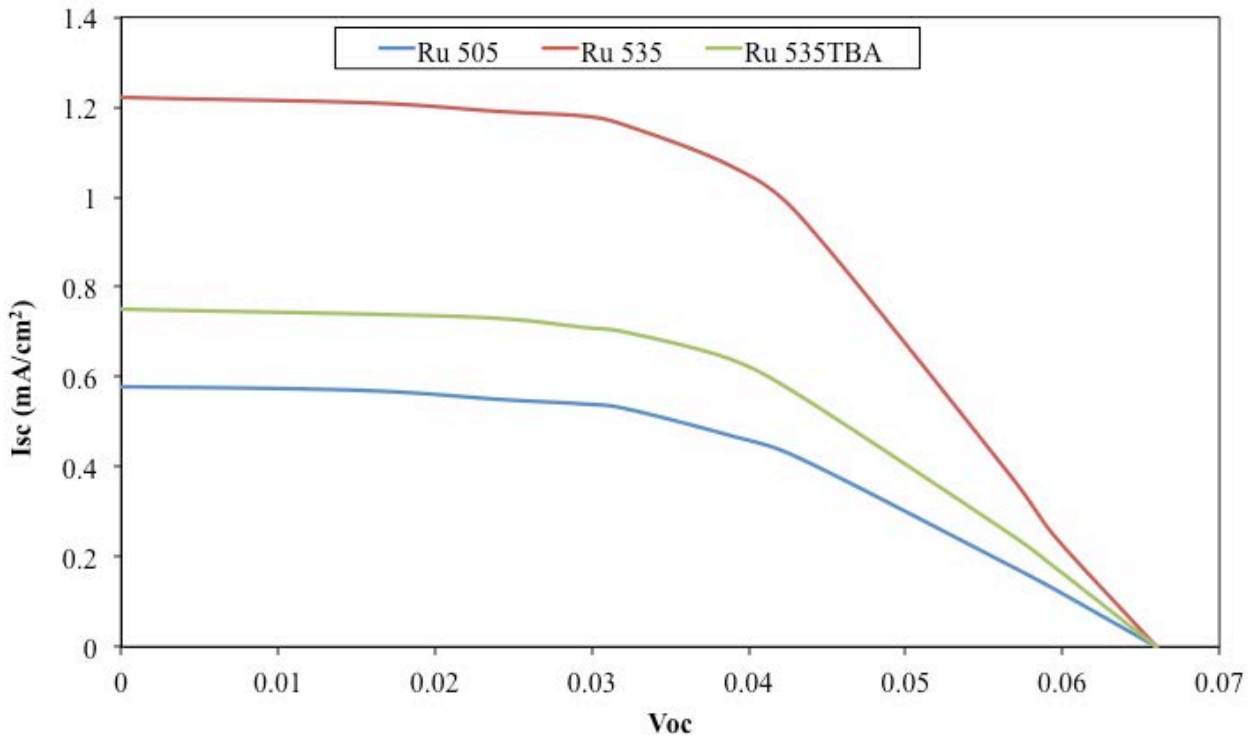

Figure 4.21*: Photocurrent-Voltage (I-V) curves of dye-sensitized solar cells with Ruthenium 505, Ruthenium 535 or N3 dye and Ruthenium 535-bis-TBA or N719 dyes combined with PN–50 electrolyte.*

Three dye-sensitized solar cells were constructed, measured and their I-V curves are presented in Figure 4.21. Cell 21 contained Ruthenium 505 dye and PN–50 electrolyte and it was measured to give a short-circuit current of 0.78 mA/cm^2, an open-circuit voltage of 0.0655 V, a fill factor of 0.30 and an overall cell efficiency of 0.161 %. Cell 23 contained Ruthenium 535 (N3) dye and PN–50 electrolyte and it was measured to give a short-circuit current of 1.22 mA/cm^2, an open-circuit voltage of 0.0592 V, a fill factor of 0.31 and an overall cell efficiency of 0.254 %. Cell 22 contained Ruthenium 535 bis-TBA (N719) dye and PN–50 electrolyte and it was measured to give a short-circuit current of 0.75 mA/cm^2 , an open-circuit voltage of 0.0601 V, a fill factor of 0.42 and an overall cell efficiency of 0.215 %.

Table 4.6 : *I – V Characteristics of dye-sensitized solar cells shown in Figure 4.21*

Cell	**Dye**	**I_{SC} (mA/cm^2)**	**V_{OC} (V)**	**Fill Factor (FF)**	**Efficiency (η) %**
Cell 21	Ru-505	0.58	0.0660	0.37	0.161
Cell 23	Ru-535	1.2	0.0592	0.31	0.254
Cell 22	Ru-535 TBA	0.75	0.0601	0.42	0.215

Table 4.4, 4.5 and 4.6 present I-V curves of dye-sensitized solar cells shown in Figure 4.19, 4.20 and 4.21 respectively. The fill factors decreased as the I_3^- concentration is lowered accompanying an increase in the total resistance. As a result, conversion efficiencies were lowered in accordance with fill factors. Recombination between the injected electrons in TiO_2 and I_3^- ions in electrolyte were established to be the main factor in determining I-V characteristics.

CHAPTER 5

SUMMARY, CONCLUSION AND RECOMMENDATIONS

5.1 SUMMARY OF MAJOR FINDINGS

5.1.1 SEM/EDX ANALYSIS

The surface morphology, surface area, TiO_2 crystal phase, and the dispersion of TiO_2 nanoparticles are the most important factors influencing the properties of a photoanode.The surface state and the morphology of the different TiO_2 films were evaluated by the scanning electron microscopy.The appearance of cracks, unevenness, lumps and roughness, TiO_2 surface morphology of the doctor-bladed photoanode presented on Figure 4.1 (a) – Figure 4.1(d) and on Figure 4.3 (a) – Figure 4.3 (b) indicated poor adherence onto the glass substrate and poor optical uniformity of the films and that the arrangement of TiO_2 particles are loosely packed as the magnification was reduced from 250 μm to 2.5 μm and could not enhance the light harvesting efficiency of the cells.

These discrepancies were supposed to be conquered by the sintering process whereby the films were heated from 400^{o}C to 450^{o}C so that the particles would form connections between each other and be interconnected to make electron percolation in the TiO_2 layer effective. Therefore it would be impossible to construct cells using the Degussa P25 and Ti-nanoxide D/SP pastes, because after sintering, their particles were not even connected to the F-doped SnO_2 layer.

Furthermore, their ohmic resistance would be increased and electrons would be unable to hop from particle to particle to reach the back contact from every part of the structure.

The commercially-coated and screen-printed TiO_2 films shown in Figure 4.5 (a) and Figure 4.6 (b), with magnifications of 2.5μm and 1.0 μm respectively, were observed to be smooth and uniform with good adherence and good optical properties. The TiO_2 particles presented in Figure 4.5 (b) were observed to be closely packed and were homogenously dispersed throughout the film. Figure 4.5 (a) showed some voids between the closely packed TiO_2 nanoparticle, which were observed on the porous TiO_2 layers. It can be concluded that from the SEM analysis the screen-printed commercial film revealed a smoother surface morphology characteristics in comparison to the doctor-bladed TiO_2 electrodes. Unfortunately, the average particle sizes presented in Figure 4.5 (a) and (b) were not measured by the scanning electron microscope, because they can only be measured by the transmission electron microscope.

The elemental analysis of this titania films were conducted using the energy dispersive x-ray analyser, which confirmed the existence of titanium atoms and oxygen atoms with different compositions.All the EDX spectra were interpreted using the x-ray microanalysis periodic table and they unanimously observed titanium at 0.326 eV due to the high oxidation state of Ti (IV) followed by its highest peak at 4.35 eV and at 4.89 eV, because of a decline of an oxidation state to Ti (III). The oxygen atom was observed at 0.523 eV in all the samples and other trace elements such as nitrogen, gold, aluminium and niobium were also observed and they emanated from the traces of some impurities and coating applied on the titania film before SEM micrographs were generated. The EDX spectrum of a TiO_2 film prepared from Degussa P25

powder presented in Figure 4.2 contained 76.5% of the TiO_2compound. The EDX spectrum of a TiO_2 film prepared from Ti – nanoxide D/SP presented in Figure 4.4 contained 84.14% of the TiO_2 compound. The EDX spectrum of a commercially screen-printed TiO_2 film presented in Figure 4.6 contained 92.25 % of the TiO_2 compound. The Degussa P25 and Ti – nanoxide titania paste samples were of less purity that the commercial TiO_2 film which contained less trace elements.

5.1.2 XRD ANALYSIS

The crystalline phases of the titanium dioxide powder and films were performed by the x-ray diffraction spectrometer and all the XRD patterns showed strong and sharp peaks which reflected good crystallinity. The patterns displayed confirmed that these films were dominated by the anatase phase and minimal amounts also existed with the films. No brookite phase was present, because its distinctive peak is normally observed at 30.8^{o}. The morphology of the anatase phase is mainly spherical and the rutile phase can exhibit both a spherical and a rod shape.

Figure 4.7, 4.8 (a) and 4.8 (b) illustrated peaks on the XRD patterns which are in good agreement and have been compared with reference to the standard spectrum (JCPDS no.: 88-1175 and 84-1286) database for the diffraction patterns of both anatase and rutile phase. The size of the particles was in the range 32–62 nm for anatase and 27–32 nm for rutile. The Degussa P25 TiO_2 powder XRD pattern presented on Figure 4.7 is composed of irregular amorphous polycrystalline structures that are composed of both the anatase phase and the rutile

phase. The diffraction peak $2\theta = 25.3^{o}$ is broadened and the intensity is increased which confirms the increase of the increased particle sizes of the powder.

The narrowing of the distinctive (101) peak at 25.3^{o} on Figure 4.8 (b) compared to Figure 4.8 (a) illustrates the increase in particle size. Furthermore, the diffraction pattern peak intensity of the Ti – nanoxide D/SP TiO_2 film in Figure 4.8 (a) commercial titania paste was higher compared to that of the commercially coated TiO_2 film in Figure 4.8 (b) to its increased particle size. The intensity of the titania film in Figure 4.8 (b) is lower than the titania film in Figure 4.8 (a) because the commercially coated TiO_2 film is commercialized and has been detected to be fully synthesized.

5.1.3 UV-VIS ANALYSIS

The electronic spectral studies of the three ruthenium-based dyes were recorded on a Perkin Elmer Lambda 35 UV – Vis Spectrophotometer from 200 nm to 900 nm of the UV-Vis spectra.The UV-Vis spectra of the ruthenium 505, ruthenium 535 and ruthenium 535 bis – TBA dye samples in ethanol revealed two broad bands which are all assigned to metal-to-ligand charge transfer (MLCT) origin from the Ruthenium metal centre to the π^* orbitals on the pyridyl ligand as shown in Figure 4.9, Figure 4.10 and Figure 4.11 respectively. The ruthenium 535 dye presented in Figure 4.10 was observed to have the highest transitions in the visible region, at 532 nm and at 395 nm than the other two dyes, which means that when it is used in a photochemical cell, the oxidized dye is expected to inject an electron into the TiO_2 and would be quickly reduced by a redox species in the surrounding electrolyte faster than other dyes.

5.1.4 FTIR ANALYSIS

The FTIR spectra of the three ruthenium-based dyes were recorded on a Perkin Elmer Spectrum 2000 FTIR on KBr discs. It has been observed in Figure 4.12, Figure 4.13 and Figure 4.14 that although the infrared spectra contain many peaks, it is very critical to outline that the positions of specific absorptions have divided the infrared region from 4000 to 400 cm^{-1} into four parts.
The infrared absorption spectra of the ligands and the complexes share many common characteristic features as series of weak to moderate absorptions in the 3,746 – 3,355cm^{-1} region which are assigned to aromatic N – H, C – H single-bond stretching motions and/or considered indicative of the presence of O – H groups in the compounds.

Therefore the region from 4000 to 2500 cm^{-1} corresponds to absorptions caused by N-H, C-H, and O-H single-bond stretching motions. N-H and O-H bonds absorb in the 3300 to 3600 cm^{-1} range; C-H bond stretching occurs near 3000 cm^{-1}. The region from 2500 to 2000 cm^{-1} is where triple bond stretching occurs. Both nitriles (RC≡N) and alkynes absorb in this region. The region from 2000 to 1500 cm^{-1} is where double bonds of all kinds (C=O, C=N, and C=C) absorb. Carbonyl groups generally absorb in the range 1680 to 1750 cm^{-1}, and alkene stretching normally occurs in the narrow range 1640 to 1680 cm^{-1}. The region below 1500 cm^{-1} is the fingerprint region of the infrared spectrum. A large number of absorptions due to a variety of C-C, C-O, C-N and C-X single-bond vibrations occur in this region.

The IR spectra of these ruthenium complexes presented on Figure 4.12, 4.13 and 4.14 were consistent to evidently present strong vibrational bands at 1364 cm^{-1}, 1635 $cm^{-1}$and at 1759 cm^{-1}

which represent carbonyl groups and would mainly suggest the dyes stood a good chance of adsorbing of anchoring on a TiO_2 surface via two carboxylate groups per dye molecule to form a bridging or bidentate chelate coordination. The spectra of N3 and N719 dyes in Figure 4.14 and Figure 4.15 revealed a sharp peak is observed at 2361 cm^{-1} and is attributed to the existence of a triple bond motion with increased intensity of the stretching band of ν(C≡N) instead of a stretching band of the thiocyanate ligand ν(N=C=S) at 2100 cm^{-1}. The thiocyanate stretching band could not be observed due to the fact it possibly suffered weak degradation either from the ultraviolet radiation during the UV – Vis spectroscopy analysis or exposure to air/humidity.

5.1.5 PL ANALYSIS

The emission or luminescence spectra of the ruthenium-based dye complexes that are dissolved in ethanol solution with excitations at various wavelengths using and are presented in Figure 4.15 to confirm that there is a direct proportionality between molecular weights and molar extinction coefficients of the dyes. Consequently, there is an inverse proportionality between the molecular weights of the dyes and emission wavelengths of the dyes. Hence, the dye with the least molecular weight was observed near the infrared region at 723 nm. The conjugated functional organic molecules are useful for the study of electron transport at the molecular scale. The most stable and effective dye is expected to be the N719 dye which has the least wavelength and greater solubility than all the dyes.

The luminescent properties of a complex as well as its ability play the role of excited state reactant or product are related to the energy ordering of its low energy excited state and,

particularly, to the orbital nature of its lowest excited state. It is crucial to note that ligands in a complex have significant effects, which in turn influence the energy positions of the metal centre (MC) and ligand centre (LC), as well as the metal-to-ligand charge transfer (MLCT). The energy of the MC excited state depends on the ligand field strength, which in turn depends on the δ-donor and π-acceptor properties of the ligands and the bite angle of the polydentate ligands. The energy of the LC excited state depends on the intrinsic properties of the ligands such as HOMO-LUMO energy gap and the singlet-triplet splitting. Moreover, the energy of the MLCT excited state is highly dependent on the reduction potential of the ligand involved in the MLCT transition, the oxidation potential of the metal in the complex and by the charge separation caused by the transition. The intense emission found in these complexes is a significant contribution to the excited state from an interaction between the metal d-orbital and the ligand π-system.

5.1.6 EIS ANALYSIS

In order to investigate the electron transport property in TiO_2, EIS measurements were employed. Figure 4.16 to Figure 4.18 present Nyquist plots of the electrochemical impedance spectra of completed cells made up of measured under 100 $mW.cm^{-2}$. All the Nyquist plots exhibited only one large semicircle in the low frequency region fitted to a transport resistance (R_w), which is ascribed to the accumulation or transport of the injected electrons within the TiO_2 films and the charge transfer across either the TiO_2/redox electrolyte interface or the TiO_2/FTO interface. Furthermore, the semicircles that are usually small and are in the frequency range of less than 0.1 M Ω, they are normally assigned to the charge transfer resistance (R_{ct}) at the

redox/electrolyte/Pt counter electrode or TiO_2 interfaces. These small semicircles were absent in all the Nyquist plots which confirmed that the electron transfer at the redox/electrolyte/Pt counter-electrode and/or TiO_2 interfaces was not efficient. The more efficient electron transfer only occurred at the TiO_2/dye/electrolyte interface due to loose mechanical contact between TiO_2 layers and the conducting glasses. The poor contact between film layers and glass substrates then led to high resistances and therefore low conversion efficiencies (Yeon S.H. *et al*., 2011).

In Figure 4.16 Nyquist plots of three cells are presented and the most stable cell was cell 22, which was composed of the N719 dye and the propionitrile-containing electrolyte followed by cell 27 with N719dye and the acetonitrile-containing electrolyte. The least stable and efficient was cell 25, which contained N719 dye and the methoxypropionitrile-containing electrolyte.
The N719 dye interacted well with the three electrolytes although the performance was not good because the highest efficiencies were exhibited by it. Figure 4.16 shows impedance spectra of the size of the middle arcs for cell 22 and cell 27 with propionitrile and acetonitrile are smaller than that of cell 25 but their characteristic frequency has been observed to be higher than that of cell 25 which contains methoxypropionitrile. Although the methoxypropionitrile solvent is highly viscous, but it possesses additives such as the alkyl benzimidazole and guanidine thiocyanate which are added to electrolytes so that they can be adsorbed on the surface of the TiO_2 electrode and prevent the leaking of injected electrons to the electrolyte and I_3^- from approaching the surface of the TiO_2 electrodes so as to improve the performances of dye solar cells. This smaller arc or semicircle that contains higher amounts of characteristic frequency suggests that a larger amount of electrons are injected in TiO_2, but the injected electrons are lost more rapidly. This is attributed by the low viscosity of solvents (acetonitrile and propionitrile) in the electrolytes.

In Figure 4.17 Nyquist plots of three cells are presented and the most stable cell was cell 28 which was composed of the N3 dye and the methoxypropionitrile-containing electrolyte followed by cell 24 with N3 dye and the acetonitrile-containing electrolyte. The least stable and efficient was cell 23 which contained N3 dye and the propionitrile-containing electrolyte.

The impedance spectra of cell 23 and cell 24 shown in Figure 4.17 show that their middle arcs were enlarged as I_3^- decreased from 150 mM (MPN) to 50 mM (PN and AN) accompanying a decrease in characteristic frequency of their semi-circles. Triiodide ions recombine with injected electrons (charge transfer at TiO_2|electrolyte) on the surface of TiO_2. The low characteristic frequency reflects long recombination lifetime of the injected electrons (electron lifetime in TiO_2). Therefore, as the fraction of I_3^- decreases in cell 23 and 24 of Figure 4.17, the arcs/semicircles expanded with an increase in the short circuit current. However, An impedance component of diffusion in TiO_2 in high concentration of I_3^-, would suggest that electron concentration became low due to frequent recombination with I_3^- under high I_3^- concentration of cell 28.

In Figure 4.18 Nyquist plots of three cells are presented and the most stable cell was cell 21 which was composed of the ruthenium 505 dye and the propionitrile-containing electrolyte followed by cell 26 with ruthenium 505 dye and the acetonitrile-containing electrolyte. The least stable and efficient was cell 17 which contained ruthenium 505 dye and the methoxypropionitrile-containing electrolyte.

The enlargement of the two arcs or semicircles in cell 17 and cell 21, is attributed by a decrease of cations in the methoxypropionitrile and propionitrile containing electrolytes. Insufficient number of cations in an electrolyte limits the diffusion of electrons in TiO_2 and consequently

charge transfer resistance in TiO_2|electrolyte interface becomes large leading to a decrease of electron concentration in TiO_2. In contrast, cell 26 had a decreased arc of semicircle due to the presence of lithium cations on the acetonitrile-based electrolyte. Lithium ions do not only stay on the surface of TiO_2 film but have a tendency of penetrating into the TiO_2 lattice and thus the energy level of the conduction band of TiO_2 results in a positive shift since Li^+ is a strong electropositive cation. Then the band gap between the excited state of the dye and conduction band of TiO_2 spreads, and electrons can be effectively injected from dye to TiO_2 accompanying an increase in the short-circuit current. However, positive lithium ions (Li^+) have a tendency of creating deeper trap sites, that can prevent injected electrons from transferring smoothly in TiO_2, and charge recombination between the injected electrons and I_3^- occurs through these sites especially when the dye in inefficient like the ruthenium 505 dye used in Figure 4.18 (Hoshikawa, et al.; 2005).

The increase in the impedances shown from Figure 4.16 to Figure 4.18 illustrated the increase of the charge transfer resistance due to the recombination of electrons at the TiO_2/electrolyte interface. Therefore, the EIS analysis proved that the N719 dye-containing cells possessed the lowest transfer resistance and would possibly have the longest electron lifetime compared to the cells made up of N3 and ruthenium 505 dyes studied.

5.2 SUMMARY OF CONTRIBUTIONS

The thin films were characterized by SEM/EDX and XRD analysis and it was observed that good adherence and optical properties, such as porosity and a smooth surface area of a titanium dioxide film, are crucial for the stability of the entire photochemical cell.The ruthenium-based dyes were characterized by UV-Vis, FTIR and PL analysis and for those complexes containing the thiocyanate ion ligand, it seemed to be the most sensitive part of the dye and to avoid degradation in dye-sensitized solar cells the cells need to be completely sealed to protect them from leakages, moisture, evaporation and UV – radiation.

The constructed cells were analyzed by the EIS spectroscopy and it has been a very powerful technique to define recombination lifetime and resistive elements on the photovoltaic performance of dye sensitized solar cells. Nyquist plots were used to investigate the resistance relation for the charge transfer process at the Pt counter electrode, resistance for TiO_2/electrolyte interface and Nernst diffusion in the electrolyte.

The high energy conversion efficiencies exhibited by dye-sensitized solar cells have been one of the reasons for the rapid interest that expanded in the DSSC research. However, it has been observed that there has been an inadequate charge transfer on the sensitizer dyes, hence the low efficiencies obtained which were less than 1%.

5.3 CONCLUSION

For dye-sensitized solar cells to be economically viable and commercially feasible, it can be concluded that they should be able to maintain a non-degrading performance in operating conditions for several years. However, the issue of long-term stability of these cells remained unsolved on this research due to the increased ohmic resistances that made it almost impossible for electrons to hop from particle to particle and reach the back contact from every part of the structure and led to a quick degradation of the cells hence the low conversion efficiencies.

Possible sources of degradation and poor performances of these dye solar cells constructed in this research are attributed to and include: the photochemical degradation or desorption of the dye i.e. replacement of ligands by electrolyte species or residual water molecules, direct band-gap excitation of TiO_2 i.e. holes in the valence band of the semiconductor act as strong oxidants, photo-oxidation of the electrolyte organic solvent by releasing protons from the solvent, catalytic reactions by TiO_2 and platinum, failure or inadequate barrier properties of the sealant material, changes in the structure of the semiconductor, dissolution of platinum from the counter-electrode, and adsorption of decomposition products onto the TiO_2 and TCO surfaces. The stability of the dye-sensitized solar cells depends greatly on the designed chemical composition and the materials of the cells as well as on any unwanted impurities possibly included during the preparation of the cells.

Therefore, these are some of the reasons why different cells exhibited some inconsistent stability. Also, the Gratzel group (Kohle et.al, 1997) reported that the other cause for the

instability of the dyes was the inadequate conditions for the re-generation of the dye, i.e. too low iodide concentrations in the electrolytes.There are certain chemicals such as the 4-tert-butylpyridine (TBP) which are found to enhance the stability of the dye solar cells. TBP is attached on the N719 dye and is known to increase tolerance towards water in the electrolyte. Pure nitrile-based organic solvents, such as acetonitrile and propionitrile are found to be the most stable amongst organic solvents. When the ruthenium-based dyes release electrons and become oxidized by the titanium dioxide, the electrolytes supply electrons to replenish the deficiency. This rearranges the dye molecules back to their original states. As a result, electrolytes become oxidized and electron-deficient and migrate towards the cathode to recover their missing electrons. When electrons migrate through the circuit they recombine with the oxidized form of the ruthenium complexes when they reach the cathode.

The photoelectrochemical and chemical stability of organic solvents such as methoxypropionitrile, propionitrile and acetonitrile were considered and were employed in dye-sensitized solar cells. In most efficient solar cell this transport of ions relies on acetonitrile and propionitrile which are known to be of low viscosity and are volatile organic solvents. Methoxypropionitrile is a low volatility organic solvent and is usually used to build stable, commercially viable solar cells. It has the ability to react with trace water in the electrolyte to produce a corresponding amide, which decreases the conductivity of the electrolyte. Methoxypropionitrile, apart from being the most stable solvent, is more viscous than propionitrile and acetonitrile solvents, inhibiting the flow of ions in the electrolyte. Slowing down the move of electrons does not only reduce the efficiency of the cell, but also contributes to

faster aging, as more of ruthenium complexes react with electrons in the semiconductor anode instead of with electrons at the cathode, resulting in rapid recombination losses.

The photochemical and thermal stabilities of ruthenium complexes have been studied investigated and reported that the NCS ligands on the Ru-535 (N3) dye and Ru-535 bis-TBA (N719) dye are oxidized to produce a cyano group (-CN) under irradiation in ethanol solution measured by UV-Vis spectroscopy. The degradation of the NCS ligand to the CN ligand by an intramolecular electron transfer reaction which reduces consequently the Ru (III) to Ru (II) state, occurs within 0.1 second to 1.0 second, whereas the rate of the reduction of Ru (III) to Ru (II) by the direct electron transfer from iodide (I^-)ions into the dye cations is on the order of nanoseconds. This illustrates that one molecule of all these ruthenium-based dyes were supposed to contribute to the photon-to-current conversion process with a turnover number of at least 10^7 – 10^8 without any degradation. Taking this into consideration, these dyes were expected to be sufficiently stable in the redox electrolyte under irradiation.

Since the photo-excited electrons of dyes that are adsorbed on the surface of semiconductor are injected in the conduction band of titanium dioxide, the injected electrons then diffuse in TiO_2 and get to the outer circuit through the back contact. Moreover, the oxidized dyes are quickly regenerated by iodide ion (I^-) and the resultant triiodide ion (I_3^-) is transferred to the counter electrode and reduced by electrons from the outer circuit. Most charge-transfer processes are involved in power generations and impedance spectroscopy has been found to be very useful for the analysis of such processes. Impedance spectroscopy analyzed a wide variety of

electrochemical processes and internal resistances which govern the performances of dye-sensitized solar cells.

Moreover, the electrolytes of the dye-sensitized solar cells used in this research project contain I^-/I_3^- redox couple and are evaluated from three essential characteristics for power generation that is efficient. The characteristics include quick regeneration of oxidized dyes and the charge transfer between TiO_2 electrodes and counter electrode. Also, the protection of the TiO_2 electrode surface is essential because tiny TiO_2 particles do not have electric barrier on the surface, and consequently, the injected electrons in the electrodes have a tendency of reacting with I_3^- in the electrolyte and therefore cause recombination. Finally, cations of the electrolyte contribute towards smooth electron transfer in the TiO_2 electrode whereby a huge portion of cations on the surface form charge pairs with injected electrons on the semiconductor in order to keep their interface neutral. Thus, the injected can transfer in TiO_2 without electric binding.
Redox couple such as I^-/I_3^- in electrolyte transfers charge between the TiO_2 electrode and the counter electrode, and redox reaction of this couple occurs at each electrode. The difference in concentrations of I^- and I_3^- have a huge impact on the performance of the dye solar cells.

Therefore, in this research project it can be concluded that recombination between the injected electrons in TiO_2 and I_3^- in the electrolyte suppressed the high performance of dye solar cells assembled and small impedance components and its low characteristic frequency is favorable for high performance of the cells. The viscosity and triiodide ion concentration of the electrolytes have the potential to influence the impedance spectrum and performance of the dye solar cells. Particularly, the impedance component of the middle arc which is attributed to diffusion of I_3^- is expected to change significantly by difference in the viscosity of the electrolyte.

5.4 RECOMMENDATIONS ON FUTURE RESEARCH

This research investigated the characterization and the electrochemistry of dye-sensitized solar cells with the aim of identifying the spectral responses and stabilities of the commercial dyes as well as understanding the electrochemical properties of dye/semiconductor/electrolyte interface. However, there are still some aspects that need to be investigated, which include:

- Construction of highly stable dye-sensitized solar cells with high photon – to – current conversion efficiencies > 10%.
- Synthesis of non-degrading dyes rather than buying ready-made dyes and also exploring other transition metals except ruthenium.
- Optimizing operating temperatures when characterizing the individual components of the dye-sensitized solar cells.
- Explore research on other electrolytes than liquid electrolyte.
- Improve on coating methods of titania pastes to avoid agglomeration of pastes.
- Optimization of the thickness of the films.
- Synthesis of dye solar cells with a high surface area which will enable larger amounts of dyes to adsorb on TiO_2 surface and produce larger amounts of photocurrent as well good performances.

Finally, for future research purposes, the long term stability of DSSCs can be enhanced by various components, such as the intrinsic photochemical stability of the sensitizer dyes adsorbed onto the TiO_2 electrode and in interaction with the surrounding electrolyte;

chemical and photochemical stability of the electrolyte; the stability of the platinum-coating of the counter-electrode in the electrolyte environment; and the quality of the barrier properties of the sealing of the cell against the intrusion of water and oxygen from ambient air, and against the loss of electrolytes from the cells through the sealing process. The interaction of these factors makes the dye solar cell operation very complex. These products may furthermore interact with the dye molecules or other species at the TiO_2/electrolyte interface with deleterious effects to the performances of the cells in the long term.

REFERENCES

Addamo M., Bellardita M., Di Paola A., and Leonardo Palmisano L. (2006) "Preparation and photoactivity of nanostructured anatase, rutile and brookite TiO_2 thin films" Royal Society of Chemistry Journal Chem. Comm., 4943 – 4945.

Adeloye A.O., Ajibade A.P., Cummings F., (2011); "Synthesis, Photophysical and Preliminary Investigation of DSSCs"; Fort Hare Institute of Technology, University of Fort Hare; 12 – 14.

Agrell H.G., (2003); "Interactions in dye-sensitized solar cells", Uppsala University; PhD Thesis; 12 – 22.

Alsema E.A., Nieuwlaar E, (2010); "Energy viability of photovoltaic systems"; Energy Policy 26-28.

Al-Arifi A.S.N., (2004); "Determination of titanium oxidation states"; Applied Polymer Science Journal; Volume 93; 56 – 62.

Athanasius J., Murphy P.J. (2012) "Dye-Sensitized Solar Cells based on poly (3-hexyl thioacetate thiophene", International Journal of Physical Science Vol 8(1); 16 – 26.

Bard A.J, Faulkner L.R (2000); “Electrochemical Methods; Fundamentals and Applications”; Wiley Interscience Publications; 6 – 8.

Bard A.J, Faulkner L.R., 1980 “Electrochemical Methods, Fundamentals and Applications” Third Edition; John Wiley and Sons, New York, 1980, 34.

Barsoukov E., Macdonald J.R, (2005); “Impedance Spectroscopy; Theory, Experiment, and Applications”; Second edition.; Wiley Interscience Publications, 1 – 5.

Bisquert J.,Palomares E .,Quiñones C.A., (2006) “Effect of Energy Disorder in Interfacial Kinetics of Dye-Sensitized Solar Cells with Organic Hole Transport Material” American Chemical Society; *J. Phys. Chem. B,* **2006**, *110* (39), 19406–19411.

Brett C.M.A, Brett A.M.O, (1993) “Electrochemistry: Principles Methods and Applications” Sixth Edition; Oxford University Press, 82.

Cahen D., 2000; “Nature of photovoltaic action in dye-sensitized solar cells”, Phys.Chem. Journal, 104, 2053 – 2059.

Ceroni P., Balzani V. (2011)“Photoinduced Energy and ElectronTransfer Processes” Department of Chemistry, University of Bologna, Italy; 21 – 36.

Chiba, Y.; Islam, A.; Komiya, R.; Koide, N. & Han, L. (2006). Conversion efficiency of 10.8% by a dye-sensitized solar cell using a TiO2 electrode with high haze. Applied Physics Letters, 88.

Chen H., (2008) "Dye-sensitized solar cells using ZnO nanotips and Ga-doped ZnO films"; University of New Jersey; PhD Thesis; 22 – 26.

Connolly J. R., (2007), "Introduction to X-Ray Powder Diffraction"; Spring – EPS400-002; 2 – 9.

Daeneke, T., Mozer, A. J., Kwon, T., Duffy, N. W., Holmes, A. B., Bach, U. & Spiccia, L. (2012).; "Dye regeneration and charge recombination in dye-sensitized solar cells with ferrocene derivatives as redox mediators." Energy and Environmental Science, 7090-7099.

Diebold,U., Surf. Sci. Rep. 48 (2003) 53.

Dykstra M. J.; (1993) "A Manual of Applied Techniques for Biological Electron Microscopy" Second Edition, Spiral Bound; ISBN 03064-44496; 272.

Feldt S., (2012) "Alternative Redox Couples for Dye-Sensitized Solar Cells"; Uppsalla University; PhD Thesis, 27.

Gamstedt H., (2005) “Ionic Liquid Electrolytes for Photoelectrochemical Solar Cells”, Royal Institute of Technology, Sweden; PhD Thesis; 2 – 6.

Gremlich, H.U.,Yan, B., (2000) “Infrared and Raman Spectroscopy of Biological Materials”, Marcel Dekker, New York; 7 – 8.

Gratzel M. (2003); “Dye-sensitized solar cells” Laboratory for Photonics and Interfaces, Swiss Federal Institute of Technology, CH-1015 Lausanne, Switzerland; 145 – 153.

Gimenez S., Rogach A. L.*, et.al*., (2011) “Energy Transfer versus Charge Separation of Ruthenium based dyes” , Department of Physics and Material Science, Applied Journal of Applied Physics, City University of Hong Kong,; 110.

Hagfeldt A., Gratzel M., (2009) “Enhancing the Light Harvesting capacity of the Photoanode Films in DSSCs”; Molecular Photovoltaics; Acc. Chem Res; 12 -16.

Halme J. (2002) “Dye-sensitized nanostructured and organic photovoltaic cells: technical review and preliminary tests” Helsinki University of Technology, MSc Thesis; 29 – 30.

Han, L.; Koide, N.; Chiba, Y.; Mitate, T. Modeling of an equivalent circuit for dye-sensitized solar cells. *Appl. Phys. Lett.,***2004**, *84* (13), 2433-2435.

Han, L.; Koide, N.; Chiba, Y.; Mitate, T.; Islam, A. Modeling of equivalent circuit for dye

sensitized solar cells: improvement of efficiency of dye-sensitized solar cell by reducing internal resistance. *Comptes. Rendus. Chime.,* **2006**, *9,* 645-651.

Hannewald K., Glutsch S., Bechstedt F., (2002)"Theory of photoluminescence excitation spectroscopy in semiconductors"; Institut für Festkörpertheorie und Theoretische Optik, Department of Applied Physics, Eindhoven University of Technology; 1 – 6.

Hara K., Arakawa H., (2003); "Dye-sensitized solar cells" National Institute of Advanced Industrial Science and Technology; John Wiley and Son Ltd; Japan, 663 – 672.

Haque S.A., Palomares E., Cho B.M., Green A.N., Hirata N., Klug D.R., Durrant J.R., (2005); "Charge separation versus recombination in dye-sensitized nanocrystalline solar cells: the minimization of kinetic redundancy"; American Chem. Society Journal; 3456 – 3462.

Henrich V.E., Cox P.A. (1994); "The surface science of metal oxides" Second Edition; Cambridge University Press, pp 43 – 48.

Hoshikawa T., Ikebe T., Eguchi K., et al.; (2006) "Effects of electrolyte in dye-sensitized solar cells and evaluation by impedance spectroscopy";Department of Energy and hydrocarbon Chemistry, Graduate school of Engineering, Kyoto University; pp 5286 – 5294.

http://cdn.intechopen.com/pdfs/8565/InTechPhoton_management_in_dye_sensitized_solar_cells.pdf

Huang S.Y., Schlichthorl G., Nozik A. J., Gratzel M., Frank A.J., (1997) Charge recombination in dye-sensitized nanocrystalline TiO2 solar cells. Phys. Chem. Journal. B., 101, 2576–2582.

Hui X., Xia T., Dong-Ting., *et al*.; (2009) "Enhanced Efficiency in DSSCs based on TiO_2 films"; Research Centre of the Ministry of High Gravity Engineering and Technology, Beijing University of Chemical Technology; 2280 – 2285.

International Energy Agency Renewables in Global Energy Supply; *An IEA Fact Sheet* 2011.

Mills S. (2011); "Integrating intermittent renewable energy technologies with coal-fired power plant"; ISBN 978-92-9029-509-9; 85.

Jaramillo, P. (2007) "A Life Cycle Comparison of Coal and Natural Gas for Electricity Generation and the Production of Transportation Fuels", Carnegie Mellon University, PhD Thesis;1 – 2 .

Jasim K. E (2009) "Dye Sensitized Solar Cells - Working Principles, Challenges and Opportunities" Department of Physics, University of Bahrain; 171- 203.

Labat F., Bahers T., Ciofini I., Adamo C., (2011) “First-Principles Modeling of Dye-Sensitized Solar Cells: Challenges and Perspectives”; University of France; 1268 – 1277.

Lee J.D., (2006) “Concise Inorganic Chemistry, Fifth Edition”; Blackwell Publishing Inc. 204 – 229.

Lee S., Yamasue E., Okumura H and Ishihara K. N., (2009) ; “Preparation of N-Doped TiO_x Films”; Japan Institute of Metals, Graduate School of Energy Science, Kyoto University, Kyoto, Japan; 1805 – 1811.

Lobato K., Peter L., Nguyen O., Jennings J, Dunn H.; (2009); “Charge Transport and Recombination in Dye-Sensitized Nanocrystalline Solar Cells”; Sustainable Energy Systems, University of Lisbon; 1– 4.

Miller F.P., Vandome A.F., MacBrewster N, (2010) “Fundamentals of X-Ray Diffraction”; Alphascript Publishers, New York; 34 – 29.

Monllor-Satoca D., Gomez R., González-Hidalgo M., Salvador P. (2007); “An Alternative kinetic approach in heterogeneous photocatalysis based on the degree of interaction of dissolved pollutant species with the semiconductor surface”; Phys. Chem. 129: 247-255.

Moom S., (2011) “State Sensitized Hetero-junction Solar Cells: Effect of Sensitizing

Systems on Performance and Stability"; Ecole Polytechnique Federal of Luassanne; PhD Thesis, 24.

Nazeeruddin M. K., Pẽchy P., Gratzel M. (1991); "Efficient panchromatic sensitization of nanocrystalline TiO_2 films by a black dye based on a trichiocyanato-ruthenium complex" Chem. Comm, 1705-1706.

Nazeeruddin M. K *et al*., (1993) "Conversion of light to Electricity by charge-transfer sensitizers on nanocrystalline TiO_2 electrodes" J. Am. Chem. Soc.**115**, 6382–6390.

O'Regan B., Gratzel M. (2001) "A low cost high-efficiency solar cell based on dye-sensitized TiO_2 films", Nature, 353-354.

Owen T., (1996); "Fundamentals of UV-Visible Spectroscopy"; Fifth Edition, Hewlett-Packard Company; Publication No: 12-5965-5123E; 10 – 14.

Park N.G, J. Lagemaat, A. J. Frank, J. Phys. Chem. B. 104 (2000) 8989.

Park N. G., Kim K., Lee M. H., (2009); "Formation of Highly Efficient Dye-Sensitized Solar Cells by Hierarchical Pore Generation with Nano-porous TiO_2 Spheres"; Materials Science & Technology Division; Korea Institute Science & Technology; 1 – 6.

R.E.H. Sims, R.N. Schock, A. X. Zhang, 2007; Energy supply. In Climate Change 2007:

Mitigation. Contribution of Working Group III to the Fourth Assessment Report of the Intergovernmental Panel on Climate Change, Cambridge University Press, Cambridge, United Kingdom and, 265 – 266.

Sauer M., Hofkens J., Enderlein J., (2011) "Handbook of Fluorescence Spectroscopy and Imaging". Copyright WILEY-VCH Verlag GmbH & Co. KGaA, Weinheim; ISBN: 978-3- 527-31669-4; 2–6 .

Smith R; (2011) "UK Future Energy Scenarios Document" 58 – 59.

Sokolsky M., Cirak J., (2010); "Dye-sensitized solar cells: Materials and Processes"; Department of Physics, Slovak University of Technology; 78 – 81.

Spectro-Educational Booklet, (2007); "Basic UltraViolet-Visible Spectrophotometry"; 3 – 8.

Stuart B., (2004); "Infrared Spectroscopy: Fundamentals and Applications"; Sixth Edition, John Wiley and Sons, Ltd; ISBN 0-470 85427-8; 1 – 5.

Tolvanen A., (2003); "Characterization and manufacturing techniques of dye-sensitized solar cells." Helsinki University of Technology"; MSc Thesis, 6-7.

Wang C.C., Ying J.Y., Chem. Mater. 11 (2004) 3113.

Wang D., Mendelsohn R., Galoppini E., (2004); “Excited State Electron Transfer from Ru(II) Polypyridyl Complexes Anchored toNanocrystalline TiO_2 through Rigid-Rod Linkers”; Phys. Chem Journal; 16642 – 16653.

Wang K., Dai K., (2003) “Optimum Nanoporous TiO_2 film and its applications to dye-sensitized solar cells”; Institute of Plasma Physics, Volume 20, 953 – 956.

Westermark K., (2001); “Dye/Semiconductor Interface - An Electron Spectroscopic Study of Systems forSolar Cell and Display Applications”; Uppsala University; PhD Thesis; 32.

Yeon S. H., Patel R., Koh J. K., (2011); “Preparation of porous TiO_2 thin films and their applications to DSSCs”; Journal of the Korean Electrochemical Society; 83 – 91.

Yu Z., (2012); “Liquid Redox Electrolytes for Dye-Sensitized Solar Cells”; KTH Chemical Science and Engineering, Royal Institute of Technology; PhD Thesis, 7 – 11.

Yurugi T., Numata Y., Ito S., Sykes K., (2001) “SEMEDX – Integrated Analysis System”; Feature Article; Hitachi Science Systems, Ltd., Oxford Instruments plc; 14 –18.

Zhang J., Zaban A.; (2008) “Efficiency Enhancement in DSSCs; Department of Chemistry, Nano – energy Research Centre, Bar – Illan University; 5670 - 5674”

Zhang S., Li L., Kumar A., (2009); “Materials characterization techniques” Second Edition;

University of Michigan; ISBN 1420042947; CRC Press Publisher; 125.